Nature and Energy Redistribution of Highly Vibrationally Excited Polyatomic Molecules

Thesis by

Joseph Walter Perry

In Partial Fulfillment of the Requirements

for the Degree of

Doctor of Philosophy

California Institute of Technology

Pasadena, California

1984

Submitted January 10, 1984

This thesis is dedicated to my parents, Joe and Dolly, and my wife Janis for their love, support and patience and to the memory of my sister, Suzy.

ACKNOWLEDGMENT

I would like to thank the many people in the Caltech community that have provided a stimulating and challenging atmosphere and have contributed to the development of this work. First, thanks go to my advisor Ahmed Zewail for his support, creative ideas, endless thirst for new scientific frontiers and for his ability to pinpoint important problems. I wish to thank my fellow students and friends who have encouraged and contributed to this work, especially: David Millar, Barry Swartz, Bill Lambert, Bill Brittain, Sam Batchelder, Duane Smith, Norbert Scherer, Lutfur Khundkar and Isaac de Melo Xavier.

I would also like to gratefully acknowledge the efforts of those people with whom I've collaborated on various projects: Professor F. Anson, Dr. S. Samson, B. Santaserio, M. Glasbeek, A. J. McQuillan, E. A. Ryabov, P. Taborek, D. Moll and Professor A. Kuppermann for providing experimental facilities which resulted in the work presented in Chapter V.

My sincere thanks go to all the Chemistry Department shops.

Finally, thanks go to Debbie Chester for spending much of her holidays typing this thesis and to my wife Janis for her careful reconstruction of the reprints included in this thesis.

This work was supported by grants from the National Science Foundation (CHE-81-12833 and DMR-81-05034).

TABLE OF CONTENTS

ABSTRACT

This thesis is a primarily experimental study of the spectroscopy and dynamics of highly vibrationally excited molecules in the ground and excited electronic states. Linear spectroscopic studies have been performed on CH-stretching overtones of medium and large sized molecules in the gas and solid phases. Also new time-resolved methods based on nonlinear multiphoton ionization spectroscopy have been applied on the picosecond time-scale to the study of ultrafast intramolecular vibrational-energy redistribution (IVR) in isolated molecules.

The first observation of high-energy CH stretching overtones of molecules in low-temperature solids is reported. Spectra of the $\nu_{CH} = 5$ transitions of many aromatic molecules at $\sim$ 2K reveal homogeneously broadened bands which are assigned to inequivalent local modes by studies of some isotopically substituted molecules. Typical linewidths give population lifetimes of $\sim$ 50 fs for aromatic compared to 100-200 fs for methyl CHs in these large molecules. The polarization ratios of durene CH overtones are in good agreement with those predicted with the localized bond-mode transition moments.

Overtone spectra of some gas-phase deuterated methanes and tetramethyl compounds have been studied. Spectra of CHD_3 have shown severe vibrational mixing at $\nu_{CH} = 6$ and 7 with an apparent tuning of the Fermi-resonance between $|\nu_{CH}\rangle$ and discrete stretch-bend combination states, e.g., $|(\nu-1)_{CH}, 2_{bend}\rangle$. Nonetheless, the lifetime of the CHD_3 overtones must be long ($\geq$ 5 ps) as evidenced by the narrow resolution limited linewidths. The splitting of the $|6,0\rangle_{\pm}$ states of CH_2D_2 is

inferred to be < 10 cm^{-1} and shows that the coupling of the CH oscillators is relatively weak in agreement with theoretical prediction. In general, the results on the CH overtones indicate a significant role of CH stretch-normal mode coupling in the spectra and dynamics.

Picosecond pump and probe multiphoton ionization is developed for the study of IVR in isolated molecules. Experimental evidence for IVR is presented. Nonexponential decay of vibronic states of S_1 trans-stilbene is analyzed in terms of a population rate equation and time-dependent Franck-Condon factor description of IVR. The thermally-averaged IVR time constant is about 2 ps. Also, the excess vibrational energy dependence of the S_1 trans-stilbene isomerization rate is determined for total vibrational energy of 2000 to 4500 cm^{-1} and good agreement is found with calculated thermally averaged rates based on independent results on jet-cooled molecules.

INTRODUCTION

This thesis reports on our work on the nature and energy redistribution of highly vibrationally excited polyatomic molecules. The motivation for such studies is inspired by several topics of current interest in chemical physics. Particularly noteworthy topics are 1) the theory and phenomenology of molecular states at energies comparable to dissociation or reaction barriers, 2) radiationless relaxation of molecules under collisionless conditions, 3) multiphoton excitation of polyatomic molecules, 4) the search for mode-selective laser-induced chemistry and 5) a problem of applied physics interest which is the dispersion and loss of optical guided modes in optical fibers. In this thesis, we shall focus on the more fundamental issues (1 and 2) which have a strong bearing on the more applied problems.

The nature of molecular states at energies comparable to dissociation energies are not well understood. Much theoretical effort has been devoted to classical, semiclassical and quantum mechanical calculations on model systems and more recently attempts have been made on "realistic" systems.[1] Most of these studies are oriented towards understanding the onset of "chaotic" motion as well as the remnants of ordered motion which are present in the presages of chaos. In addition to the development of refined and highly powerful model systems and mathematical techniques there is always much interest in especially simple models which serve as conceptually and computationally convenient tools. The local mode model[2] of molecular vibrations is one such simple model.

The local mode model[2] is a model which takes as a starting point the description of vibrations as localized displacements of particular internal coordinates (valence coordinates) of the molecule. In particular, stretching vibrations involving hydrogen attached to a relatively heavy atom (eg., C, N, O, etc.) are well suited to such a description. The simplest form of this model uses an adiabatic separation of the high-frequency stretching vibrations from the remaining vibrations. The Hamiltonian for the high-frequency modes is written as a sum of single mode operators. The single model operators are, of course, sums of kinetic and potential energy operators which are diagonal in the stretch internal coordinate. The potential is taken to be an anharmonic form such as a Morse potential[3a] or a truncated power series expansion.[3b]

The Morse potential is convenient since the corresponding Schrodinger equation is analytically soluble.[4] The wavefunctions generated in this approach form an extremely convenient basis. These basis states are thought to be especially good since they give a reasonable description of dissociation in terms of single bond breakage rather than the energetically unfavorable process envisioned in proceeding to dissociation via an anharmonic normal mode where all oscillators in an N-fold degenerate system will rupture. Also, this model readily rationalizes the very simple "one-dimensional" transition energy expression ($\Delta E = A\nu + B\nu 2$)[5] found to successfully fit spectroscopic data for many polyatomic molecules.[6] In addition, the local mode model reinforces the long-known phenomenological idea of group vibrations[7] where a subsystem of oscillators (e.g., a methyl group

or a carbonyl group) in a molecule behave essentially independently of the remainder of the system.

There has been much work on the theoretical basis of the local mode model. Wallace,[2c] for example, has examined the derivation of the local mode Hamiltonian starting from a very general form. The approximations involved are 1) a neglect of the variation of the G-matrix with respect to the internal coordinate and 2) a neglect of all off-diagonal terms in the kinetic and potential energy when written in the internal coordinate representation. The off-diagonal terms in the kinetic energy can be shown to be $\sim$ 1/12 of the diagonal term for a CH_2 fragment due to the scaling of the off-diagonal term by the reciprocal mass of the adjoining atom. The magnitudes of the off-diagonal potential terms are not readily estimated so that in the absence of experimental information their neglect is an outright assumption. Given the rather extensive level of approximation it is clear that we should view this model as a starting basis for theoretical considerations rather than as a rigorous description for an understanding of the exact eigenstates of the system. The use of a symmmetry-adapted basis of local mode functions in theoretical applications is necessary due to the commutation relations of the symmetry point group operators and the Hamiltonian and is convenient since it greatly simplifies the rather large coupling matrices which must be dealt with at higher vibrational quanta. The spirit of this work will be to stick with the simplest form of the model as far as possible and to introduce the coupling of the oscillators when experimental evidence so requires.

Theoretical models which develop the treatment of coupling of the oscillators have been advanced by several groups.[8] Of particular interest is the work by Childs et al. and Mortensen et al. In the work of Childs et al. the authors use variational calculations based on symmetrized local mode basis functions. The useful feature of their treatment is the simplification of the coupling Hamiltonian to a form which expresses the coupling strength as a single parameter. The full range of behavior of the system of oscillators is then realized by performing a complete diagonalization of the interbond coupling for varying amounts of diagonal anharmonicity. Then, when the eigenvalues are plotted as a function of the ratio of coupling to diagonal anharmonic constants, a complete correlation from limiting local mode to limiting normal mode cases can be achieved. This correlation can be a useful tool for assessing the degree of localization. Of particular interest in this regard is the splitting of the spectroscopically dominating lowest energy local mode level (of the form $|\nu,0,0...\rangle$) as the ratio of coupling to diagonal anharmonicity is increased. It may be the case that this splitting takes place only very close to the normal mode limit in which case the lack of a splitting in the observed spectrum does not allow a conclusion on the extent of localization. On the other hand if a splitting of significant size can be observed then in most realistic cases the extent of delocalization will be high. It is clearly of interest to attempt to observe these splittings experimentally with the proper level of caution exerted in the literal interpretation of a relatively small splitting.

The other main point of focus in this thesis is determination of the timescale for intramolecular vibrational redistribution. Stated very simply, IVR is the total energy conserving process which results after excitation of a nonstationary vibronic state in a molecular system. The initially excited state is often characterized in terms of some dominant zero-order state where a given number of quanta are in a particular mode. The IVR process then serves to redistribute the vibrational quanta until all states within a certain width (given by the uncertainty principle) become equally probable. The timescale of this process is extremely important for laser-induced chemistry with respect to the proper description of the energy distribution of the excited molecules. Contrasting theories which have been compared recently[9] are the RRKM theory[10] where it is assumed that[10] the energy redistribution is complete (thermalized) on the timescale of the chemical reaction and the Slater theory[10] where energy is not assumed to be statistically distributed and mode occupations and state-to-state rate constants must be specified. Clearly, from the viewpoint of desired selective laser-induced chemistry much could be gained if IVR is found to be slow relative to reaction times in molecules which undergo photochemical reactions, and if these molecules can be strongly excited selectively.

The empirical efforts of this work will be divided into spectral and time-resolved studies. In the spectral studies CH stretching overtone spectra of polyatomic molecules in crystals at very low temperature ($\sim$2K) will be investigated. These studies will focus on bandwidths, lineshapes, and broadening mechanisms with effort devoted to energy levels and spectral splittings, also. The use of low-temperature crystal media will permit elimination of effects due to thermal

congestion and exploitation of the crystal anisotropy to obtain information on the nature of the transition dipole moments. In conjunction with these low-temperature studies room temperature studies of crystals and gases will be performed to obtain some thermally-averaged properties or spectra of somewhat smaller molecules under "isolated" conditions.

Finally, a laser multiphoton ionization method will be described in a study directed towards making time domain measurements of IVR. This method involves the picosecond pulsed excitation of molecules in a low-pressure vapor to a vibrational state in some electronic state (S_1 in the cases studied here). The time evolution of the system is monitored by applying a probing pulse which is capable of elevating the molecules from the given electronic state to the ionization continuum. Ion current is detected as a function of the time delay between the pump and probe pulses and thus the dynamics of the intermediate level are mapped out. The method is capable of monitoring IVR because of the change in Franck-Condon factors as the vibrational probability distribution evolves from the initial to the "equilibrated" form. The process is modelled in terms of population rate equations and effective Franck-Condon factors for the initial and final distribution.

This extremely sensitive and versatile method is applied to the study of the low pressure vapors of trans-stilbene and aniline.

REFERENCES

1. a) D. W. Noid, M. L. Koszykowski and R. A. Marcus, Ann. Rev. Phys. Chem. **32**, 267 (1981); b) S. A. Rice, Adv. Chem. Phys. **47**, 117, (1981); c) P. Brumer, ibid. **47**, 201 (1981); d) M. Tabor, ibid **46**, 73 (1981); e) C. Jaffe and P. Brumer, J. Chem. Phys. **11**, 5646 (1980); f) M. Sage and J. Jortner, Chem. Phys. Lett. **62**, 451, (1979); g) E. L. Sibert, III. W. P. Rinehardt and J. T. Hynes, Chem. Phys. Lett. **92**, 455 (1982); h) J. S. Hutchinson, W. P. Rinehardt and J. T. Hynes. J. Chem. Phys. **79**, 4247 (1983) and references therein.
2. a) B. R. Henry and W. Sibrand, J. Chem. Phys. **49**, 5369 (1968); b) B. R. Henry, Acc. Chem. Res. **10**, 207 (1977); c) R. Wallace, Chem. Phys. **11**, 189 (1975).
3. a) P. M. Morse, Phys. Rev. **34**, 57 (1929); b) R. L. Swofford, M. E. Long and A. C. Albrecht, J. Chem. Phys. **65**, 179 (1976).
4. D. ter Haar, Phys. Rev. **70**, 222 (1946).
5. R. T. Birge and H. Sponer, Phys. Rev. **28**, 259 (1926).
6. a) H. L. Fang and R. L. Swofford, Adv. in Laser Spectroscopy **1**, 1 Ed. B. A. Garetz and J. R. Lombardi, Heyden Publ. Philadelphia (1982); b) B. R. Henry, Vib. Spectra Struct. **10**, 269 (1981).
7. a) W. T. King and B. Crawford, Jr., J. Mol. Spectrosc. **5**, 421 (1960); b) G. Herzberg, Infrared and Raman Spectra of Polyatomic Molecules, Van Nostrand, New York (1945).
8. a) M. L. Sage and J. Jortner, Adv. Chem. Phys. **47**, 293 (1981); b) M. S. Burberry and A. C. Albrecht, J. Chem. Phys. **71**, 4631 (1979); c) H. S. Moller and O. Sonnich Mortenson, Chem. Phys.

Lett. **66**, 539 (1979); d) R. T. Lawton and M. S. Child, Mol. Phys. **40**, 773 (1980); e) O. Sonnich Mortensen, B. R. Henry and M. Ali Mohammadi, J. Chem. Phys. **75**, 4800 (1981); f) L. Halonen and M. S. Child, Mol. Phys, **11**, 1 (1982); g) M. L. Sage and J. A. Williams, III, J. Chem. Phys. **78**, 1348 (1983); h) L. Halonen and M. S. Child, J. Chem. Phys. **79**, 4355 (1983).

9. E. Thiele, M. F. Goodman and J. Stone, Opt. Eng. **19**, 10 (1980).

10. P. J. Robinson and K. A. Holbrook, Unimolecular Reactions John Wiley & Sons, New York (1972).

CHAPTER I

Observation of high-energy vibrational overtones of molecules in solids: Local modes and intramolecular relaxations

J. W. Perry and A. H. Zewail[a)]

Arthur Amos Noyes Laboratory of Chemical Physics, [b)] *California Institute of Technology, Pasadena, California 91125*
(Received 15 September 1978)

In the last few years, the spectra of vibrational overtones[1] (at ~ 15–20,000 cm^{-1}) in large molecules have received considerable attention. The focus is on three problems dealing with the origin of relaxation at such high energies, the association of spectral band positions with the local modes (LM) in molecules, and the relevance of these spectra to possible selectivity in laser-induced chemistry.

Albrecht and co-workers[2–4] using the technique of thermal lensing has identified overtones in *liquid* benzene and in several other aromatic liquids. Typically, the fifth overtone is around 6000 Å and the width (FWHM) is ~ 300 cm^{-1}. A similar transition has been found in *gaseous* benzene by Bray and Berry[5] but with a width of 90 cm^{-1} ascribed to broadening by intramolecular relaxation.[6]

We report here on the observation of CH-stretching overtones ($v = 2 - 6$) in *solid* naphthalene. The experiments offer the following: (a) the molecules can be frozen to low temperatures (1.3 K) so that the contribution of rotational states to the width of the resonance may be eliminated; (b) at 1.3 K the excitation is from $v = 0$ and hence spectral congestion can be avoided; (c) unlike gases and liquids polarization spectroscopy in solids assigns the bands; and finally (d) the inhomogeneous broadening may be realized by comparing the width of the overtone to that of nearby crystal electronic states.

Naphthalene (Aldrich Gold label) was extensively zone refined,[7] and crystals (2–70 mm) were grown in a Bridgman furnace. The crystals were cooled carefully from room temperature to 1.3 K. The optical spectrometer used in these experiments is a home-built double beam apparatus[10] whose photomultiplier output

was phase sensitive detected and digitally processed in order to obtain accurate line shape functions.

Figure 1 shows the overtone spectrum at 300 °K together with the least squares fit for the anharmonic relationship: $\Delta E(v)v^{-1} = A + Bv$, where $A = X_1 + B$. X_1 is the fundamental frequency and B is the anharmonicity. Using this relationship, we obtain $A = 3086 \pm 6$ cm^{-1} and $B = -55.8 \pm 1.4$ cm^{-1} for crystalline naphthalene, thus establishing good agreement with the liquid phase work.

The linewidth of the 0 – 5 transition at 300 K is 220 cm^{-1}, much *narrower* than the liquid line, but still broader than that of the CH overtone in benzene gas. At 1.3 K, however, the line shows a new feature; a splitting into two peaks whose apparent relative intensity is temperature dependent. The question now: Is the resonance homogeneously or inhomogeneously broadened (IB)?

To answer this question we must first eliminate two effects; the inhomogeneous crystal broadening and *inter*-molecular vibrational splittings (IB). To disentangle the contribution of the former, we have located the triplet state in the *same* crystal (see Fig. 2). The 0, 0 which exhibits a Davydov splitting of 10 cm^{-1}, is in excellent agreement with previous photoexcitation experiments.[9] The first vibrational band shows a smaller (~ 5 cm^{-1}) splitting. If this picture applies to the overtone progression we can then neglect the IB due to crystal "irregularities" and vibrational resonance interactions. The splitting shown in Fig. 2, we therefore ascribe as due to different CH oscillators (say the two inequivalent sets of naphthalene).[11] The broadening (99 ± 7 and 147 ± 5 cm^{-1} from the computer fit results, Fig. 2) must have the contribution of both dephasing and energy relaxation processes. At room temperature the broadening increases and masks the splitting. To confirm that this temperature dependence is real and that the splitting is not due to different "local" crystallites in the long crystal used, we have taken room temperature spectra, 1.3 K spectra and then room temperature spectra again. No differences between the first and the last scan were detectable. The splittings will undoubtedly contribute to the linewidth in the liquid and in the gas also. One must therefore be cautious about spectral changes in bandwidth as a function of v simply because the splitting might become smaller for higher v's due to the difference in anharmonicity between modes.

The line shape (Fig. 2) at 1.3 K can be fit near perfectly to Lorentzians and not to Gaussians. The width of the Lorentzians compares very well with the benzene data.[5] However, in the gas and liquid, there might be some low frequency molecular or reservoir vibrations that are populated at room temperature and will contribute to the width. In benzene, there are no very low frequency molecular modes, but the reservoir modes (e.g., librations) might heavily influence the

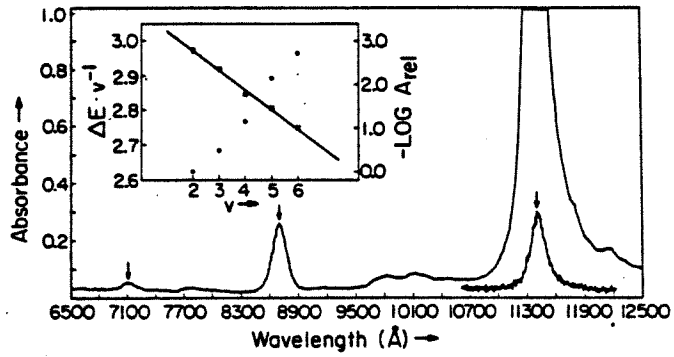

FIG. 1. Vibrational overtones of crystalline naphthalene. Only $v = 0 \rightarrow 3, 4$, and 5 are shown. Absorbance scale is relative to the background and the scan is of low resolution. The actual background absorption cannot be separated from scattering which in turn makes the absorbances reported here relative and dependent on the quality of the crystal. The repeat trace of $v = 0 \rightarrow 3$ was obtained with a thin crystal. In the insert, the relative absorbance is based on the absorbance at λ_{max} and $\Delta E\, v^{-1}$ is in $cm^{-1} \times 10^{-3}$.

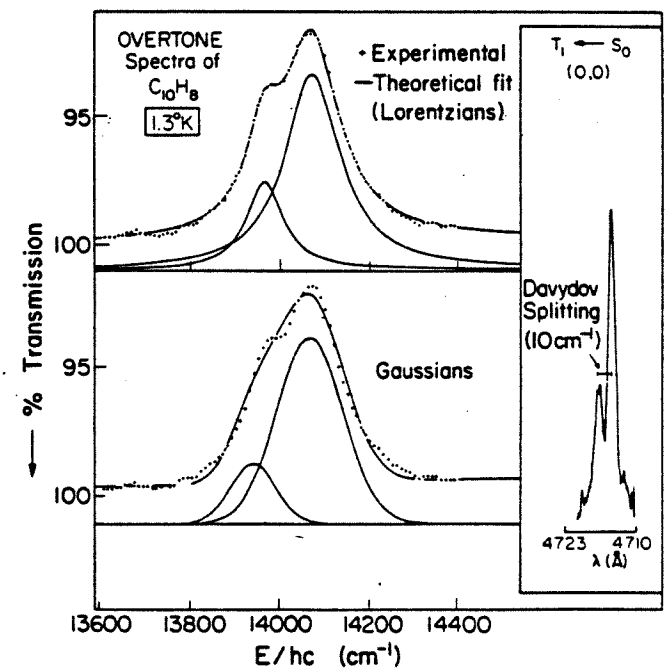

FIG. 2. The low-temperature, $0 \rightarrow 5$ overtone spectra, and the $T_1 \rightarrow S_0$ direct absorption of crystalline naphthalene. The temperature (measured from the vapor pressure of He) is 1.3 °K and the resolution is 2 Å for the overtone and <1 Å for the triplet–singlet absorption. The solid lines are the best computer fits, and the crosses are the digitized experimental data with a stepping resolution of 5 Å. Transmission is relative to background.

liquid band contour, making it broader.[4,12] In the solid at 1.3 K the ground state crystal modes will not contribute to the width, while those built on overtones will. Thus the line will be narrower than the liquid as is evident in Fig. 2. We have made preliminary analysis on the effect of crystal modes on these line shapes and find that although the line will narrow at 1.3 K relative to 300 K, the *asymmetry* of the line is a measure of the homogeneous width $(\pi T_2)^{-1}$, where T_2 is the total dephasing time. If T_2 is "long" ($\approx$ 10 ps) the line is asymmetric, while if T_2 is short ($\approx$ 0.3 ps), the line[13] is essentially symmetric. With this in mind we infer that $T_2 \approx 0.1$ ps and that the overtone transition in the solid (no rotation!) is a limiting intrinsic one, resembling the equivalent CH modes of benzene in the gas phase. What we do not know at the moment is the contribution of T_1 to T_2. Theoretically[14] this contribution has been estimated classically to be negligible on the psec time scale and on the order of 10^{-11} s by Robinson.[15] The contribution of T_1 to T_2 is now experimentally under investigation.

[a]Alfred P. Sloan Fellow.
[b]Contribution No. 5886. This work is supported by a grant from the National Science Foundation.

[1]B. R. Henry, Acc. Chem. Res. 10, 207 (1977).
[2]R. Swofford, M. Burberry, J. Morrell, and A. Albrecht, J. Chem. Phys. 66, 5245 (1977).
[3]R. Swofford, M. E. Long, and A. C. Albrecht, J. Chem. Phys. 65, 179 (1976).
[4]A. C. Albrecht, in *Advances in Laser Chemistry*, edited by A. H. Zewail, Springer Series in Chemical Physics 3 (Springer-Verlag, Berlin, 1978), p. 235.
[5]K. V. Reddy, R. G. Bray, and M. J. Berry, in *Advances in Laser Chemistry*, edited by A. H. Zewail, Springer Series in Chemical Physics 3 (Springer-Verlag, Berlin, 1978), p. 48.
[6]D. Heller and S. Mukamel (to be published); see also M. Elert, P. Stannard, and W. Gelbart, J. Chem. Phys. 67, 5395 (1977).
[7]Extensive zone refining of naphthalene[8,9] will not remove certain impurities. However, since we are not dealing with emission and because the major remaining impurity[8,9] has no strong absorption in the region of interest, these low-concentration impurities do not interfere with the spectra especially at high energies.
[8]D. M. Hanson and G. W. Robinson, J. Chem. Phys. 43, 4174 (1965).
[9]G. Castro and G. W. Robinson, J. Chem. Phys. 50, 1159 (1969).
[10]J. W. Perry and A. H. Zewail (to be published).
[11]E. Lippincott and E. O'Reilly, Jr., J. Chem. Phys. 23, 238 (1955); W. Person, G. Pimentel, and O. Schnepp, *ibid.* 23, 230 (1955).
[12]Recent work by A. Albrecht indicates that anharmonic librational modes can cause a large asymmetric broadening in the line shape of the liquid.
[13]Note that it is basically the same reason which makes the gas phase line shape appear homogeneous when rotational levels have a very wide width.
[14]P. Nagy and W. Hase, Chem. Phys. Lett. 54, 73 (1978).
[15]G. W. Robinson (private communication).

CHAPTER II

HIGH-ENERGY VIBRATIONAL OVERTONES OF POLYATOMIC MOLECULES IN SOLIDS: INEQUIVALENT LOCAL C–H MODES AND SUBPICOSECOND DEPHASING OF NAPHTHALENE AT 1.3 K

J.W. PERRY and A.H. ZEWAIL *

Arthur Amos Noyes Laboratory of Chemical Physics ‡, California Institute of Technology, Pasadena, California 91125, USA

Received 27 March 1979; in final form 7 May 1979

We report on the assignment of inequivalent C–H local modes in naphthalene by observation of overtones of symmetrically deuterated naphthalene (α-d_4) at low temperatures (1.3–2 K). Careful lineshape analysis gives information on the dephasing of these high-energy states as inferred from homogeneous linewidths. We observe new trends in the linewidths that suggest the relative importance of local–normal and local–local mode coupling.

1. Introduction

In our first communication [1] we reported on the observation of C–H stretching overtones of cooled naphthalene. We observed the overtones ($\Delta v_{CH} = 2 \rightarrow 6$) at room temperature, thereby obtaining the average diagonal anharmonicity ($B = -56$ cm^{-1}) and "mechanical" frequency ($A = 3086$ cm^{-1}) of the CH stretching modes. Observing the $\Delta v_{CH} = 5$ transition at low temperature (1.3 K) showed a splitting of the resonance. The lineshape was fit well by the sum of two lorentzians and was not fit by gaussians. The best values for the width (fwhm) were 100 and 150 cm^{-1}. Experiments, which showed the inhomogeneous broadening to be small relative to the observed linewidths, were presented to support the contention that the overtone resonances ($\Delta v_{CH} = 5$) are homogeneously broadened at low temperatures. From the symmetric lorentzian lineshapes we concluded the total dephasing time, T_2, is $\approx$0.1 ps.

In this paper we report on: (1) the origin of the splitting of the CH stretching overtone observed at low temperature; (2) the local mode parameters derived from overtone spectra of crystals of naphthalene-h_8, -αd_4, and -d_8 at room temperature, and (3) the dynamics of the high energy CH local mode states as inferred from lineshape analysis of the overtones observed at low temperature. We conclude with discussion of the observed trends in terms of local modes and coupling of local modes to other modes (local, normal, and lattice) which produce broadening of the overtones.

2. Experimental

Naphthalene-1,4,5,8-d_4 and naphthalene-d_8 were obtained from Merck, Sharp and Dohme of Canada, Ltd. The materials were extensively zone refined before use. Crystals were grown by standard Bridgman techniques. Mass spectral analysis and NMR studies provided the isotopic composition for the N-αd_4 sample. Spectra were obtained using a double beam spectrometer which will be described in a future publication. All spectral analyses of the line shapes were done using a nonlinear regression computer program.

3. Assignment of inequivalent local modes

On observing the CH stretching overtone ($\Delta v_{CH} = 5$) of the naphthalene-h_8 crystal at low temperature

* Alfred P. Sloan Fellow.

‡ Contribution No. 5989.

(1.3 K), we reported previously that the bandshape showed clearly 2 lorentzian components. Our initial hypothesis was that the splitting was due to the resolution of the overtones of the two inequivalent sets of CH oscillators in naphthalene. The two sets are labeled α and β. The approach we used to confirm this assignment was to observe the overtone spectrum of the symmetrically deuterated naphthalene, henceforth referred to as N-αd_4. The N-αd_4 should, of course, show one of the component bands (at $\Delta v = 5$) greatly diminished in intensity at low temperature, if the assignment is correct.

The spectra of N-αd_4 and N-h_8 in the region of the $\Delta v = 5$ transition at 2 and 1.3 K, respectively, are shown in fig. 1 (there was no observable temperature dependence of the lineshapes at liquid He temperatures). Indeed, the spectrum of the N-αd_4 corroborates our hypothesis and provides a basis for positive assignment of the CH α and β local oscillators. Thus, since the peak at higher energy has been greatly reduced in intensity we assign this resonance as the α-CH stretching absorption. The lower energy peak is, therefore, the β-CH stretching absorption.

The relative intensities of the peaks in N-αd_4 should scale, with respect to N-h_8, by the percentage

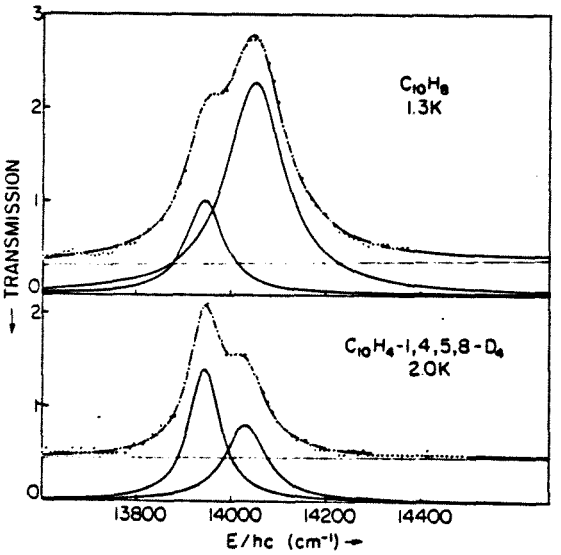

Fig. 1. The low-temperature, 0 → 5 overtone spectra of naphthalene-h_8 (1.3 K) and naphthalene-1,4,5,8-d_4 (2 K). The solid lines are the best computer fits, and the crosses are the digitized experimental data. Transmission is relative to background, and in arbitrary units.

deuteration of the α and β positions. Since the deuteration was not complete at the α position we were able to observe the residual α-CH stretching absorption, as is evident in the spectrum. We calculate ‡ a ratio of *areas* of the high energy peak to the low energy peak to be ≈3.5 for N-h_8. The ratio of the areas for N-αd_4 was found to be 0.8. The predicted ratio based on the percent deuteration and the assignment of the two groups of oscillators is 0.7 ± 0.2. The agreement with the predicted value is seen to be reasonable, which further supports the assignment and the locality of the different CH modes.

The spectrum of N-d_8 in the region of the CH $\Delta v = 5$ transition at room and low temperature was also observed in the solid phase. We found no measurable absorption that could be distinguished from the structureless background, again consistent with our assignment.

4. Local mode parameters of CH and CD oscillators in solid naphthalene

The spectra of vibrational overtones of molecules provide direct information on the vibrational potential function [2], along the coordinate of the mode being probed. Diagonal anharmonicity expresses itself as a convergence of the vibrational levels which leads to dissociation of the bond. Contributions from the higher terms in the potential (cubic, quartic) are observed, but the coefficients of the potential expansion are not uniquely determined [3]. Terms in the potential higher than quartic (contributions of terms $\propto v^3$) simply do not show up in CH stretching vibrations of organic molecules up to at least $\Delta v = 8$ [3].

In the usual local mode analysis [4] of the overtone spectra of X–H oscillators, the energies of the "pure" local mode overtones are fit to the anharmonic relationship

$$\Delta E_i = A_i v_i + B_i v_i^2 \qquad (1)$$

for oscillator i. A is the local mode frequency and B is the anharmonicity. This equation is linearized, $\Delta E_i/v_i$ is plotted against v_i, yielding the local mode parameters as the slope and intercept of the straight line.

‡ Calculated from the integrated areas of the best fit lorentzian components. (Details will be published elsewhere.)

In the case of naphthalene there are two sets of inequivalent oscillators, therefore the energy spectrum of the "pure" local mode vibrational states is given in terms of A_α, A_β and B_α, B_β where α and β refer to the two sets of CH stretch. In principle one could determine the local mode parameters for the individual inequivalent oscillators. However, in the solid at *room temperature* the high energy overtone spectra do not show resolution of the two sets of oscillators. This is due to interactions of phonons with the local modes which cause broadening of the resonances and results in complete overlap of the peaks as will be the case in liquids. We have not yet attempted to obtain lower overtone spectra at low tempertures, therefore we will have to deal with average local mode parameters in this section of the paper.

The positions of the CH and CD stretching overtones in the molecules studied are given in table 1. The positions of the β CH stretching overtones in N-αd_4 are much the same as the average position of the CH stretches in N-h_8. Similarly the positions of the α-CD stretching overtones of N-αd_4 are the same as the average position of the CD stretches in N-d_8. Even though these spectra are of low resolution the results emphasize the similarity of the α and β CH or CD stretches in naphthalene. This makes the resolution of the α and β CH stretch at $\Delta v = 5$ at low temperature an interesting finding in that it demonstrates the importance of observing the high energy overtones at low temperature to resolve positions and widths of slightly different oscillators!

Table 1
CH and CD stretching overtone spectra [a,c] of naphthalene crystals

Molecule	CH stretch				
	$\Delta v = 2$	$\Delta v = 3$	$\Delta v = 4$	$\Delta v = 5$	$\Delta v = 6$
N-h_8	16820 [b]	11420	8730	7130	6070
N-αd_4	16820	11440	8740	7130	–
	CD stretch				
N-αd_4	22360	15110	11440 [d]	–	–
N-d_8	22360	15120	11490	9320	–

a) Peak positions (λ_{max}) in A. b) Nominal uncertainty ±10 A.
c) Spectra obtained with air as reference.
d) Overlapped with CH $\Delta v = 3$, therefore that value is given; not used in estimation of L.M. parameters.

The average local mode parameters of the molecules studied, which were derived from the overtone spectra, are presented in table 2. It is seen that the local mode parameters for the CH stretching overtones are insensitive to partial deuterium substitution. This is in agreement with other studies on CH oscillators [4,5]. One expects the "remote" isotope effect (i.e., effect of deuterium substitution in one part of a molecule on the energy of vibration of an adjacent fragment) to be small in the case of CH stretching modes on the basis of the large inertial difference of the atoms in the local oscillator as well as the fact that the aromatic ring is fairly rigid with respect to the CH stretch [8]. These ideas are indicative of the concept [4] that the oscillators are independent and correspond primarily to hydrogen (deuterium) atom based motion. The parameters for CD stretch are also very similar for N-αd_4 and N-d_8.

The shift of the fundamental local mode frequency in going from CH to CD is in accord with the change in reduced mass of the oscillator. One predicts using $A_{CD} = (\mu_{CH}/\mu_{CD})^{1/2} A_{CH} \approx 2270\ cm^{-1}$ for the CD stretch on the basis of the reduced mass change. Using the relation [3] $B_{CD} = (\mu_{CH}/\mu_{CD}) B_{CH}$, one predicts 29.6 cm^{-1} for the CD anharmonicity. The much smaller diagonal anharmonicity for CD indicates, as is well-known, that the CD stretch is a much more harmonic vibration. This is also in accord with the faster drop in oscillator strength with vibrational quantum for CD stretching overtones.

It is noted here that the effect of phase on the vibrational potential function [9–11] of molecules is

Table 2
Average local mode parameters of N-h_8, N-αd_4 and N-d_8

Molecule	A [a]	B [a]	Correlation coefficient
	CH stretch		
N-h_8	3088 ± 6	−56.5 ± 0.7	0.9998
N-αd_4	3086 ± 3	−56.6 ± 0.8	0.9998
	CD stretch		
N-αd_4	2296 [b]	−30 [b]	– [c]
N-d_8	2296 ± 2	−30.1 ± 0.6	0.9996

a) Parameters from $\Delta E/v = A + Bv$, in cm^{-1}.
b) Estimated by fitting two points only.
c) Not able to calculate (see b).

consistent with our solid state work. We note that the anharmonicity of both the CH stretch and CD stretch are slightly less in the solid than in the liquid. (For comparison: benzene liquid phase values are 59 cm^{-1} for CH and 32 cm^{-1} for CD [3,12].) This observation of less anharmonicity of CH stretching vibrations in the solid state is consistent with the observations of Greenlay and Henry [9] and with the theory of Dellinger and Kasha [10,11]. The effect is that the solvent produces a viscosity dependent barrier to dissociation which reshapes the vibrational potential yielding a more harmonic vibration. In the case of a molecular crystal the van der Waals forces on neighboring molecules provide the repulsive term at short separation.

5. Intensities of local modes

In our early work [1] we have measured the average peak intensity of the different overtones as a function of v. We found that the absorbance versus v gives essentially an exponential decrease in intensity as v increases. These data were recently fit to a Morse oscillator and excellent agreement between theory [13] and experiment [1] was found. This agreement is different from the results on benzene [16]. However, there are several problems involved in measuring these intensities. First, as pointed out in ref. [1], the absorbance is relative to the background which is not yet identified (scattered light versus molecular absorption). Second, in liquids the lines are severely inhomogeneously broadened and this broadening may change as a function of v. Third, although the inhomogeneous broadening in solids is less than in the liquid, the α and β bands are unresolved (at room temperature) and the measured intensity is an average one. Fourth, the dependence of the actual homogeneous broadening on v is still unknown in the low-energy region. Finally, from some preliminary data we have observed changes in intensity when polarized light is used. These studies, which will be complete soon, indicate that different bands might exhibit different intensities depending on the net polarization. As a result of all the above mentioned effects, to us an agreement between the results on naphthalene, benzene, and others to within 20% or so for the slope of $\log I$ versus v is reasonable at this point and one cannot improve this uncertainty factor without further experimentation.

6. Dynamics of CH oscillators from linewidths: dephasing processes

Local mode concepts [1,17–23] have recently been applied to the description of relaxation of CH oscillators [1,6]. In benzene [7], the coupling of the local modes was assumed to be stronger than the local–normal coupling. The assumption results in description of the relaxation in terms of states of the form $|v, 0, 0...\rangle$ coupled to states $|v-1, 1, 0...\rangle$ which are damped by interactions with the dense manifold of normal modes. These theoretical descriptions have been prompted by recent experiments [6] ‡ which report on the widths of the CH overtone resonances in benzene *gas* as a function of vibrational quantum number and deuteration. The overtone spectra were obtained for gas phase benzene by intracavity dye laser spectroscopy utilizing photoacoustic detection. The results of their studies indicate that there is a narrowing of the overtone resonances with increasing v for all molecules studied, except benzene-h_1d_5, and that there is relatively no effect on the widths of the CH overtones in the partially deuterium substituted benzenes.

We report here on the narrowing of CH overtones ($\Delta v = 5$) of N-αd_4 with respect to N-h_8 in the solid at low temperature. Our main purpose in observing the overtone resonances in the low temperature crystal was to obtain direct information on the broadening of the overtones. As mentioned previously [1], we contend that the CH overtone $\Delta v = 5$ is homogeneously broadened at low temperature. This conclusion was reached through lineshape analysis of the N-h_8 resonances. We obtained, for N-h_8, the widths of the α and β CH overtones at $\Delta v = 5$. The widths were 98 ± 7 cm^{-1} (T_2 = 0.11 ps) and 145 ± 5 cm^{-1} (T_2 = 0.073 ps) for the β and α CH modes, respectively. If we assume that the differences in widths are due to energy relaxation and not pure dephasing, the widths may give us some information on the coupling of modes. We do not expect the pure dephasing to be very rapid for CH modes as the bath (inter- and intramolecular modes) is very cold at 2 K. Also, it is not obvious why the pure dephasing of the α and β modes should be different at such low temperature. The 50 cm^{-1} difference in width is not easily interpreted in terms of a density of states argument alone since the splitting of the resonances is only $\approx$100 cm^{-1} and the

‡ See also ref. [19].

density of states does not vary appreciably over the high energy region of the $\Delta v = 5$ CH overtone. If one assumes that the local–local interactions are similar for the inequivalent oscillators, the difference is interpretable in terms of stronger local–normal coupling for the α-CH oscillators. This view is advantageous in that it rationalizes the *benzene-like width of the β-CH* resonance and the broader width for the α-CH oscillators which are coupled to ring vibrations that have no counterpart in the benzene ring modes [14,15].

The lineshape analysis of the N-αd_4 CH resonances was carried out and it was found that widths of the overtone ($\Delta v = 5$) had narrowed with repsect to the N-h_8. The observed widths were 75 ± 5 cm^{-1} (0.14 ps) and 115 ± 10 cm^{-1} (0.092 ps) for the β and residual α-CH stretching overtones. The narrowing of the resonances is surprising in light of the Bray–Berry experiments which suggest no such narrowing. It should be mentioned, however, that there was a narrowing of the CH $\Delta v = 5$ overtone in benzene-$h_1 d_5$ compared to benzene-h_6 (85 versus 100 cm^{-1}) but there was not a consistent trend in the intermediate deuterium substituted molecules. It is possible that the observed narrowing in our case is due to the fact that inequivalent CH oscillators have been deuterium substituted and in the benzene case, the CH oscillators are equivalent. This would indicate that there is stronger coupling to nonequivalent local modes than to equivalent modes. However, we feel that in the present study the observed narrowing is mostly due to the removal of CH local mode states which are coupled to a larger extent with the prepared overtone than are the CD local mode states. Thus, even though the density of states at the $\Delta v = 5$ energy is higher for the deuterated molecule, the effective density of states (coupling matrix element times the real density of states) of strongly coupled levels is lower and the relaxation is slower. The naphthalene data would then suggest that the direct local–normal coupling (for specific normal modes) is very important and that the CH oscillators are coupled more strongly to other CH oscillators than to CD oscillators. The trends in the linewidths indicate that a plausible coupling scheme for describing relaxation in aromatic CH stretching (in the low-temperature phase) is as follows:

(1) The radiation field excites states which are a combination of "pure" local mode overtone states, "mixed" local mode combination states and "mixed" local–normal mode combination states; the excited overtone becomes increasingly "localized" as the quantum number increases.

(2) These states, prepared according to (1), interact with the dense manifold of lower energy modes which are not radiatively coupled to the ground state. In the solid these modes are both lower energy normal modes and lattice modes. This scheme results in homogeneous broadening in accord with the radiationless relaxation of overtones which are in an intermediate-dense level structure [24–26]. (Note that our thinking of the preparation and the coupling scheme is different from the picture depicted in fig. 2 of ref. [7].) If the dense manifold interacting with the discrete state has a finite transition moment, then a lorentzian, a continuum and interference between them is expected [27]. As pointed out by Jortner [28], these interference effects might wash out if the coupling is random.

7. Conclusions

We have presented evidence which assigns the CH stretching overtones of cold naphthalene as due to α and β modes #. The room temperature overtone spectra ($\Delta v = 2 \rightarrow 5$) of solid N-$h_8$, N-$\alpha d_4$ and N-d_8 are consistent with the local mode description of the CH or CD stretching modes. The overtone spectra at low temperature give us information on the broadening mechanisms and indicate that the widths of the overtones are sensitive to subtle molecular parameter variation. The variation of the homogeneous linewidths between α-CH and β-CH oscillators in naphthalene suggest that intramolecular interactions cause more rapid relaxation for the α-CH modes. The partial substitution of CD for CH oscillators in naphthalene gives rise to smaller homogeneous linewidths for the remaining CH stretching modes, thus slower relaxation. The trends of the linewidths indicate that significant local–local mode coupling and local–normal mode coupling contribute to the ultrafast (subpicosecond) relaxation. At the moment we cannot rule

In a private communication with B. Henry, we were informed that inequivalent CH oscillators have been found in cycloalkanes and cycloalkenes in the *liquid* phase. It will be very interesting to resolve their relaxation properties by using the low-temperature (1–2 K) approach discussed here.

out the effect of energy exchange between equivalent and inequivalent oscillators on the overall resonance width. This point is under current investigation.

We plan to further untangle the contributions of inequivalent local modes on the homogeneous broadening of the overtones by observing overtone spectra of benzene at low temperature. Also, the deuterium substitution effect on CH linewidths will be tested by studying overtone spectra of partially deuterated benzenes.

Acknowledgement

This work was supported by a grant from the National Science Foundation. We thank Professors J. Jortner and B. Henry for sending us preprints of their work.

References

[1] J.W. Perry and A.H. Zewail, J. Chem. Phys. 70 (1979) 582.
[2] E.B. Wilson Jr., J.C. Decius and P.C. Cross, Molecular vibrations (McGraw-Hill, New York, 1955).
[3] R.L. Swofford, M.E. Long and A.C. Albrecht, J. Chem. Phys. 65 (1976) 179.
[4] B.R. Henry, Accounts Chem. Res. 10 (1977) 207.
[5] R.L. Swofford, M.S. Burberry, J.A. Morrell and A.C. Albrecht, J. Chem. Phys. 66 (1977) 5245.
[6] R. Bray and M.J. Berry, J. Chem. Phys., to be published.
[7] D.F. Heller and S. Mukamel, J. Chem. Phys. 70 (1979) 463.
[8] R. Wallace, Chem. Phys. 11 (1975) 189.
[9] W.R.A. Greenlay and B.R. Henry, Chem. Phys. Letters 53 (1978) 325.
[10] B. Dellinger and M. Kasha, Chem. Phys. Letters 36 (1975) 410.
[11] B. Dellinger and M. Kasha, Chem. Phys. Letters 38 (1975) 9.
[12] T.E. Martin and A.H. Kalantar, J. Chem. Phys. 49 (1968) 235.
[13] I. Schek, J. Jortner and M. Sage, to be published.
[14] D.E. Freeman and I.G. Ross, Spectrochim. Acta 16 (1960) 1393.
[15] D.B. Scully and D.H. Whiffen, Spectrochim. Acta 16 (1960) 1409.
[16] M.S. Burberry and A.C. Albrecht, J. Chem. Phys. 70 (1979) 463.
[17] P.L. Nagy and W.L. Hase, Chem. Phys. Letters 54 (1978) 73.
[18] A.C. Albrecht, in: Advances in laser chemistry, ed. A.H. Zewail (Springer, Berlin, 1978) p. 235.
[19] K.V. Reddy, R.G. Bray and M.J. Berry, in: Advances in laser chemistry, ed. A.H. Zewail (Springer, Berlin, 1978) p. 48.
[20] B.R. Henry and W. Siebrand, Chem. Phys. Letters 3 (1969) 327.
[21] W. Siebrand and D.F. Williams, J. Chem. Phys. 46 (1967) 403; 49 (1968) 1860.
[22] B.R. Henry and W. Siebrand, J. Chem. Phys. 49 (1968) 5369.
[23] R.J. Watts and S.J. Strickler, J. Chem. Phys. 49 (1968) 3867.
[24] G.W. Robinson, in: Excited states, Vol. 1, ed. E.C. Lim (Academic Press, New York, 1974) p. 1;
S. Rice, in: Excited states, Vol. 2, ed. E.C. Lim (Academic Press, New York, 1975) p. 111.
[25] J. Jortner and S. Mukamel, in: The world of quantum chemistry, eds. R. Daudel and B. Pullman (Reidel, Dordrecht, 1974).
[26] K.F. Freed, Topics Appl. Phys. 15 (1976) 23.
[27] U. Fano, Phys. Rev. 124 (1961) 1866.
[28] J. Jortner, in: Advances in laser spectroscopy, Vol. 113, ed. A.H. Zewail (SPIE Publishing Co., 1977) p. 88.

Appendix to Chapter 2

High-Energy CH-Overtone Spectra of Benzene at 1.8K

It is now well established that the transition energies of CH-stretching overtones in large molecules can be fit to the Birge-Sponer relationship.[1] The description of the bandwidths of these transitions, however, has not been as clearly ascertained. Previous experimental work has determined the homogeneous broadening (from Lorentzian lineshape fits) of the CH-stretch overtones of benzene[2] and naphthalene[3] in the gas phase and low-temperature (2K) crystals, respectively. In a subsequent study[4] of durene (tetramethylbenzene) at low-temperature ($\sim$ 2K) a rather large difference in the bandwidths of methyl bands ($\sim$ 25 cm^{-1}) compared to the aromatic band ($\sim$ 100 cm^{-1}) at $\Delta\nu_{CH} = 5$ was found. The contributions of energy and phase relaxation to the homogeneous broadening have been discussed recently.[4] At room temperature, both types of bands are rather broad ($\sim$ 200 cm^{-1}) and approach the linewidths usually observed for liquids which have significant congestion due to sequence progressions (eg. librational modes).[5]

Benzene overtone spectroscopy has been the subject of many theoretical and experimental studies of the gas and liquid phases. However, due to some experimental difficulties the overtone spectra of benzene at very low temperature crystals have not previously been reported. In this Communication we report on such a measurement for $\Delta\nu = 5$ at 1.8K. We resolve the observed spectrum into three bands and obtain the individual local mode linewidths. The widths ($\sim$ 70-130 cm^{0-1}) are comparable to the widths of gas-phase benzene reported by Bray and Berry, and compare well with the width of other aromatic CH-transitions studied by us at low-temperature. This low-temperature

measurement on benzene shows the intrinsic nature of the width of the CH-overtones and the absence of a thermal congestion contribution, a point which has been of some concern recently.[6] Finally, we provide results on related molecules at low-temperatures for comparison.

The spectroscopic methods have been described previously.[3,4] The benzene crystals were grown by very slowly lowering the sample into a dewar with a decreasing temperature gradient achieved with solid CO_2 at bottom. The single crystals, which showed good optical quality, were cut in a cold glove bag and transferred to an optical dewar precooled to $\sim$ 100K. The dewar was evacuated to a lower pressure to allow slower cooling. The crystals were then immersed in liquid He which was cooled to below the -transition by pumping. The sensitivity of the direct-absorption double-beam spectrometer which used phase sensitive detection, allowed an optical density of $\sim$ 0.003 to be recooled at 1:1 signal to noise with a resolution of 0.3 cm^{-1}. Finally, the lineshapes were analyzed using a nonlinear least-squares fitting routine.

Figure 1 shows the benzene $\Delta\nu_{CH} = 5$ overtone spectrum at 1.8K along with the fitted sum of Lorentzians and components. The benzene lindwidths are presented in Table I along with results for the other molecules studied.

Several important conclusions can be drawn from these results. The benzene spectrum displays an overall width of 225 $\pm$ 10 cm^{-1} at 100K and resolves into three bands at 1.8K. The benzene crystal is known to have a site symmetry of C_i[7] and inhomogeneous broadening of less than a few cm^{-1}.[8] In the rigorous site symmetry the six CH local modes of benzene split into 3 pairs. It is therefore expected that

three bands would be observed as is actually found experimentally.[9]

The linewidths of the low-temperature benzene bands are quite similar to the gas phase linewidths ($\sim$ 100 cm^{-1}). We conclude from this result that the aromatic CH stretch ($\Delta\nu$ = 5) overtones have an intrinsic width of a minimum of 70 cm^{-1}. Furthermore, in contrast to the durene methyl overtones with a width as low as 25 cm^{-1}, the aromatic CH width of benzene is much broader and compares with that of the durene aromatic CH. Tetrachlorobenzene has only two CH's related by the inversion symmetry and since the site symmetry is again C_i only one band is predicted. For $\Delta\nu$ = 5 we observe (Figure 2) one main band and a smaller one (A_{rel} $\sim$ 0.2) with widths of $\sim$ 80 cm^{-1} and 45 cm^{-1}, respectively, which are in Fermi-Resonance.

With this analysis in mind we reexamined the analysis of the naphthalene $\Delta\nu_{CH}$ = 5 spectra. In our previous work we fit the naphthalene-h_8 spectrum with two Lorentzians and the partially deuterated naphthalene-α-d_4 again showed two Lorentzians with the higher energy band substantially reduced in intensity. The higher energy N-α-d_4 band was taken to be due to residual α-hydrogens. However, quantitative NMR analysis shows the residual α-H content of the N-α-d_4 to be < 5% so that it could not be the source of the observed higher energy band. Considering the rigorous site symmetry of naphthalene (C_i) we expect further splitting of the β-CH's just as discussed for benzene.[9] Analysis of the N-h_8 spectrum using three Lorentzians was performed (Figure 3) and the fit was quite good.[10] The width parameters of the higher and lower energy bands did not change appreciably from those reported previously. The primary change was the relative

intensity which is now consistent with the isotopic composition. Finally, it is interesting to note the narrowing of the benzene CH-overtone in going from the liquid phase to the vapor or low temperature solid. In the former phase the width is 223 cm^{-1}[1,11] while in the latter two it is $\sim$ 100 [2] and 70-130 cm^{-1}, respectively.

The important question is what causes the intrinsic broadening of the gas and cold molecules? Armed with the durene data we have attributed the broadening to population relaxation. We showed previously[4] that the ratio of methyl to aromatic linewidths did not quantitatively scale with an estimate of the local-bath total density of states. However, qualitatively, the total density of states for the aromatic ring was much higher than for the methyl group so it is reasonable that the aromatic CH's relax faster. We expect the effective coupling of aromatic CH overtone to the bath to be greater than for the methyl CH's. This idea seems to be borne out by recent quantitative theoretical calculations[12] where the coupling of the CH stretch to bending modes is modelled via the G-matrix coupling. The coupling in this model is due to the stretch coordinate dependence of the effective mass for bending motions (or possibly other modes) involving significant displacements of the CH bond.

In conclusion, we have obtained the very low temperature (1.8K) overtone spectra of the prototypical aromatic molecule; benzene, the only molecule for which the overtones have now been studied in all phases. The aromatic CH bands remain relatively broad ($\sim$ 100 cm^{-1}) even at 1.8K in contrast to aliphatic methyl bands (of durene) which become narrower by up to a factor of 4. This shows that thermal

congestion is not the origin of widths of the aromatic CH overtones and that it is certainly possible to obtain information on the dynamics of CH-overtones in benzene (or comparable molecules) from the spectra. A full account of this work will be published later.

This work was supported by a grant from the National Science Foundation.

REFERENCES

1. H. L. Fang and R. L. Swofford in "Advances in Laser Spectroscopy", Vol. 1, eds.: B. Garetz and J. Lombardi, Heyden Publ. Co., Philadelphia, (1982).
2. R. Bray and M. J. Berry, J. Chem. Phys. **71**, 4909 (1979); K. V. Reddy, D. F. Heller and M. J. Berry, J. Chem. Phys. **76**, 2814 (1982).
3. J. W. Perry and A. H. Zewail, J. Chem. Phys. **70**, 582 (1979).
4. J. W. Perry and A. H. Zewail, J. Phys. Chem. **86**, 5197 (1982).
5. G. M. Korenowski and A. C. Albrecht, Chem. Phys. **38**, 239 (1979).
6. G. J. Scherer, K. K. Lehmann and W. Klemperer, J. Chem. Phys. **78**, 2817 (1983).
7. E. G. Cox, D. W. J. Cruickshank and J. A. S. Smith, Proc. Roy. Soc. (London) **A247**, 1 (1958).
8. E. R. Bernstein, S. D. Colson, D. S. Tinti and G. W. Robinson, J. Chem. Phys. **48**, 4632 (1968); G. C. Nieman and D. S. Tinti, J. Chem. Phys. **46**, 1432 (1967).
9. The possibility of Fermi-Resonance precludes a definite assignment. A higher effective site symmetry along with a Fermi-Resonance could also explain the 3 bands.
10. Since there was no structure on the naphthalene-h_8 spectrum to define the third band we fixed the band positions, the width and the relative intensity of the center band to the lower energy band according to the values of the N-α-d_4 spectrum.
11. C. K. N. Patel, A. C. Tam and R. J. Kerl, J. Chem. Phys. **71**, 1470 (1979).

12. J. S. Hutchinson and W. P. Reinhardt (private communication).

Table I

Low-Temperature ($\tilde{\nu}$ 2K) Bandwidth and Position

of CH-Overtones ($\Delta\nu = 5$) of Large Aromatic Molecules

Molecule	Band	$\bar{\nu}$(cm^{-1})	FWHM (cm^{-1})	A_{rel}
Benzene	α	14123 (4)	133 (10)	0.7
	β	14053 (5)	65 (10)	0.3
	γ	14007 (4)	70 (6)	1.0
1,2,4,5-tetra-chlorobenzene[a]	α	14226 (4)	77 (8)	1.0
	α'[b]	14289 (4)	45 (5)	0.2
naphthalene-h_8[a]	α	14055 (2)	133 (10)	3.0
	β	13952 (4)	90 (10)	1.0
-1,4,5,8-d_4[a]	β'	14036 (8)	113 (10)	1.0
	β	13952 (3)	66 (7)	0.9
durene aromatic-methyl[c]-	α	13872 (4)	103 (6)	---
	a	13620 (4)	43 (5)	∿1
	b	13532 (4)	25 (4)	∿1
	c	13344 (4)	50 (5)	∿2

[a] Parameters given for two peak fit to spectrum.

[b] Combination band in Fermi-Resonance.

[c] Assignments have been presented in ref. 4.

Figure 1: Direct CH-stretching overtone absorption spectrum ($\Delta v = 5$) of crystalline benzene at 1.8K. The crystal pathlength was about 4 cm. The points are the experimental data and the solid lines are the best fit sum of Lorentzians and the components. The spectral resolution for this scan was $\sim$ 5 cm^{-1}. The abscissa is in $cm^{-1}/100$ measured from 13656 cm^{-1}.

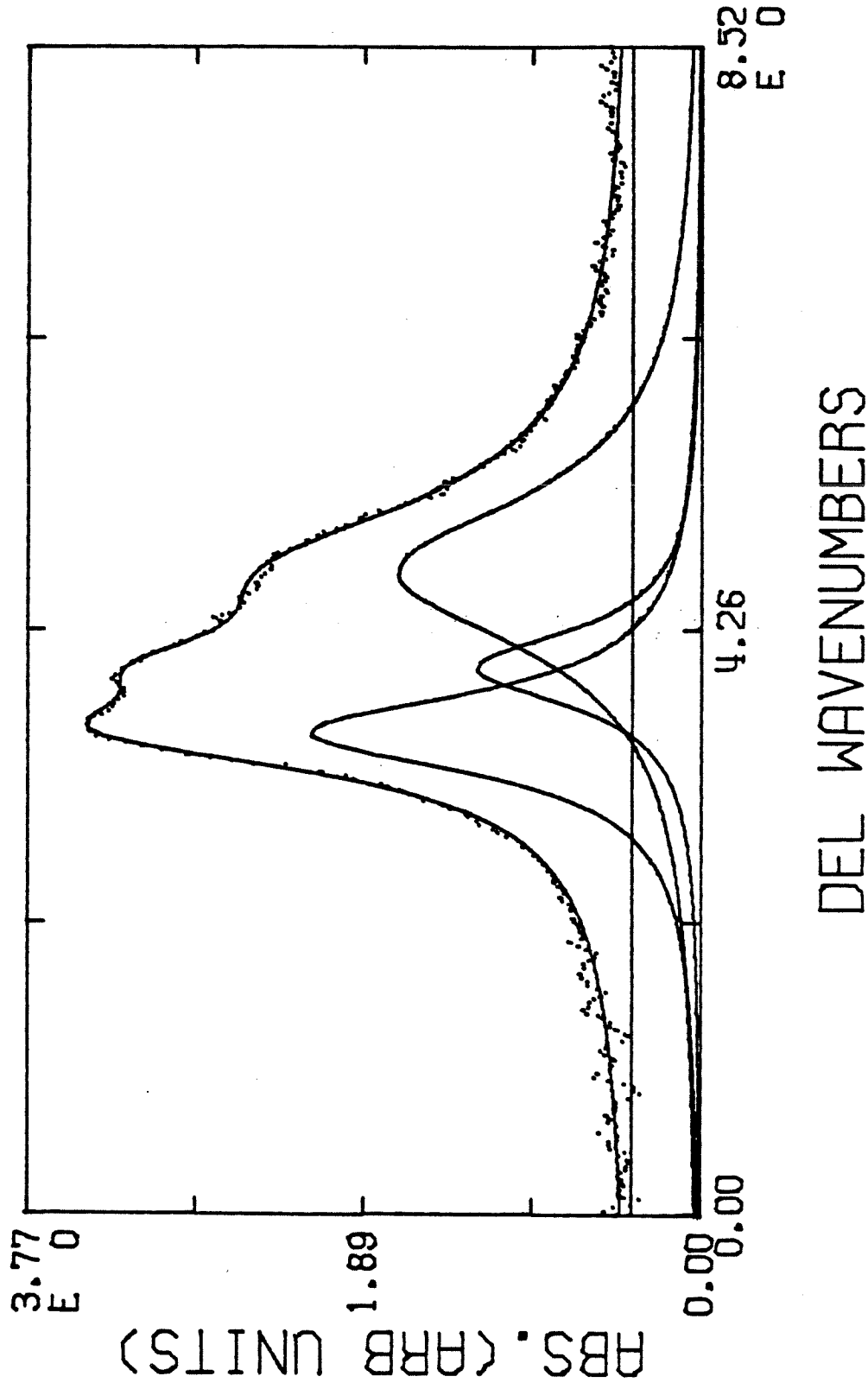
3.77
E 0
1.89
0.00
0.00
4.26
8.52
E 0
RBS.(ARB UNITS)
DEL WAVENUMBERS

Figure 2: CH-stretching overtone spectrum ($\Delta\nu$ = 5) of 1,2,4,5-tetrachlorobenzene at 2.1K. The crystal pathlength was $\sim$ 4 cm and the spectral resolution was $\sim$ 5 cm^{-1}. The points are the experimental data and the solid lines are the best fit Lorentzians. The abscissa is in $cm^{-1}/100$ measured from 13800 cm^{-1}.

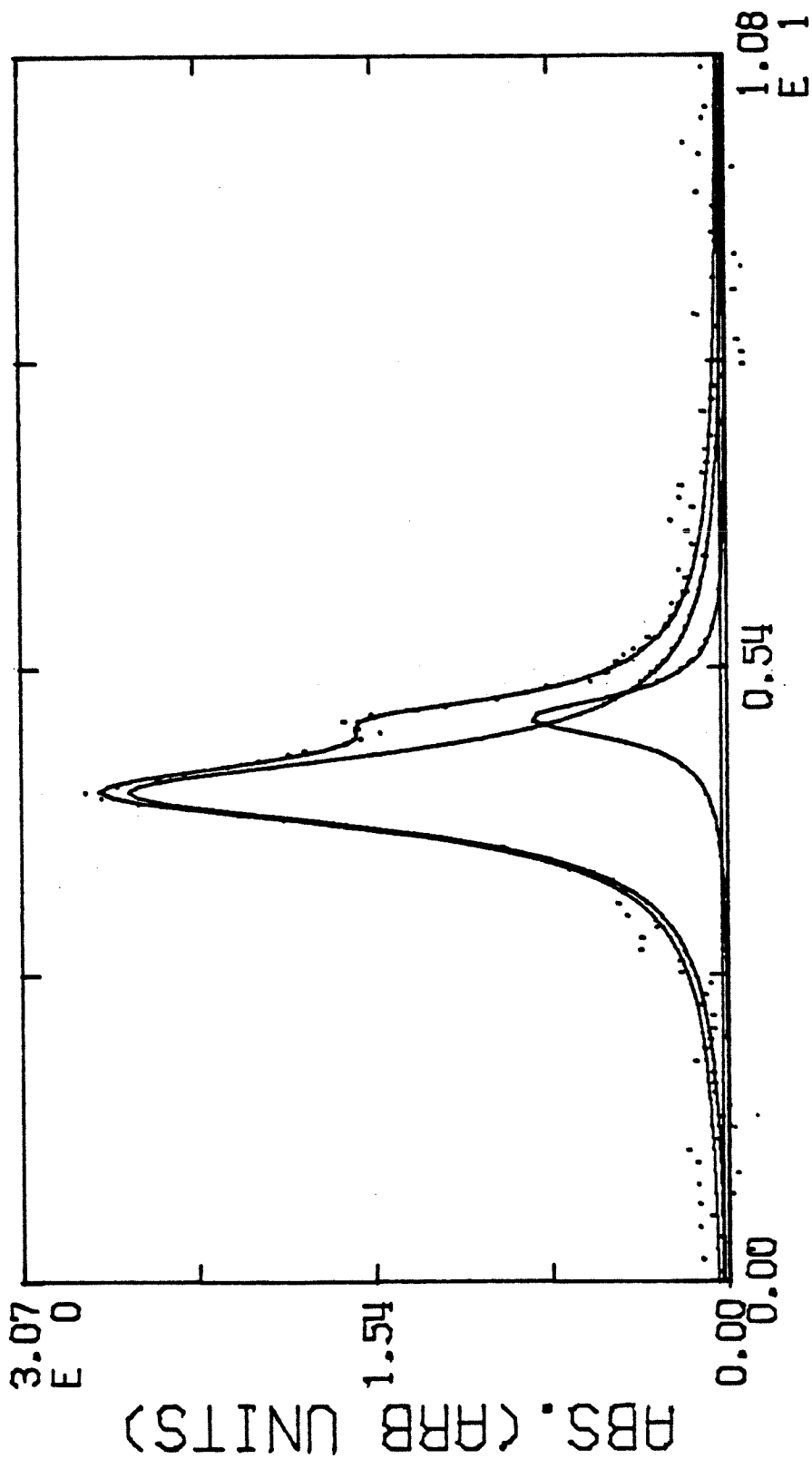
3.07
E 0
1.54
0.00
0.00
0.54
1.08
E 1
ABS. (ARB UNITS)
DEL WAVENUMBERS/100

Figure 3: CH-stretching overtone spectrum ($\Delta\nu$ = 5) of naphthalene-h_8 at 2.0K showing a fit to a sum of three Lorentzians as discussed in the text. The spectral resolution is < 5 cm^{-1}. The abscissa is in $cm^{-1}/100$ measured from 13500 cm^{-1}.

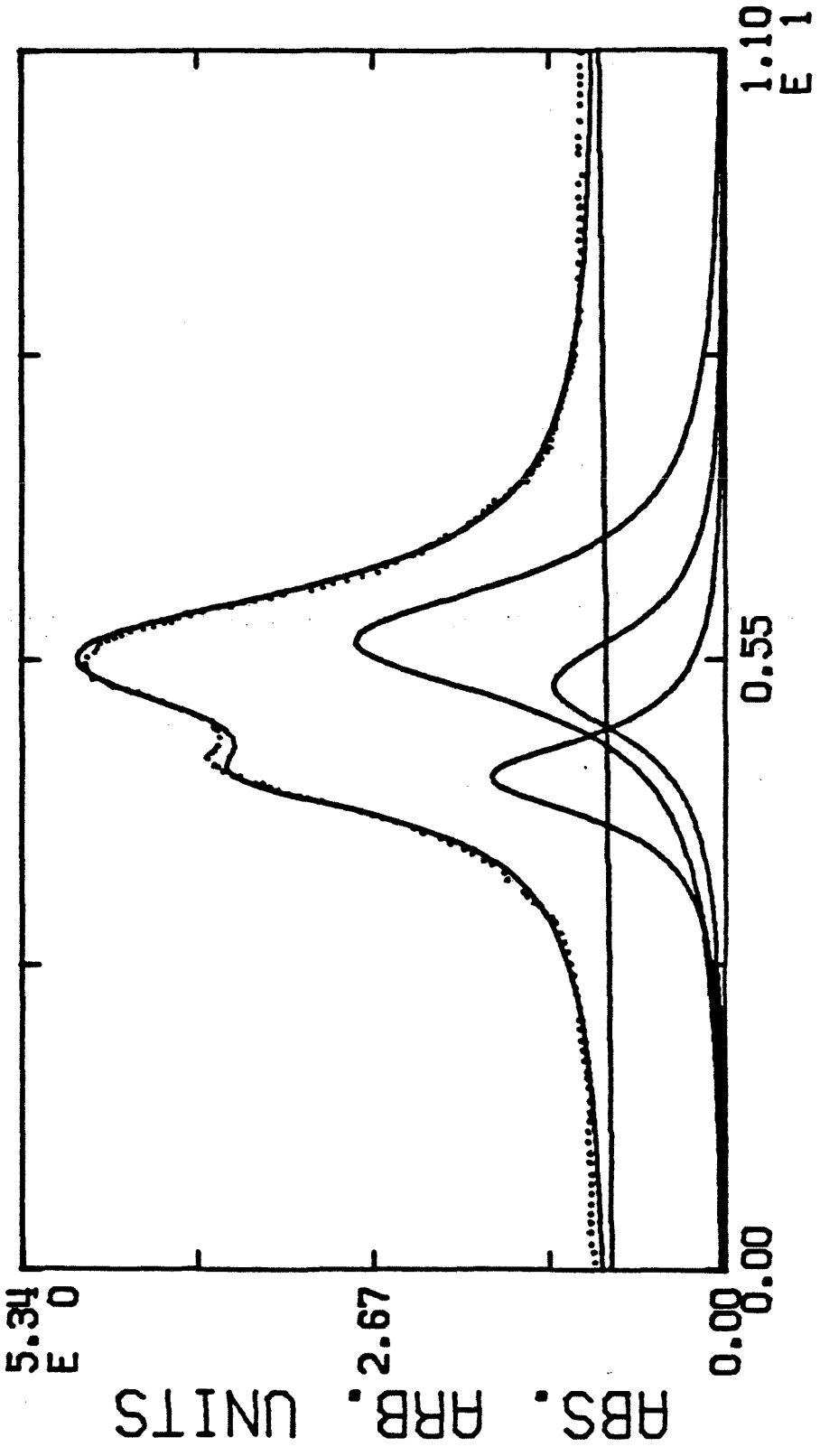
ABS. ARB. UNITS
5.34
E 0
2.67
0.00
0.00
0.55
1.10
E 1
DEL CM-1/100

CHAPTER III

Observation of Large Splittings, Narrow Resonances, and Polarization Extinction in the High-Energy Overtone Spectra of Large Molecules. Experimental Tests of Locality of Excitation in Bonds

Joseph W. Perry and Ahmed H. Zewail*†

Arthur Amos Noyes Laboratory of Chemical Physics,‡ California Institute of Technology, Pasadena, California 91125
(Received: October 24, 1980; In Final Form: February 6, 1981)

In this paper we report on several new spectral features in the high-energy overtone region of the large molecule durene in a crystal at ~2 K, in particular, large splittings, narrow resonances, and polarization extinction. The results are used to test the locality of vibrational excitation at high energies (the fifth harmonic of the CH stretch).

Introduction

In recent years, there has been much interest in the nature of vibrational states of molecules at high energies. The important problems in this field are centered around the following questions: (a) is the excitation in the high-energy states localized or delocalized; (b) what is the time scale for vibrational energy redistribution; and finally (c) what is the relevance of these states and their relaxation to possible mode-selective chemistry? Overtone spectroscopy, including direct absorption[1-3] and emission,[4] thermal lensing[3,5] and photoacoustic spectroscopy,[6,7] has been the primary experimental technique used to obtain information in attempts to answer these questions. The spectra of X–H stretching overtones obtained in liquids,[2,3,5,7] gases,[6] and solids[1,4] have been consistent with the local-mode model in which the vibrational excitation is considered to be localized in certain bonds. Also, from spectral bandwidths (typically 100 cm^{-1}), relaxation times for these high-energy (Δv = 5, 6, 7, ...) overtone states were inferred to be ≈100 fs or shorter.

In this paper we report on the observation of narrow resonances, large spectral splittings, and polarization extinction in the Δv = 5 spectral region of the large molecule durene in a crystal at low temperature (~2 K). Because experiments were done with the samples at low temperature, intrinsic line widths as small as 20–25 cm^{-1} and clear spectral splittings of 200 and 86 cm^{-1} were observed for the aliphatic CH-stretching overtones. We assign bands due to aliphatic and aromatic CH-stretching modes with

selective isotopic substitution. Finally, we report on the essentially complete polarization extinction for the aliphatic bands. The narrow spectral line widths of the methyl peaks provide evidence for slower relaxation of the aliphatic relative to the aromatic CH-stretching modes. The polarization results are used to compare various models of the overtone states on the basis of the directions of the transition dipole moments. Based on our observations and comparison, questions are raised regarding the general applicability of the local-mode model.

Experimental Section

Durene (Aldrich Chemical Co.) and durene-d_2 (Merck Sharp and Dohme) were zone refined extensively. Long crystals (4–6 cm) were grown by using standard Bridgman techniques. The orientation of the crystals used to obtain polarized spectra was determined with X-ray crystallographic techniques. Crystals of durene are monoclinic,[8] space group P_{2_1}/a, thus possessing a twofold axis (b axis) and a mirror plane perpendicular to it. The direction of the b axis was determined with the Laue method by locating first the mirror plane and then the twofold axis. The length of the b axis (b_0 = 5.77 Å) was confirmed by oscillation photographs. The orientation of the a and c axes were determined with the use of zero-layer Weissenberg photographs, taken with the b axis as the rotation axis. The orientation of all three axes was determined relative to the crystal morphology, thus enabling us to orient the crystallographic directions appropriately in our spectrometer.

Absorption spectra were obtained with a locally built conventional double-beam optical spectrometer. The light output of a 1000-W quartz–halogen lamp was band pass filtered for the appropriate spectral range. The filtered light was split with a mirror into a reference and a sample beam. Each beam was chopped independently at a different frequency. Both beams were recombined after the sample and were focused onto the slit of the spectrometer ($^3/_4$-m Spex or $^1/_2$-m Jarrell Ash). The signals from the two beams were processed with a two-phase lock-in amplifier (Brookdeal/9505) referenced at the two chopping frequencies. The sample and reference signals were divided by a logarithmic ratiometer and the log ratio was recorded. Polarized spectra were obtained in the usual manner by inserting a polaroid-film polarizer before the sample and a calcite depolarizer after the sample.

Samples were cooled slowly to ~100 K (overnight) with the use of a Janis 10-DT optical-research dewar. The outer jacket was filled with liquid nitrogen and the inner jacket was pressurized with helium gas. Subsequently, the crystals were immersed in liquid helium and the temperature was reduced to less than 4.2 K by pumping. The temperature was measured with a calibrated diode thermometer or inferred from the measured vapor pressure. It should be noted that the samples retained good optical quality after thermal cycling. X-ray diffraction patterns obtained at room temperature after thermal cycling indicated *no* substantial increase in the mosaic spread.

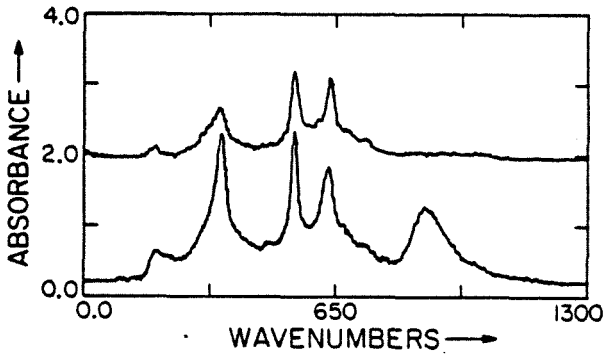

Figure 1. Low-temperature (<2 K) CH-stretching $\Delta v = 5$ overtone spectra of durene (lower) and durene-d_2 (upper) crystals. The spectral bandwidth was <5 cm^{-1}. The absorbance scale is in arbitrary units and the horizontal scale is in wavenumber change from 12990 cm^{-1}.

Results and Discussion

Assignments and the Dynamics. The local-mode model has been successfully applied in the interpretation of the available spectroscopic data on X–H stretching overtones of polyatomic molecules. Relatively simple spectral line shapes and invariance of the scaled line shape with respect to partial isotopic substitution have constituted the strongest evidence for locality of excitation.

In the low-temperature durene crystal spectra we observe several narrow bands with distinct polarization. We attempt to explain these bands within the local-mode model and also within other models which involve various degrees of delocalization in order to determine which model best accounts for the data.

In Figure 1 we present the low-temperature $\Delta v = 5$ CH-stretching absorption spectrum of durene and durene-d_2 (henceforth d_2). The first feature we wish to point out is the absence of the broad band at $\Delta\bar{\nu} \approx 900$ cm^{-1} ($\lambda = 7209$ Å) in the d_2 spectrum and the qualitative consistency of the remaining features of the spectrum.[9] On this basis we assign the band at 7209 Å as the aromatic $\Delta v = 5$ CH-stretching mode. The other bands around $\Delta\bar{\nu} = 300$–600 cm^{-1} ($\lambda \approx 7400$ Å) are methyl-based CH-stretching modes. Although some of the weak bands may be due to vibrational side bands, we rule out that possibility for the main bands because two bands are polarized perpendicular to the other and the required Franck–Condon envelope would be unusual.

In the region of the methyl CH-stretching modes, the line widths of the bands vary from ~20 to ~50 cm^{-1} in contrast to the ~100-cm^{-1} width of the aromatic CH-stretching band. *The methyl CH-stretching mode bandwidths are the smallest bandwidths yet observed in high-energy overtone spectra of polyatomic molecules.* The small widths of the methyl bands imply that these modes relax slower than the aromatic CH-stretching modes. Provided that pure dephasing is negligible, this can be explained as a larger population relaxation time constant for the methyl CH-stretching modes. The slower relaxation of the methyl modes makes sense qualitatively since there is a carbon–carbon bond separating the methyl CH-bonds from the benzene ring. This separation reduces the average potential or kinetic energy coupling of methyl CH-stretching modes to the ring modes relative to the aromatic analogue.

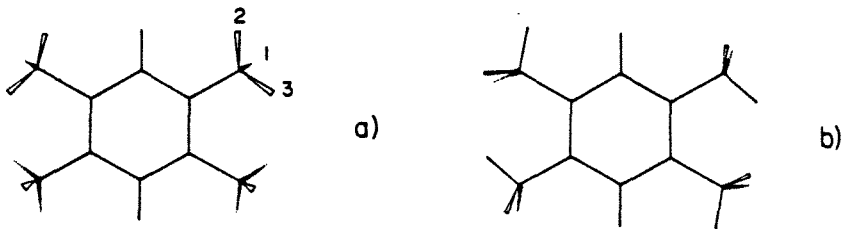

Figure 2. Conformers of durene: (a) "cogwheel" and (b) "bisected" arrangement of methyl groups.

The Nature of the States Excited. The narrowness and the large spectral splittings of the aliphatic bands relative to the aromatic band leads us to consider two important points: (a) there are two distinct types of relaxation of the different CH's to other modes within the molecule, and (b) that the states prepared optically may be different in nature for the aliphatic and aromatic CH's. The vibrational relaxation problem here is strongly connected with the problem of vibronic or electronic relaxation.[12]

In the intermediate coupling case, the states prepared with narrow-band excitation are nonstationary (i.e., have finite width) because of interactions with the manifold of bath modes, but the states of the "optically-active" manifold (at a given quantum level) are separated by an amount (Δ) which is larger than the corresponding line widths (W), thus $W/\Delta < 1$ and one is able to approximately resolve the individual "eigenstates". Since for the aliphatic CH subset of modes $W/\Delta \sim 0.2$–0.1, the modes should belong to the intermediate-coupling case. However, the origin of the splitting must be fully elucidated before classifying the nature of these modes, a point that we shall come to later. In the usual aromatic CH-stretching modes case (e.g., benzene), the line widths are broad ($\sim$100 cm^{-1}) and the spacing of the states is small ($W/\Delta > 1$). Thus, one can excite only a superposition of symmetry-adapted states leading to localization of the excitation. In this sense, the aromatic CH-stretching modes belong to the statistical limit and correspond approximately to local modes with ultrashort lifetimes.

The durene molecule may exist in various rotomeric conformational states of the methyl groups. Previous work on hexamethylbenzene has described the average minimum energy conformation as a "cogwheel" arrangement of methyl groups involving two hydrogens up and one down from the benzene ring plane with the adjacent methyl groups in the opposite orientation.[13] That this is the minimum energy conformation makes sense from steric interaction considerations. The other reasonable conformation would have an arrangement such that one methyl hydrogen would be up from the plane, one would be down, and the other would lie in the plane. The adjacent methyl groups would be in a "bisected" geometry. For durene, both conformers would possess C_{2h} symmetry (see Figure 2). However, for the "bisected" conformer the in-plane CH bond would be eclipsed with the ring resulting in in-

creased steric repulsion. We will extend the conclusion drawn on hexamethylbenzene to durene and assume that the durene molecule is locked in a "cogwheel" conformation. This assumption is further supported since we slowly cooled the crystals to low temperature and the barrier to rotation of the methyl group is relatively high in energy, thus the molecules should be "locked" in the lowest energy conformation.

The spacing of the three main methyl CH-stretching peaks involves splittings of 200 and 86 cm^{-1}. These splittings contain several contributions. If one uses a local-mode model to discuss the states, the observed spectrum would be the result of the diagonal perturbation of the threefold degenerate methyl group by the benzene ring and by the ortho methyl–methyl interactions, thus, in first order, one expects to observe three bands. Alternatively, if one uses a delocalized symmetry adapted basis set for individual methyl groups (C_{3v} effective point group) to discuss the states, the observed spectrum would be described as the electric dipole-allowed absorption by the a_1 and e modes. In this basis, one introduces the previously mentioned perturbations which influence further the a_1 and e mode spacing and also split the e modes; again, in first order, the result expected is three bands. Other symmetry-adapted models for the stretching modes would be based either on the symmetry corresponding to interacting adjacent methyl groups (C_2) or on the full symmetry of the molecule (C_{2h}). In either case, there are six electric dipole-allowed modes. It it obvious that the number of bands alone cannot be used to distinguish between the possible models since some of these six modes might be relatively weak.

Similar to the molecular field splittings we discussed before, crystal field splittings might also contribute. However, in view of other data, the large observed (200 and 86 cm^{-1}) splittings are not completely dominated by the crystal and molecular field splittings. Gas-phase studies of CH_3NC $\Delta v = 5$ overtones[10] reveal a splitting of 100 cm^{-1} and in the gas-phase overtone spectrum of toluene[11] a similar splitting of $\sim$150 cm^{-1} is observed. In the absence of Fermi resonances,[14] the splitting observed for CH_3NC (C_{3v} molecule) is not interpretable without a symmetry-adapted basis for the CH modes and, in our opinion, this implies delocalization. These results suggest that the molecular field splitting due to the benzene ring is $\sim$50 cm^{-1}. For durene the observed total splitting of 286 cm^{-1} therefore contains an $\sim$140-cm^{-1} contribution from other sources such as the crystal field and methyl–methyl interactions.

In principle, the polarization properties of the bands provide support for the determination of the best model. In a local-mode model (LM) the transition moment is along the appropriate CH bond, whereas this is not necessarily true in the symmetry-adapted models. Our polarized absorption spectra of d_2 are shown in Figure 3. The spectra were taken at normal incidence to the bc^* plane of the crystal, with polarized light along b or c^*. There is essentially complete extinction of the various bands in the "orthogonal polarization". We note that, in the polarized spectra of durene-h_2, the aromatic band was polarized along the same direction determined to be c^* for d_2, consistent with the known crystal structure.[8,15]

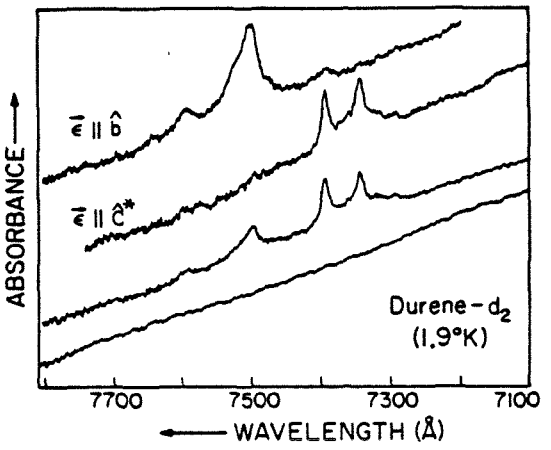

Figure 3. Polarized overtone spectra of durene-d_2. The lowest trace is a baseline scan. The trace above is the unpolarized spectrum at normal incidence to bc^* and the upper traces are the polarized spectra as indicated. The absorbance is in arbitrary units.

TABLE I: Experimental and Calculated Polarization Extinction Ratios

		calculations		
λ,[a] A	exptl[b]	LM	IM[c]	DM[d]
7497 (methyl)	0.95	0.87 (1)	0.46 (a_1)	0.98 (a or b)
7392	0.9	0.83 (2)		0.98 (b)
7342	1.0	0.05 (3)		0.98 (b)
7209 (arom)	1.0	0.98		0.98

[a] Values are ±3 A. Methyl wavelengths are the same for durene-d_2 and -h_2. [b] Values are ±10%. Methyl values are the average of results for durene-d_2 and -h_2. [c] Only result for the C_{3v} z-polarized transition is given. [d] Results are the same for C_2 and C_{2h} models. In C_{2h} the representations are ungerade.

We have calculated the extinction, $(1 - A_\perp/A_\parallel)$, for various models of the vibrational transition moments, where the parallel direction referred to is the direction of the maximum absorbance for a particular band. The calculations were based on the known crystal structure of durene (direction cosines were taken from ref 8), the direction of polarization of the light, standard geometrical coordinates for the durene molecule in the "cogwheel" conformation, and the model for the transition dipole moments. We have assumed the validity of the oriented gas model and we use the same direction cosine matrix for the two molecules in the unit cell. The orientation of the durene molecules in the crystal is such that the short molecular axis (y) is almost along c^* ($\angle yc^* \sim 7°$) and the molecular planes make approximately a 45° angle with the bc^* plane. For the local-mode model (LM), the transition-dipole moments were taken as along the individual CH bonds. Also, the calculated extinction was averaged over all equivalent bonds. The results of the calculations are presented in Table I. For the independent methyl symmetry-adapted model (IM), the transition moments were taken such that the C_{3v} z component was along the "threefold" axis of the methyl group and the x and y components were in a plane normal to the axis. The models based on the delocal mode models (DM) of C_{2h} or C_2 symmetry were indistinguishable on the basis of the polarization, since in both cases z is along the long mo-

lecular axis and y and x could be taken equivalently as along the short axis and normal to the plane or vice versa, respectively.

The results of the calculation are presented in Table I. The local-mode model calculation predicts near complete extinction (0.87 and 0.83) for two bands but predicts no extinction (0.05) for the other band. The independent methyl mode model is ruled out since the predicted extinction for the z component is 0.46. The results for the C_{2h} or C_2 models predict complete extinction ($\sim$0.98) for all bands, thus in agreement with experiment. The agreement suggests some degree of delocalization within the aliphatic CH subset to form symmetry-adapted states.

Burberry and Albrecht[17] have calculated the splittings of the symmetry-adapted a_1 and e modes of the individual methyl groups of tetramethylsilane up to $v = 6$, by using *quadratic* potential and kinetic energy coupling terms in the LM basis. They find that, at high v, the splitting becomes negligible, which implies localization. It should be noted that the agreement of the calculation with the observed liquid phase spectra is reasonable, however, there are features in the $\Delta v = 5$ spectrum which suggest a splitting on the order of 50 cm^{-1}. In view of the fact that the liquid-phase spectra were taken at room temperature, it is possible that line broadening[18] is masking these splittings. With these considerations in mind, we believe that further theoretical and experimental work is needed to sort out the exact nature of the coupling of local modes, and the actual extent of delocalization. Currently, we are examining the nature of methyl–methyl interactions with studies of the overtone spectra of other compounds such as *p*-xylene.

Conclusions

Our observations suggest that relatively slow intramolecular CH-stretching relaxation ($\tau = 0.5$ ps in contrast with the 0.075 ps of the aromatic mode) in sizeable molecules such as durene (24 atoms) is possible at high energies ($\Delta v = 5$). Also, the polarized absorption spectra lead to interpretation in terms of symmetry-adapted states for the aliphatic CH-stretching modes. We have discussed how the interplay between spectral splittings and line widths may determine the nature of the vibrational state excited. However, the actual extent of delocalization is a matter still under investigation.

Acknowledgment. We thank Dr. S. Samson for his great help in guiding one of us (J.W.P.) with the X-ray crystallography. We also thank Professor M. El-Sayed (Sherman Fairchild Distinguished Scholar at Caltech), Professor W. Gelbart, and the two referees for their interest in and discussion of this problem. Finally, the contribution of Professor A. Albrecht to this work was important and is gratefully acknowledged. This material is based upon work supported in part by the National Science Foundation under Grant No. CHE79-05683.

† Alfred P. Sloan Fellow and Camille and Henry Dreyfus Foundation Teacher–Scholar

‡ Contribution No. 6331.

(1) J. W. Perry and A. H. Zewail, *J. Chem. Phys.*, **70**, 582 (1979); *Chem. Phys. Lett.*, **65**, 31 (1979).

(2) B. R. Henry, *Acc. Chem. Res.*, **10**, 207 (1977).

(3) H. L. Fang and R. L. Swofford, *J. Chem. Phys.*, **73**, 2607 (1980).

(4) D. D. Smith and A. H. Zewail, *J. Chem. Phys.*, **71**, 540 (1979).

(5) R. Swofford, M. E. Long, and A. C. Albrecht, *J. Chem. Phys.*, **65**, 179 (1976).

(6) R. Bray and M. Berry, *J. Chem. Phys.*, **71**, 4909 (1979).

(7) C. K. N. Patel, A. C. Tam, and R. J. Karl, *J. Chem. Phys.*, **71**, 1470 (1979).

(8) J. M. Robertson, *Proc. R. Soc. London*, **141**, 594 (1933); A. N. Winchell, "The Optical Properties of Organic Compounds", Academic Press, New York, 1954, p 76; J. Michaluk, Ph.D. Thesis, University of Pennsylvania, 1972.

(9) The apparent broadening of the band at 7500 Å is the only remaining feature in the spectrum of d_2 which is somewhat different from h_2. This should not affect the main points of our discussion. More on this point will be published later.

(10) K. V. Reddy and M. Berry, *Chem. Phys. Lett.*, **52**, 111 (1977).

(11) D. Heller and M. Berry, private communication of unpublished results.

(12) M. Sage and J. Jortner, *Chem. Phys. Lett.*, **62**, 451 (1979); D. F. Heller, *ibid.*, **61**, 583 (1979); E. J. Heller, *J. Chem. Phys.*, **72**, 1337 (1980); E. Heller, E. Stechel, and M. Davis, *ibid.*, **71**, 475 (1979).

(13) B. Henry and W. Greenlay, *J. Chem. Phys.*, **72**, 5516 (1980); W. C. Hamilton, J. W. Edmonds, and A. Tippe, *Discuss. Faraday Soc.*, **48**, 192 (1969).

(14) By using frequencies given by Herzberg, we find one binary combination level, with one quantum of C–H stretch and five quanta of C–N stretch, which is in quasi-resonance with the CH $\Delta v = 5$ overtone. This suggests that the coupling of modes (e.g., the CH stretch–CN stretch) by Fermi resonance is possible but unlikely.
Finally, spectroscopic data are strongly in favor of a linear C–N–C array in the structure of CH_3NC (ref 16).

(15) The direction of c^* for the d_2 crystal was determined by X-ray crystallographic techniques as mentioned previously. Spectroscopically it was found that the doublet of the d_2 spectrum was polarized along c^*. Subsequent studies of h_2 crystals showed the aromatic band to be well polarized along the same direction as the doublet.

(16) G. Herzberg, "Infrared and Raman Spectra", Van Nostrand, Princeton, 1945.

(17) M. S. Burberry and A. C. Albrecht, *J. Chem. Phys.*, **71**, 4631 (1979).

(18) G. M. Korenowski and A. C. Albrecht, *Chem. Phys.*, **38**, 239 (1979).

CHAPTER IV

Local Modes: Their Relaxation, Polarization, and Stereoselective Excitation by Lasers

Joseph W. Perry and Ahmed H. Zewail*

Arthur Amos Noyes Laboratory of Chemical Physics,[†] California Institute of Technology, Pasadena, California 91125
(Received: June 28, 1982; In Final Form: September 9, 1982)

In this paper, we present new results concerning the nature and relaxation of methyl and aromatic CH stretching overtones of low-temperature crystalline durene (1,2,4,5-tetramethylbenzene). The experimental polarization ratios of the bands ($\Delta v_{CH} = 5$) are used to compare three limiting models (local modes, independent methyl modes, and fully delocalized modes) in light of new information on the conformation of durene obtained by low-temperature X-ray diffraction. Armed with these results, we provide a picture for the origin of the splittings observed for the $\Delta v_{CH} = 5$ spectra at 1.7 K and discuss the nature of the vibrational energy distribution of the single-photon excited states of the methyl and aromatic subsets; the aromatics are equivalent local modes by symmetry (line width > observed splitting) whereas the methyls are inequivalent local modes which are split (line width < splitting) by the molecular and crystal fields. The dynamics of the high-energy states ($\Delta v_{CH} = 5$) are inferred from the line widths. The methyl bands, which are much narrower than the aromatic band at low temperature, are broadened as the temperature is increased by a process which results in partial coalescence at room temperature. Consequently, specific inequivalent bond modes on nonrigid groups (e.g., methyl) can be selectively excited by optical pumping at low temperatures. In addition, crystal field splittings of the CH modes, particularly at low temperature, can be large enough to allow selective excitation of bond modes which would be equivalent in the isolated molecule. Thus we propose the use of low-temperature matrices or crystals as a molecular environment for (polarized) photoselection experiments on high-energy overtones.

I. Introduction

The understanding of the spectra and dynamics of high-energy vibrational states of molecules is of great importance to possible selective laser chemistry.[1] Systems where energy can be "localized" in a specific mode (or a small number of vibrational modes) for times on the order of reaction or collision times are being sought for such experiments. Consequently, molecules exhibiting local mode characteristics (e.g., CH oscillators) are especially enticing as candidates for bond-selective laser chemistry.

Evidence for bond localization of vibrational excitation (local modes) has involved the modeling of spectroscopic energies and intensities[2] and chemical and isotopic substitution in high-symmetry molecules.[3] In our work on the CH overtones of molecules at very low temperature ($\sim$2 K), we were motivated to test the local mode model by using polarization spectroscopy,[4] and to examine the homogeneous broadening of these transitions in the absence of thermal congestion.[5] Specifically, the following was shown for durene (1,2,4,5-tetramethylbenzene): (a) resolution of the aromatic and aliphatic CH stretching bands of the $\Delta v = 5$ transitions, (b) large splittings ($\simeq$200

cm^{-1}) of the aliphatic bands, (c) narrow spectral bands for the aliphatic band (bandwidth as low as 25 cm^{-1}) in contrast with the aromatic band (width ~ 100 cm^{-1}), and finally (d) polarization extinction along b and c^* axes for the different aliphatic bands in the [100] plane of the crystal.

The equilibrium conformation of durene, unknown at that time, was taken in analogy to the low-temperature hexamethylbenzene conformation.[6] Using the polarization ratios, splittings, and bandwidths, we discussed several models for the vibrational energy distribution in the aliphatic subset, but the modeling depended crucially on the choice of the conformation. To establish the best description of the states (local or extended) and their relaxation, we initiated new experiments on this system.

In this paper, we report on (a) the low-temperature (16 K) conformation of the durene molecule in the crystal determined by X-ray diffraction methods, (b) experimental and calculated (with the new conformation) polarization ratios for the Δv = 3–5 overtones in the [100] and [001] planes, (c) the Birge–Sponer plots for the aromatic and aliphatic bands, and (d) the relaxation of and effect of temperature on the durene overtones. Determination of the conformation has allowed us to rule out the model of independent delocalized methyl modes. Our results are consistent with bond localization of vibrational energy in the aliphatic and aromatic subsets. Because of this localization, molecular site selective or stereoselective (polarized) excitation of CH stretching overtones by lasers is possible, particularly in matrices or solids at low temperature. Finally, we compared our low-temperature results with those of some gas-phase molecules to assess the role of intramolecular interactions.

II. Experimental Section

The materials and experimental methods for overtone spectroscopy of durene in the Δv = 5 region have been described in a previous paper.[4] The spectra for Δv = 2–4 were obtained with a Cary-17 spectrophotometer. Details of the X-ray diffraction study at low temperature (16 K) will be given elsewhere.[7]

III. Molecular Structure and Vibrational Energy Distribution

A. Low Temperature Conformation. The durene crystal at 16 K is monoclinic ($P_{2_1/a}$) with two molecules in the unit cell. The unit cell parameters at this temperature were found to be a = 11.51 Å, b = 5.60 Å, and c = 6.87 Å, with β = 113.2°. The important aspect of the molecular structure (see Figures 1 and 2) for this work is the conformation which is in agreement with the room temperature structure of durene[8,9] and hexamethylbenzene[6] but is in contrast with the low-temperature structure of hexamethylbenzene,[6] which undergoes a conformational transition at low temperature (~120 K).

The conformational state of the methyl groups here was somewhat surprising to us in that in this form there exist some fairly close eclipsed contacts (~2.4 Å) for the out-of-plane hydrogens on adjacent methyl groups. The site symmetry of the molecule in the crystal is C_i. Therefore, there are six sets of inequivalent methyl hydrogens; two sets of the hydrogens are in-plane and four sets are out-

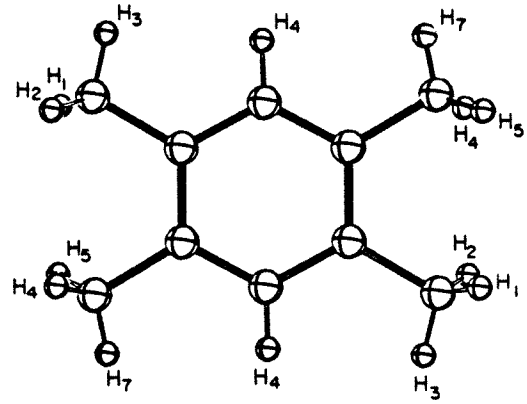

Figure 1. Low-temperature (16 K) molecular structure of durene determined by X-ray diffraction. The structure has been plotted by use of isotropic thermal factors.

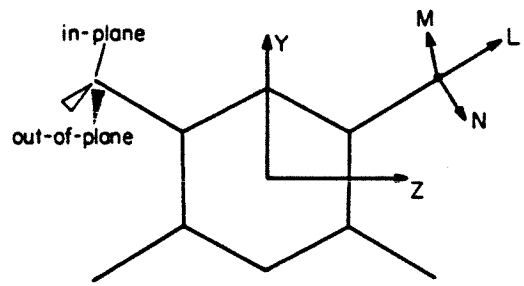

Figure 2. Coordinate systems used for vibrational models and local CH type modes.

of-plane. The molecules are arranged in the crystal such that the aromatic CH bond vector makes ~7° angle with the c* axis of the crystal, and the molecular plane makes ~45° angles with the [100] crystal plane.

The torsional potentials of the methyl groups in durene have been much studied, for example, by inelastic neutron scattering,[10,11] modeling of neutron diffraction data,[9] NMR spectroscopy,[12] and atom–atom potential calculations.[13] The barrier to methyl rotation has been found to be ~2 kcal/mol (~700 cm^{-1}) for durene. Even at room temperature only a small fraction of the molecules have sufficient energy to cross the rotational barrier. In equilibrium at very low temperature the molecules would exist predominantly in the lowest ground torsional quantum level. Since the adjacent wells of the torsional potential are not equivalent, degeneracy is removed and therefore tunneling between the wells is relatively less probable. One may then view the methyl groups at low temperature as being "trapped" in a particular potential well and carrying out thermal torsional oscillations in that well. We have used the determined low-temperature equilibrium position of the methyl groups in our calculation of the polarization of the methyl modes.

B. Models for the High-Energy Vibrational States. We have previously discussed in detail the interpretation of the durene CH overtones in terms of various models.[4] Here, a brief description of the models is given. In Figure 3, a correlation table is given for the modes of various models under the influence of molecular and crystal fields.

In the local mode model the high-energy bands are described as due to the various inequivalent bond mode

TABLE I: Carbon-Hydrogen Bond Vector Coordinates[a] and Local Mode Intensities[b]

type of hydrogen	*a*, Å	*b*, Å	*c**, Å	I_a	I_b	I_{c^*}
H_1[c] op[d]	1.046	−0.099	−0.062	1.10	0.01	0.00
H_2 op′	−0.229	0.856	−0.140	0.05	0.73	0.02
H_3 ip[d]	−0.156	−0.269	0.924	0.02	0.07	0.85
H_4 arom	−0.072	−0.034	0.926	0.00	0.00	0.86
H_5 op″	−0.924	0.115	−0.316	0.85	0.01	0.10
H_6 op‴	0.290	−0.925	−0.238	0.08	0.85	0.06
H_7 ip′	0.052	0.057	0.901	0.00	0.00	0.81

[a] Coordinates given in the orthogonalized crystallographic system. [b] Intensities are taken as proportional to the squares of the bond vector projection onto the indicated crystal axis (as discussed in section IIIC). [c] Hydrogens numbered as in Figure 1 (after ref 9). [d] op refers to out-of-plane and ip refers to in-plane. Primes distinguish various sets.

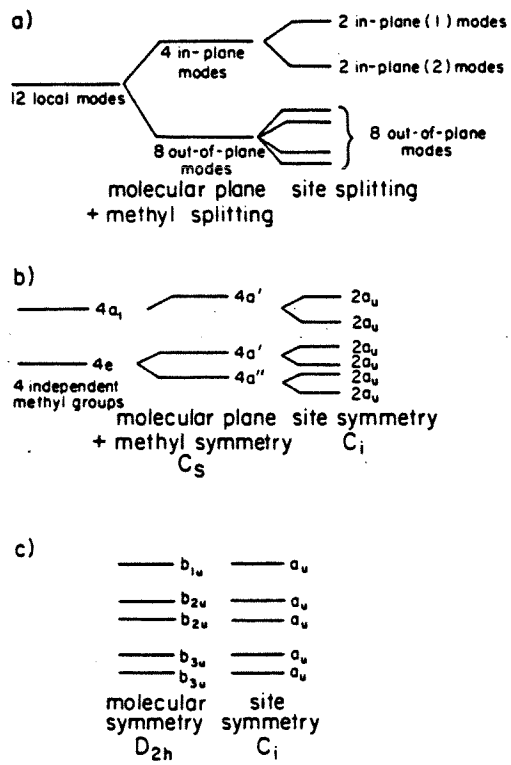

Figure 3. Correlation diagram showing the splitting of vibrational modes of various models under the influence of the molecular field and the crystal field. The relative positions of the levels are arbitrary, only the qualitative splitting is significant.

overtones (and combinations). As mentioned above, there are six sets of inequivalent methyl CH bonds: two in-plane sets and four out-of-plane sets (Figures 1 and 2). (The coordinates of the CH bond vectors in the crystal are given in Table I.) The directions of the vibrational transition moments are along the CH bonds in this model.

In the model of independent methyl modes, one must treat the bands as due to four independent methyl groups (C_{3v} effective symmetry for each group). The eigenstates which we deal with in this case are the symmetry-adapted states (a_1 and e) of the pure local mode overtones (i.e., $|v_1 00\rangle$, $|0 v_2 0\rangle$, and $|00 v_3\rangle$ for a given methyl). These states

TABLE II: Independent Methyl Mode Transition Moment Direction Cosines[a] and Intensities

	methyl group 1			methyl group 2		
	L_1	M_1	N_1	L_2	M_2	N_2
a	0.485	0.803	0.37	0.613	0.688	−0.89
b	0.617	−0.596	0.50	0.640	−0.726	0.32
c^*	0.622	0	−0.78	−0.459	0	0.33

	I_a	I_b	$I_c{}^*$
L_1	0.235	0.381	0.387
M_1	0.645	0.355	0
N_1	0.137	0.250	0.608
L_2	0.376	0.384	0.211
M_2	0.473	0.527	0
N_2	0.79	0.102	0.109

[a] Direction cosines and numbering after ref 33, see Figure Figure 2.

TABLE III: Direction Cosines for Delocalized Mode Moments (Molecular Symmetry Axes[a]) and Intensities

	X	Y	Z
a	0.746	−0.118	0.655
b	−0.661	−0.021	0.750
c^*	0.067	0.993	0.097

	I_a	I_b	I_c
X	0.557	0.437	0.004
Y	0.014	0.000	0.986
Z	0.429	0.562	0.009

[a] Axes defined in Figure 2. [b] Note that while only one compound (Y) has significant intensity along c^*, there are two independent Y-polarized modes given by symmetry. Therefore the observation of two c^*-polarized bands at $\Delta v = 5$ (Figure 4) does not rule out the fully delocalized mode model for the methyl CH stretching states.

are then subject to the molecular field symmetry and the C_i site symmetry. The e modes of each methyl are therefore split into symmetric and antisymmetric components with respect to the molecular plane. The site field splits the methyl degeneracy into two sets of two equivalent methyls. There could be up to six bands in this model. For a given methyl, the polarizations are directed along the C–C axis, out of the molecular plane and in the plane (Figure 2). The direction cosines of this axis system and the crystal axes are given in Table II.

As for the delocal mode model we can treat the system as having vibrational amplitude delocalized in all CH bonds (full molecular symmetry, D_{2h}) or on adjacent methyls (C_{2v} symmetry). In the D_{2h} case, there are two $b_{2u}(Y)$, two $b_{3u}(X)$, and one $b_{1u}(Z)$ mode(s) whereas for the C_{2v} case there are two $a_1(Z)$, one $b_1(X)$, and two $b_2(Y)$ mode(s) that are electric dipole allowed. All these modes correlate with a_u modes in the C_i site symmetry. The transition moments are directed in the molecular axis system along the short (Y), long (Z), and out-of-plane (X) axes. The direction cosines of this coordinate system with respect to the crystal axes are summarized in Table III.

C. The Polarization Ratios. The polarization ratios of the various transitions are found for the different models by calculating the projections of the transition dipoles (as discussed above) on the crystallographic axes of the or-

iented crystal. The absorption by the ith band in the αth direction of polarization is

$$I_{i\alpha} \propto \sum_{k=1}^{l} |\vec{\mu}_k \cdot \vec{\epsilon}_\alpha|^2 = \sum_{k=1}^{l} \cos^2 \theta_{k\alpha}$$

where $I_{i\alpha}$ is the intensity, the sum is over all l moments contributing to the band, $\vec{\mu}_k$ is the transition moment vector, $\vec{\epsilon}_\alpha$ is the radiation electric field polarization vector, and $\theta_{k\alpha}$ is the angle between $\vec{\mu}_k$ and $\vec{\epsilon}_\alpha$. Because of the crystal birefringence, the radiation polarization was always directed along a crystallographic principal axis. With the direction cosines and coordinates in Tables I–III, the calculation of the relative absorption in the a, b, and c^* directions of the crystal was performed for the various models. The validity of the oriented gas model has been assumed and the refractive indices of the crystal have been taken as equal since $n_a = 1.584$ and $n_b = 1.619$.[14] The calculated relative intensities are given in the corresponding table of direction cosines.

The local mode polarizations are quite remarkable for the experimentally determined conformation used in this calculation. The various sets, inequivalent by the site symmetry, are all polarized very well in the a, b, c^* system. This is in contrast with the calculated methyl CH local mode polarizations for other durene conformers.[4]

The independent methyl modes model polarization calculation shows that the symmetric (L) component is not polarized along any crystallographic axis. Also, the in-plane (N) component is not well polarized in the crystallographic system. The out-of-plane (M) component is polarized along b in [100] but not well polarized in [001].

The delocal mode model, which has transition dipoles aligned in the molecular symmetry axis system, shows that the X transition (out-of-plane axis) is b polarized in [100], the Y transition (short axis) is c^* polarized in [100] or [010], and the Z transition is b polarized in [100]. Note that the Y transition is extinguished in [001].

D. Polarization Extinction and Vibrational Energy Distribution in the Aliphatic Subset. In Figure 4 are presented the polarized absorption spectra and the calculated polarized spectra for the $\Delta v = 5$ CH-stretching region of the [100] plane of durene-d_2. In our previous study[4] we assigned the bands due to methyl and aromatic CH-stretching modes, by comparison of spectra of durene-d_2 and durene-h_{14} (see Figure 5b). The d_2 spectra show three main methyl CH bands. The higher energy bands (doublet) are c^* polarized and the lower energy band is b polarized in the [100] plane (see Table IV). Since all the bands are well polarized in this plane it is possible to rule out the independent methyl modes model as only one type of mode is well polarized in this model. Both the local mode and delocal mode models predict complete polarization for all the bands along the crystal axes. Thus we are not able to rule out either of these models on the basis of the polarizations. However, note that (1) there are only three main methyl bands in the $\Delta v_{CH} = 5$ region, (2) six bands are expected for full molecular symmetry-adapted modes even in the absence of the crystal field, and (3) two bands are expected for the methyl local modes in the absence of the crystal field. We therefore favor interpretation in terms of local modes since the crystal field splitting of the local modes explains the presence of more bands in the

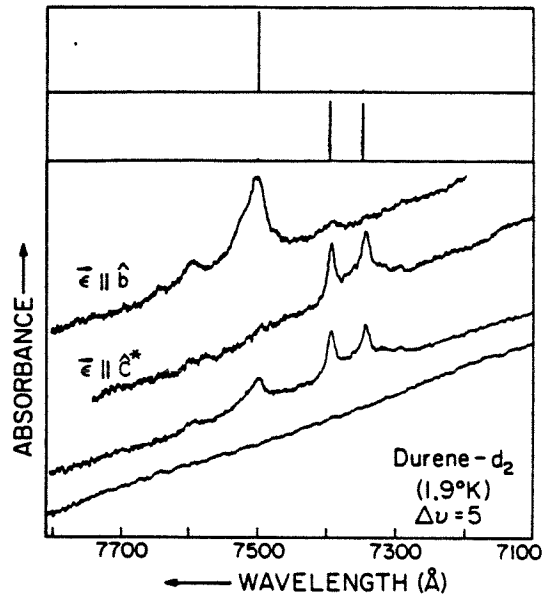

Figure 4. Polarized overtone spectra ($\Delta\nu_{CH} = 5$) of [100] plane of durene-d_2 at low temperature (1.9 K). The lower traces are the baseline and unpolarized spectrum and the upper traces are the polarized spectra as indicated. The absorbance is in arbitrary units. The "stick" spectra above are the calculated polarized spectra for the local mode model. The crystal pathlength was ~4 cm.

TABLE IV: Experimental and Calculated Polarization Extinction Ratios of the $\Delta\upsilon = 5$ Bands in the [100] Plane

	λ, A	E_{expt}[a]	E_{LM}[b]	E_{IM}[c]	E_{DM}[d]
Me	7497	0.95 (*b*)	0.97 (op)	−0.42 (*L*)	0.98 (*X*, *Z*)
	7392	0.9 (*c**)	0.96 (ip)	1.0 (*M*)	1.0 (*Y*)
	7342	1.0 (*c**)	0.99 (ip′)	0.33 (*N*)	1.0 (*Y*)
arom	7209	1.0 (*c**)	1.0		

[a] Experimental ($T = 1.9$ K) extinction defined as $E = 1 - A_\perp/A_\parallel$. Direction of $A_\parallel$ indicated in parentheses. [b] Local mode model extinction. The out-of-plane value is the average over the various sets of out-of-plane hydrogens. [c] Independent methyl mode model extinction. Values are the average of the type 1 and 2 methyls (Figure 2 and Table II). In this model the symmetrical component (*L*) is expected to be the longest wavelength band. [d] Delocalized mode model extinction. Since two bands are polarized along *c**(*Y*) experimentally then *X* and *Y* modes must be assumed to be accidentally degenerate to obtain a consistent assignment.

spectrum but an explanation of the absence of several bands in the delocal (symmetry adapted) model is not obvious.

In terms of the local mode model, our polarization and X-ray data allow a simple assignment of the bands in terms of conformation. The doublet being *c** polarized in [100] must correlate with the in-plane methyl CH modes as these are the only ones that polarize as such in [100]. The other band must correlate with the out-of-plane CH modes of which there are four sets. Two of the sets are extinguished in [100] so that the statistical weight of these modes is equal to that of the doublet, consistent with the roughly equal total intensity of the doublet to the other band.

The doublet splitting (86 cm^{-1}) can be attributed to crystal field splitting since the in-plane hydrogens are not split by the molecular field. The crystal field splitting of the out-of-plane modes must be relatively smaller as two sets remain unresolved (< 50 cm^{-1}) even at very low temperatures. There are signs of structure on the *b*-polarized band (Figure 4) consistent with the small splitting hypothesis. The splitting of the *b*-polarized band from the center of the doublet (~240 cm^{-1}) contains contributions from the molecular plane field and the crystal field. If we assume the crystal field splitting of the in-plane and out-of-plane modes is the same as the doublet splitting, then the molecular field splitting is estimated to be ~150 cm^{-1}, somewhat larger than estimated previously,[4] but in very good agreement with the observed splitting of the gas-phase toluene methyl CH (Δv = 5) bands (~150 cm^{-1}).[15]

E. Comparison with the Overtone Splittings of Liquid and Gas Phase Molecules. There has been much interest recently in the use of overtone spectroscopy to probe molecular conformation. Resolution of bands due to conformationally inequivalent CH bonds has also been accomplished in studies of toluene,[15] hexamethylbenzene,[16] *o*-xylene,[17] *o*- and α-methylstyrene,[17] α-methylnaphthalene,[17] alkanes,[18,19] alkenes,[18-20] cycloalkanes,[21,22] cycloalkenes,[21,22] acetone,[20,23] and acetaldehyde.[23] Of particular relevance to our work on durene is the study of the xylene isomers in liquids.[17] The double peak structure of the Δv = 4 and 5 methyl bands of *o*-xylene was associated with the in-plane (higher energy peak) and out-of-plane hydrogens of the methyls in an eclipsed conformation. Our interpretation of the durene methyl bands is in agreement with the conclusions on *o*-xylene which were inferred from relative intensities and bond length data. Unlike in liquids, the polarization and X-ray data of this work provide an unequivocal confirmation of the molecular conformation and assignment of the overtone bands.

The splittings of high-symmetry methyl CH stretching overtone bands may contain other contributions such as Fermi resonance. Splitting of high energy overtones in the halomethanes,[24,25] in haloethanes,[18] and in CHD_3, CH_2D_2, CH_3D, CH_4, tetramethylsilane, and neopentane[26] have been observed recently. Many of these splittings were interpreted in terms of Fermi resonance between the "pure" overtone and combination bands involving one less CH stretch quantum and two CH bending quanta (shown schematically in Figure 5c). Similarly, splittings for CH_3NC and CH_3CN[27] can be interpreted in terms of Fermi resonance of the same type. The CH stretch quantum region which may become affected by this type of coupling depends on the CH stretch anharmonicity, frequency, and on the bending mode overtone (or combination) frequency.[26] Qualitatively, Fermi resonance may become significant for the vth CH quantum level when the bending overtone (or combination) energy equals approximately the energy defect between $|v_{CH}\rangle$ and $|v_{CH} - 1\rangle$ (Figure 5c). The existence of these Fermi resonances are most easily identified by a study of a progression of CH stretching overtones in conjunction with a Birge–Sponer plot of the transition energies. The resonances manifest themselves, as usual, as shifts of the bands from the Birge–Sponer line

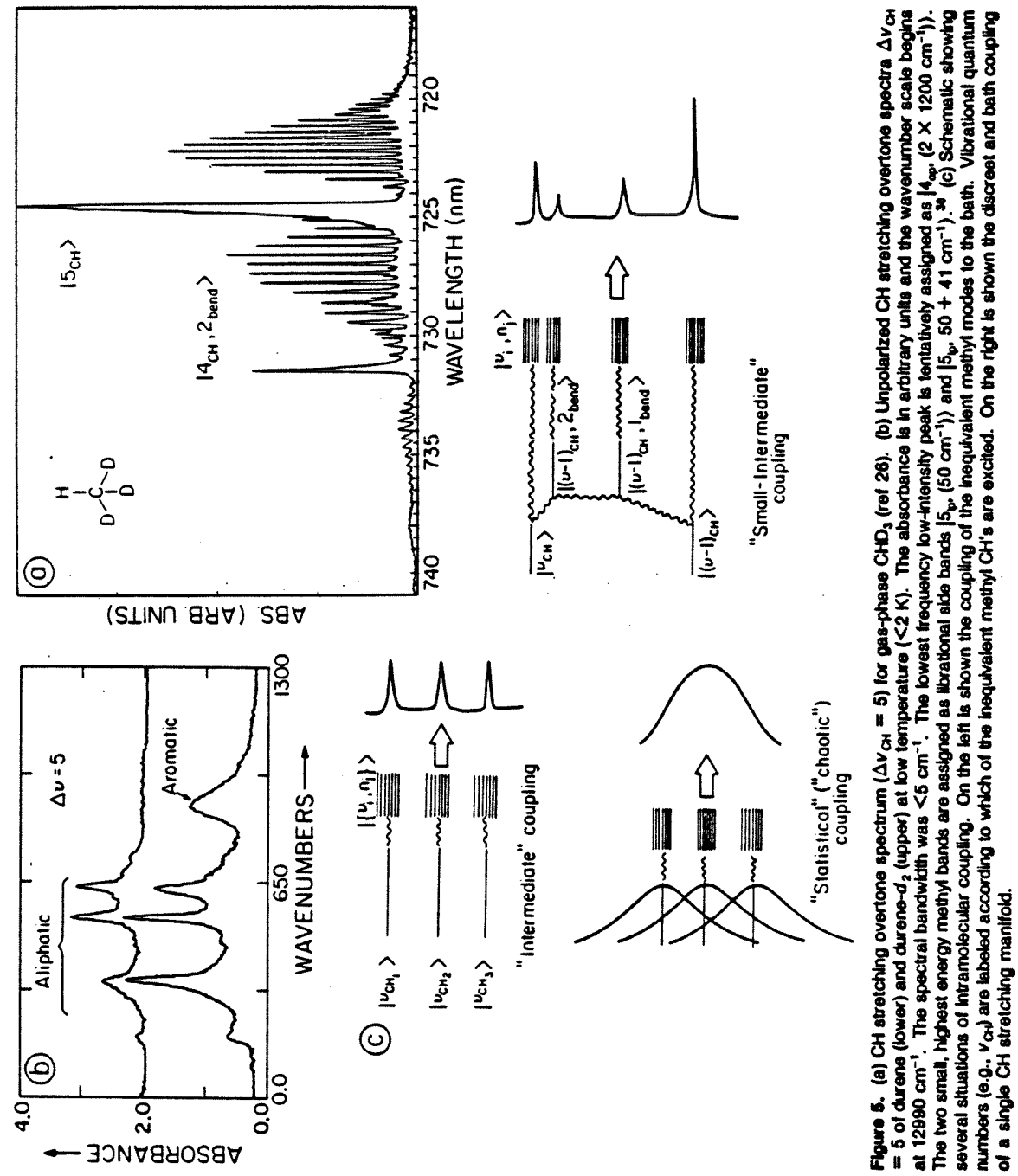

Figure 5. (a) CH stretching overtone spectrum ($\Delta v_{CH} = 5$) for gas-phase CHD_3 (ref 26). (b) Unpolarized CH stretching overtone spectra $\Delta v_{CH} = 5$ of durene (lower) and durene-d_2 (upper) at low temperature (<2 K). The absorbance is in arbitrary units and the wavenumber scale begins at 12990 cm^{-1}. The spectral bandwidth was <5 cm^{-1}. The lowest frequency low-intensity peak is tentatively assigned as $|4_{op}$, (2 × 1200 cm^{-1})). The two small, highest energy methyl bands are assigned as librational side bands $|5_{lp}$, (50 cm^{-1})) and $|5_{lp}$, 50 + 41 cm^{-1}).[38] (c) Schematic showing several situations of intramolecular coupling. On the left is shown the coupling of the inequivalent methyl modes to the bath. Vibrational quantum numbers (e.g., ν_{CH}) are labeled according to which of the inequivalent methyl CH's are excited. On the right is shown the discreet and bath coupling of a single CH stretching manifold.

and qualitatively different spectral profiles (relative intensities) for the affected levels. As discussed later, the high-energy overtones of durene do not show Fermi resonance type deviations from the Birge–Sponer line, consistent with our assignment presented above. We should emphasize that in the establishment of the nature of the vibrational energy distribution from observed splittings one must separate the contributions of local-normal coupling (Fermi resonances) and splitting due to bond inequivalence.

An interesting question now arises: *What is the effect of the density of states on the spectra in the high-energy overtone region*? We have calculated the total vibrational density of states for several molecules using the Whitten–Rabinowitch approximation.[28] The total density of states for CHD_3 at $\sim$13000 cm^{-1} is $\sim$12 states/cm^{-1} whereas for benzene it is $\sim 9 \times 10^6$ states/cm^{-1}. In Figure 5a is shown the $\Delta v = 5$ CH stretching region for CHD_3. The CHD_3 spectrum is comprised of two vibrational bands in this region: $|5_1\rangle$ and $|4_1 2_5\rangle$,[26] where v_1 is the CH stretch and v_5 is the e symmetry CH bending mode. Considering the large increase in the density of states for durene one might expect a very complex spectrum compared to CHD_3. It is clear that the durene methyl region is comprised of more bands than in CHD_3 due to the inequivalent CH stretches. However, it is also clear that the presence of the combination bands in the durene spectrum is not dominant, that is, the effect of the greatly increased total density of states for the methyl groups attached to the benzene ring in durene has not had a strong effect on the number of bands in the spectrum. This is consistent with the selective single-quantum exchange local-normal coupling model discussed above where the pure overtone interacts strongly only with a small subset of discreet combination levels. A calculation of the restricted quantum exchange density of states[29] may provide useful insight into the prediction of the onset complex combination activity in the high overtone spectra. The effect of the density of states on the line widths will be discussed later in this work.

F. Lower-Energy States. The unpolarized absorption spectra of the lower-energy overtones (Δv = 2–4) in the [100] and [001] planes of the durene-d_2 crystal are shown in Figure 6. The durene CH stretch fundamental[30-32] and first overtone[33] spectra have been reported before, and our spectra ($\Delta v = 2$) are in good agreement with ref 33, except for a systematic shift ($\sim$35 cm^{-1}) of their spectra (our spectra are of somewhat higher resolution). A main feature of these spectra is that the c^*-polarized bands are extinguished in the [001] plane. These include the $\Delta v_{CH} = 3$ band at 1184 nm and several of the $\Delta v = 2$ region bands. Note that much of the splitting of the $\Delta v_{CH} = 2$ region bands is absent in the $\Delta v_{CH} = 3$ region (Figure 6). The $\Delta v = 3$ region of the [001] plane spectrum is dominated by two main bands at 1184 and 1197 nm. Polarized absorption studies of these crystal planes show the 1184-nm band is in fact c^* polarized in [100] and that the 1197-nm band is b polarized in [100] (Figure 7). The 1197-nm band is not polarized at all in the ab plane [001] of the crystal, consistent with the fact that two different sets of out-of-plane local modes contribute along a and b giving equal contributions and thus no polarization.

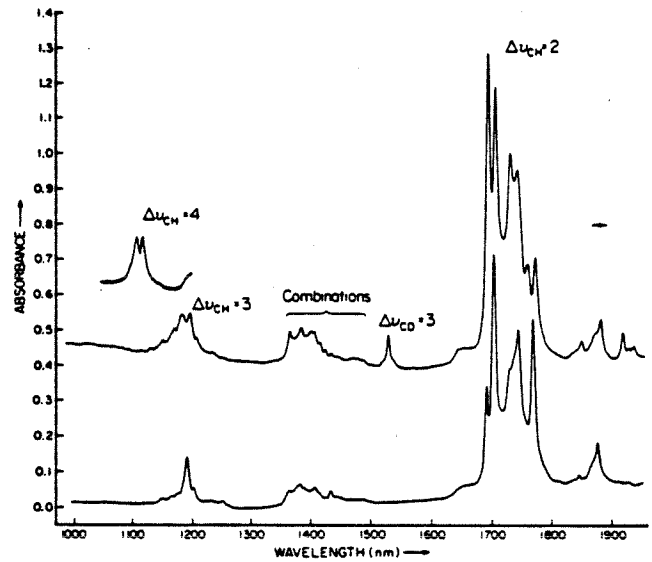

Figure 6. Unpolarized overtone spectrum ($\Delta v_{CH} = 2, 3$) of [100] plane (upper) and [001] plane (lower) of durene-d_2 at room temperature (18 °C). The crystal pathlength was 0.83 mm for upper spectrum and 0.37 mm for lower spectrum. The insert is the $\Delta v = 4$ absorption region (1000–~850 nm) of the [100] plane obtained with a 5.6-mm crystal and the vertical scale is ×2.5. The spectral bandwidth was less than or equal to that marked on the spectrum (~1 nm). The baseline levels are arbitrary.

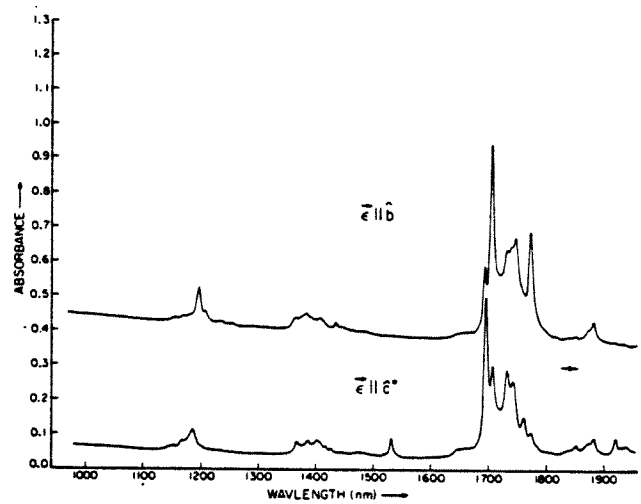

Figure 7. Polarized overtone spectrum ($\Delta v_{CH} = 2, 3$) of [100] plane of durene-d_2 at room temperature (18 °C). The crystal pathlength was 0.83 mm. The baseline levels are arbitrary.

TABLE V: Spectral Positions of Durene Methyl CH Stretching Bands[a]

region ($\Delta\upsilon$)	λ, nm	$\bar{\nu}$, cm^{-1}	assignment
1[c]		2865 (1)[b]	combination
		2885	combination
		2920	Me, $\Delta\upsilon = 1$
		2937	Me, $\Delta\upsilon = 1$
		2969	Me, $\Delta\upsilon = 1$
2[d]	1773	5640 (2)	combination
	1761	5679	$\Delta\upsilon_{CH} = 2$
	1747.5	5722.5	$\Delta\upsilon_{CH} = 2$
	1743	5737	not reported
	1732	5774	$\Delta\upsilon_{CH} = 2$
	1706	5862	$\Delta\upsilon_{CH} = 2$
	1694.5	5901	$\Delta\upsilon_{CH} = 2$
3	1235	8097 (3)	combination
	1207	8285	combination
	1197	8354	$\Delta\upsilon = 3$, op (a,b)
	1183.5	8449.5	$\Delta\upsilon = 3$, ip (c^*)
	1170	8547	combination
	1154	8665.5	combination
4	915.3	10930 (5)	$\Delta\upsilon = 4$, op (ab)
	904.3	11060	$\Delta\upsilon = 4$, ip (c^*)
5	750.5	13324 (10)	$\Delta\upsilon = 5$, op (ab)
	740.2	13510	$\Delta\upsilon = 5$, ip (c^*)

[a] Room temperature data. [b] Nominal standard errors given. [c] Reference 32. [d] Assigned in terms of C_{3v} modes for methyls in ref 33.

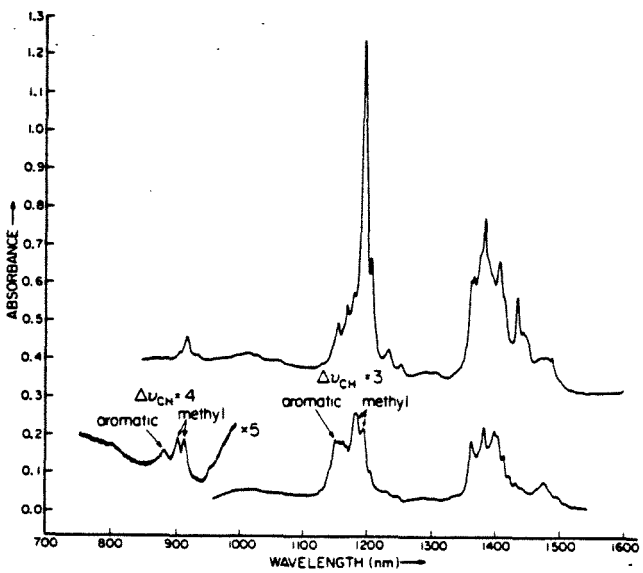

Figure 8. Unpolarized overtone spectra ($\Delta\upsilon_{CH}$ = 2, 3, 4) of the [100] (lower) and [001] (upper) planes of durene at room temperature. Different pathlengths were used for the upper and lower crystals.

In Figure 8 the unpolarized spectra of the $\Delta\upsilon_{CH} = 3$ and 4 regions for the [100] and the [001] plane of durene are shown. The $\Delta\upsilon_{CH} = 4$ spectrum is comprised of an aromatic and two methyl bands, and once again the higher energy methyl band (904.3 nm) is extinguished in [001] along with the aromatic similar to the $\Delta\upsilon_{CH} = 3$ region. Figure 8 shows clearly that, although there is sizeable combination activity in the region of 1400 nm, the combination activity is weak in the near vicinity of the methyl $\Delta\upsilon_{CH} = 3$ band (1197 nm). The spectral positions of the durene methyl CH stretching bands are summarized in Table V.

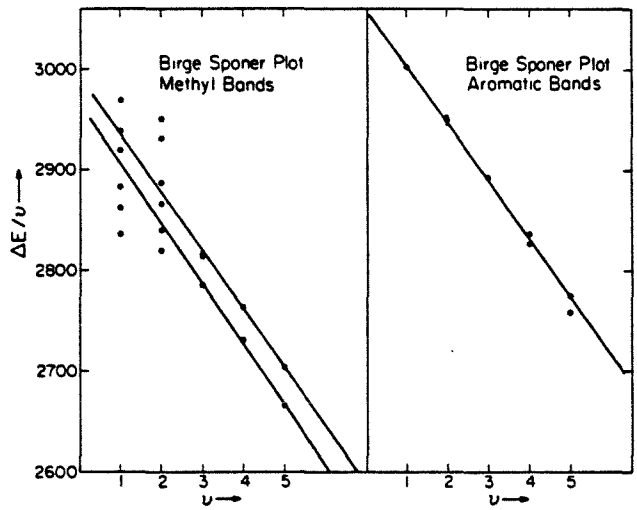

Figure 9. Birge–Sponer plots for the durene aromatic and methyl bands. The lower points for $v = 4$ and 5 in the aromatic plot are room temperature data, the upper points are low-temperature (~2 K) data. The methyl data are at room temperature. In the methyl plot, the lower two points at $v = 1$[32] and the lowest point at $v = 2$[33] have been assigned as combination bands. The highest energy points for $v = 1$ and 2 are c^* polarized and the lower point is b polarized ([100] plane). The high-frequency methyl line corresponds to the c^*-polarized bands ([100] plane) and the lower line to the (a,b)-polarized bands for $v = 3$–5.

TABLE VI: Parameters[a] of Linear Least-Squares Fits to Birge–Sponer Plots

	A, cm^{-1}	B, cm^{-1}	R^b	D_e,[d] kcal/mol
aromatic	3062 (3)	−57 (1)	−0.9996	122
in-plane methyl[c]	2987 (14)	−57 (3)	−0.998	116
out-of-plane methyl[c]	2968 (15)	−60 (4)	−0.998	109

[a] Parameters of equation $\Delta E/\upsilon = A + B\upsilon$. [b] Linear correlation coefficient. [c] Fit of $\Delta\upsilon = 3$–5 only. [d] Morse oscillator dissociation energy.

In Figure 9 the Birge–Sponer plots for the main methyl bands and the aromatic bands are shown. The $\Delta\upsilon = 3$–5 methyl bands fit reasonably well to straight lines, one for the higher energy bands (c^* polarized in bc^*) and one for the lower energy bands (b polarized in bc^*). However, the similarly polarized bands in the $\Delta\upsilon = 1$ and 2 regions are displaced from the line. This may be due to the nature of the modes being different at low energy, that is, delocalized within each methyl, as other work[33] has suggested, or due to Fermi resonance. More work is needed to clarify this problem at lower energies. For now, it suffices to consider that for higher overtone levels ($\Delta\upsilon = 3$–5) there is resolution of the c^*- and b-polarized (in the bc^* plane) transitions and we assign these as the in-plane and out-of-plane methyl local modes, respectively.

As for the Birge–Sponer plot for the aromatic band, the straight line fit is good for all harmonics from $\Delta\upsilon = 1$ to $\Delta\upsilon = 5$. However, the room temperature values for the energies of the $\Delta\upsilon = 4$ and 5 levels are displaced from the line toward the methyl bands. The shift of the band is

temperature and quantum level dependent, a point that we will return to later, so we have used the low-temperature points for the straight line fit. The parameters of the fits to the Birge–Sponer plots are given in Table VI.

The diagonal anharmonicities in Table VI are seen to be roughly independent of the mode type while the frequencies of the aromatic and various methyl bands are different, which implies a characteristic force constant for each type of local mode. Since the lengths of the CH bonds are related to the force constants,[34] we can predict the order of the bond lengths as $r_{arom} < r_{ip} < r_{op}$. It is interesting to note that the average bond lengths for these sets determined from the low-temperature X-ray data are consistent with this trend: $r_{arom} = 0.93$ (0.03) Å, $r_{ip} = 0.94$ Å, and $r_{op} = 0.98$ Å. It is well-known that the X-ray method yields CH bond lengths which are shorter than the actual values. The relative lengths, however, of the in-plane and out-of-plane CH bonds are corroborated by room temperature neutron diffraction results[9] which give $r_{ip} = 1.065$ and $r_{op} = 1.096$. Also given in Table VI are the dissociation energies of the CH bonds calculated by use of the expression for a Morse oscillator

$$D = -(A - B)^2/4B$$

The values obtained here are in good agreement with those determined for *o*-xylene.[17] The out-of-plane CH's, being slightly more anharmonic and having a lower frequency, are found to be the weaker methyl CH bonds.

IV. Bandwidths, Intramolecular Relaxation, and the Effect of Temperature

As discussed previously,[4] the very low-temperature line width of the aromatic CH band ($\sim$100 cm^{-1}) at $\Delta v = 5$ was larger than the widths of the methyl bands (25–50 cm^{-1}). This suggests that, in the absence of pure dephasing[35] at very low temperature, the population relaxation for the methyl bands is slower than the aromatic. With the assignment given above, the in-plane methyl bandwidths are $\sim$25 cm^{-1} whereas the apparent bandwidth of the out-of-plane band is $\sim$50 cm^{-1}. Since the out-of-plane band may have some site splitting contribution, as discussed above, we can say that the homogeneously broadened line width is <50 cm^{-1} for this band.

The difference in the line widths of the aromatic and methyl bands is rationalized in terms of a greater density of strongly coupled states for the aromatic CH which is attached directly to the aromatic ring ("bath"), whereas the effective density of states for the methyl groups is much lower. However, as we indicated in section IIIE, the relative total density of states is on the order of $\sim 10^6$ for the benzene ring bath compared to the CHD_3 bath (taken as indicative of the methyl bath). If the coupling of the methyl CH stretches to the bath was comparable to the aromatic then the low-temperature methyl band shape would be far less structured. Taken to the limit of statistical coupling, the broadening would likely wash out the observed splitting (Figure 5c, schematic), in contrast with observation. Thus the use of the CHD_3 total density seems a reasonable crude estimation. The bandwidth of the aromatic is not scaling relative to the methyl according to this estimation of the relative total density of states. It is clear that the total density of vibrational states is not

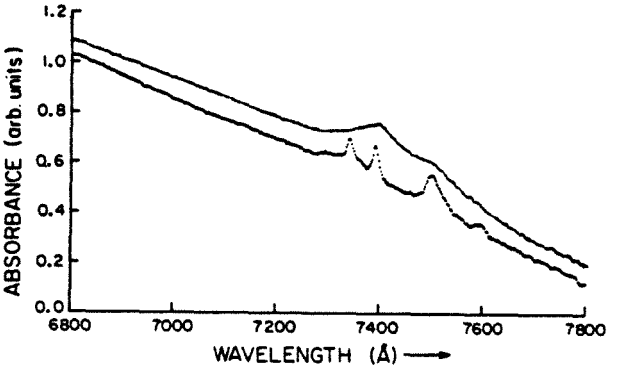

Figure 10. CH stretching overtone spectra ($\Delta v = 5$) of durene-d_2 at low temperature (2 K) (lower) and room temperature (293 K) (upper). The absorbance scale is in arbitrary units. Note that the horizontal axis has been reversed compared to Figure 4.

involved directly in the relaxation, but that the relaxation and the spectral splittings are determined by some restricted or effective form of the density of states.

Figure 10 shows the effect of temperature for the methyl $\Delta v = 5$ overtone transitions. There is in general a broadening of the bands and a shift which eventually leads to coalescence. Several models can be discussed in connection with these results, for example, thermally induced population relaxation, exchange dephasing,[36] or torsional motion induced dephasing.[37]

In a very recent detailed study[37] of the fundamental CH stretching region of various deuteriotoluene isomers, the temperature dependence of the line shape of a single CH oscillator was investigated. Two models were analyzed: one in which stochastic jumps of the CH between conformational minima dephases the vibration and another in which the torsional fluctuations of the oscillator within a given potential well causes dephasing. In both cases, the CH stretching frequency was taken as a function of the angle of the oscillator with respect to the plane and both cases provided efficient relaxation channels. Here, we have not performed a detailed enough study to warrant explicit modeling; however, these considerations provide a possible explanation of the breadth of overtone transitions of some gas-phase methyl-containing compounds where the widths (typically $\gtrsim 70$ cm^{-1}) are larger than the durene low-temperature methyl bandwidths. Clearly torsional oscillations of the methyl groups in these molecules can cause dephasing as discussed above. Thus, the population relaxation times of these gas-phase molecules may be significantly longer than inferred from the line widths.

V. Conclusions and Implications for Bond Selective Laser Chemistry

(A) By using the experimentally determined low-temperature conformation of the durene molecule, we have been able to confidently test models for the vibrational energy distribution in the high CH overtones by using direct absorption of oriented crystals in polarized light. Our polarization data are consistent with the local mode transition moments and with molecular principal axes transition moments. Based on the polarizations and on the number of bands, we believe that the simplest and most useful model is the local mode model. This model

successfully accounts for all observations and is consistent with the weak coupling[39] situation for the low-energy $\Delta v = 1, 2$ region.[30-33] Within this model, the in and out-of-plane methyl modes have been distinguished. Also, a crystal field splitting (smaller than the molecular field) of the in-plane modes is suggested by our analysis. The use of polarization spectroscopy to assign different inequivalent bond modes may be applied to other systems where stereoselectivity of excitation is desired.

(B) The overtone splittings of the durene methyl groups have been compared to the splittings of methyl groups in gas-phase molecules such as toluene and CHD_3. In general, the effects of Fermi resonance on the splittings, especially between $|v_{CH}\rangle$ and $|v_{CH} - 1,2_{bend}\rangle$, must be considered. We emphasize that if the Fermi resonance is truly between $|v_{CH}\rangle$ and $|v_{CH} - 1, n_{bend}\rangle$ manifolds, then even if the mixing is strong the energy in the mixed states is mainly within the CH stretching modes, for $v_{CH} > n_{bend}$. Thus, this form of mixing does not present a serious problem for selective excitation.

(C) Splitting due to inequivalence of CH bonds (due to crystal or molecular fields) is the other main contribution to the observed spectral splittings. These splittings can be separated from Fermi resonance by a study of a progression of overtones. The Birge–Sponer plot for CH stretching progressions usually shows significant deviations from the best straight lines for overtones perturbed by Fermi resonance. These deviations are not observed for higher methyl overtones ($\Delta v = 3$–5) of durene, suggesting that Fermi resonance is not important in this case.

(D) Deviations from the Birge–Sponer line have been observed for the aromatic high overtones, but these shifts are temperature dependent. The dependence is viewed as evidence against Fermi resonance for the aromatic. The temperature-dependent shift and broadening of the durene bands suggests that some dephasing or exchange process is involved.

(E) The analysis of the Birge–Sponer plots gives frequencies and anharmonicities for the in- and out-of-plane methyl bands and for the aromatic band. The frequencies suggest a trend of the bond lengths: $r_{arom} < r_{in\text{-}plane} < r_{out\text{-}of\text{-}plane}$. The computed bond dissociation energies follow the reverse trend.

(F) The narrow bandwidths of the methyl modes suggests that the relaxation times of these modes may be long ($\geq$0.5 ps) compared to previous estimates of CH stretching overtone relaxation times ($\leq$0.1 ps). These times are perhaps on the order of those needed to enhance reactions for example of neighboring molecules in matrices, where the collision frequencies are high.

(G) The well-resolved bands due to various inequivalent hydrogens (assigned experimentally with polarized light) implies that bond-selective and stereoselective excitation is possible and that laser-induced reaction with such selectivity is feasible, especially at low temperature.

(H) Finally, the comparison of the durene results with those of gas-phase CHD_3 shows that the effect of the increased density of states of durene is not as expected from the total density, i.e., the coupling involves a restricted density of some form.

Acknowledgment. This work was supported by a grant from the National Science Foundation, No. CHE8112833. We thank Professor G. Rossman of the Department of Geology at the California Institute of Technology for the use of the Cary-17 spectrophotometer. We also thank Professor B. Henry for useful comments and suggestions.

(1) Zewail, A. H. *Phys. Today* **1980**, *33*, 25.
(2) For example: (a) Henry, B. *Acc. Chem. Res.* **1977**, *10*, 207. (b) Wallace, R. *Chem. Phys.* **1975**, *11*, 189. (c) Burberry, M.; Albrecht, A. *J. Chem. Phys.* **1979**, *70*, 147. **1979**, *71*, 4631. (d) Elert, M. C.; Stannard, P. R.; Gelbart, W. M. *Ibid.* **1977**, *67*, 5395. (e) Sage, M.; Jortner, J. *Chem. Phys. Lett.* **1979**, *62*, 451. **1981**, *79*, 9. (f) Lawton, R. T.; Child, M. S. *Mol. Phys.* **1980**, *40*, 773. (g) Møller, H. S.; Mortensen, O. S. *Chem. Phys. Lett.* **1979**, *66*, 539.
(3) (a) Swofford, R. L.; Burberry, M. S.; Morrell, J. A.; Albrecht, A. C. *J. Chem. Phys.* **1977**, *66*, 5245. (b) Bray, R.; Berry, M. J. *Ibid.* **1979**, *71*, 4909. (c) Perry, J. W.; Zewail, A. H. *Chem. Phys. Lett.* **1979**, *65*, 31.
(4) Perry, J. W.; Zewail, A. H. *J. Phys. Chem.* **1981**, *85*, 933.
(5) Perry, J. W.; Zewail, A. H. *J. Chem. Phys.* **1979**, *70*, 582.
(6) Hamilton, W. C.; Edmonds, J. W.; Tippe, A.; Rush, J. J. *Discuss. Faraday Soc.* **1969**, *48*, 192.
(7) Santaserio, B.; Samson, S., to be published.
(8) Stam, C. H. *Acta Crystallogr. Sect. B* **1972**, *28*, 2630.
(9) Prince, E.; Schroeder, L. W.; Rush, J. J. *Acta Crystallogr. Sect. B* **1973**, *29*, 184.
(10) Rush, J. J. *J. Chem. Phys.* **1967**, *47*, 3936.
(11) Livingston, R.; Grant, D. M.; Pugmire, R. J.; Strong, K. A.; Brugger, R. M. *J. Chem. Phys.* **1973**, *58*, 1438.
(12) Allen, P. S.; Cowking, A. *J. Chem. Phys.* **1968**, *49*, 789.
(13) Mirskaya, R. V.; Ivanova, L. V. *Sov. Phys. Cryst.* **1973**, *18*, 101.
(14) Winchell, A. N. "The Optical Properties of Organic Compounds"; Academic Press: New York, 1954; p 76.
(15) Reddy, K. V.; Berry, M. J.; Heller, D. F. *J. Chem. Phys.* **1982**, *76*, 2814.
(16) Henry, B. R.; Greenlay, W. R. A. *J. Chem. Phys.* **1980**, *72*, 5516.
(17) Nakagaki, R.; Hanazaki, I. *Chem. Phys. Lett.* **1981**, *83*, 512.
(18) Henry, B. R.; Ali Mohammadi, M. *Chem. Phys.* **1981**, *55*, 385.
(19) Wong, J. S.; Moore, C. B. *J. Chem. Phys.* **1982**, *77*, 603.
(20) Fang, H. L.; Swofford, R. L. *Appl. Opt.* **1982**, *21*, 55.
(21) Henry, B. R.; Hong, I. F.; MacPhail, R. A.; Strauss, H. L. *J. Am. Chem. Soc.* **1980**, *102*, 515.
(22) Wong, J. S.; MacPhail, R. A.; Moore, C. B.; Strauss, H. L. *J. Phys. Chem.* **1982**, *86*, 1478.
(23) Nakagaki, R.; Hanazaki, I. *J. Phys. Chem.* **1982**, *86*, 1501.
(24) Fang, H.; Swofford, R. *J. Chem. Phys.* **1980**, *72*, 6382. **1980**, *73*, 2607.
(25) Sonnich Mortensen, O.; Henry, B. R.; Ali Mohammadi, M. *J. Chem. Phys.* **1981**, *75*, 4800.
(26) Perry, J. W.; Moll, D.; Kuppermann, A.; Zewail, A. H. *J. Chem. Phys.*, to be submitted for publication.
(27) Reddy, K. V.; Berry, M. J. *Faraday Discuss. Chem. Soc.* **1979**, *67*, 188.
(28) Robinson, P. J.; Holbrook, K. A. "Unimolecular Reactions"; Wiley-Interscience: New York, 1972.
(29) Stone, J.; Thiele, E.; Goodman, M. F. *Chem. Phys. Lett.* **1980**, *71*, 171.
(30) (a) Le Calvé, N.; Carrigou-LaGrange, C.; Forel, M. T.; Tomczak, Z.; Tramer, A. *J. Chem. Phys.* **1966**, *63*, 1445. (b) Tramer, A.; Tomczak, Z. *Spectrochim. Acta, Part A* **1968**, *24*, 2051.
(31) Forel, M. T. *Spectrochim. Acta, Part A* **1968**, *24*, 311.
(32) Fruwert, J.; Galli, J. *Z. Phys. Chem.* **1974**, *255*, 1069.
(33) Rohleder, J. W.; Luty, T. *Acta Phys. Pol.* **1967**, *31*, 653.
(34) McKean, D. *Chem. Soc. Rev.* **1978**, *7*, 399.
(35) Zewail, A. H. *Acc. Chem. Res.* **1980**, *13*, 360.
(36) Marks, S.; Cornelius, P. A.; Harris, C. B. *J. Chem. Phys.* **1980**, *73*, 3069.
(37) Cavagnat, D.; Lascombe, J. *J. Chem. Phys.* **1981**, *76*, 4336.
(38) Prasad, P. N.; Kopelman, R. *J. Chem. Phys.* **1973**, *58*, 5031.
(39) The local mode coupling, at the quadratic level, has been calculated by Burberry and Albrecht[2] to be very small for methyl CH local modes at high energy ($\Delta v \geq 3$) and our current interpretation is consistent with this theoretical finding.

* Alfred P. Sloan Fellow and Camille and Henry Dreyfus Foundation Teacher–Scholar.
† Contribution No. 6665.

CHAPTER V

High-Energy Overtone Photoacoustic Spectroscopy of Some Methyl-Containing Molecules: Vibrational Analysis*

ABSTRACT

Pulsed photoacoustic spectroscopy of gas phase CHD_3 ($\Delta\nu_{CH}$ = 5,6 and 7), CH_2D_2, CH_3D, CH_4 and neopentane ($\Delta\nu_{CH}$ = 6) and tetramethylsilane (combination of the form $|(5,1)_{CH}>$) is reported. We present an analysis of the Fermi-resonances of CHD_3 which indicates strong interactions of the CH stretch with degenerate bending modes. Preliminary calculations implicate interactions between the CH stretching overtones or low order combinations and combinations of CH stretch and high numbers of bending quanta in $\tilde{\nu}_5$ (degenerate CH binding mode) as responsible for the anomalous rotational constants reported in a companion paper [D. Moll, J.W. Perry, A. Kuppermann and A.H. Zewail, J. Chem. Phys., submitted for publication.] An upper limit of 10 cm^{-1} is obtained for splitting of the $|6,0>_{\pm}$ local mode states for CH_2D_2, giving support to a description based on the local mode picture. For CH_3D and CH_4 the spectra are apparently congested by overlapping overtone and combination bands and perhaps other mechanisms not identified in this work. Very slow population relaxation of CHD_3 (for $\Delta\nu_{CH}$ = 5 and 6) is implied by the lower limit (5 ps) of the lifetime obtained from the

---

*This chapter is based on a manuscript which has been submitted for publication
[J.W. Perry, D.J. Moll, A.H. Zewail and A. Kuppermann, J. Chem. Phys., submitted).

relatively narrow bandwidths of some CHD_3 transitions, in contrast with the larger bandwidths obtained for some larger molecules. The spectra obtained for neopentane and tetramethylsilane are reasonably well fit by sums of Lorentzian bandshapes and homogeneous broadening (50-100 cm^{-1}) is argued to be dominant. However, since a thermal population of low-frequency methyl torsions exists, dephasing processes may be very significant and thus the lifetimes may be longer than inferred from the bandwidths. Generally, our results emphasize the importance of the proper inclusion of interactions of CH stretching with CH bending motions in the theoretical prediction of high overtone spectra and dynamics.

I. INTRODUCTION

The high energy vibrational states of polyatomic molecules have attracted much interest in recent years. Much of this interest stems from the relevance of these states and their dynamics to selective laser-induced vibrational photochemistry. Other phenomena whose understanding will certainly benefit from studies of high energy vibrational states include radiationless relaxation and multiphoton excitation and dissociation. In regard to selective laser-induced chemistry, the ability to localize a large fraction of the dissociation energy in specific modes or bonds for periods of time about equal to reaction or collision times is the main qualitative prerequisite for possible selectivity.

The local mode model[1] (and the local mode picture) has been used widely in the description of high-energy X-H (X=C,N,O) vibrational states.[2] Refinements of the theory which include the effects of coupling of the X-H stretches in two or more oscillator systems[3-6] have consistently shown that high energy states are most easily described within the local mode picture. The reason for this situation is that for X-H bonds the interbond coupling is less than the diagonal bond anharmonicity. The splitting of the symmetrized states has been shown to decrease with increasing ν_{XH}, resulting in increased localization at higher energy. Also, the intensity of the lowest energy state in each ν_{XH} manifold typically increases, relative to other states in the manifold, with increasing ν_{XH}.

Recently, new information on the nature of high-energy CH-stretching overtones has been obtained.[7] The polarizations of the CH

stretch overtones of durene (1,2,4,5-tetramethylbenzene) crystals have been measured and analyzed. Using the molecular conformation of durene determined by X-ray diffraction methods, the calculated polarizations and the spectral assignments were compared for several models of the vibrational states. The results were found to be consistent with the local mode model for the durene CH stretching overtones.

From the studies of the bandshapes of overtone transitions, information on the relaxation of the high energy states of polyatomic molecules has been obtained. For aromatic CH stretching overtones the bandwidths are typically ≥ 50 cm^{-1} for high ν_{CH},[7-9] implying ultrafast population relaxation times of ≤ 0.1 ps, for molecules in the gas phase or low temperature solid.

Perry and Zewail[7] have shown that for the methyl CH stretching overtones ($\Delta\nu_{CH} = 5$) of durene the bands become quite narrow, ~ 20 cm^{-1} at low temperature ($\sim 2K$). This suggests that the relaxation of methyl CH stretches is slower than for aromatic CH stretches (linewidth ~ 100 cm^{-1}) and the greater widths were rationalized in terms of a larger effective density of states for the aromatic CHs.

In a companion paper[10] (henceforth paper I) we presented a rotational analysis of the high-energy ($\Delta\nu = 5,6$ and 7) CH stretching overtones of gas phase CHD_3, obtained by pulsed photoacoustic spectroscopy. In this paper, we present a vibrational analysis of the CHD_3 spectra as well as spectra and vibrational analyses of the following gaseous molecules in the $\Delta\nu_{CH} = 6$ region: CH_2D_2. CH_3D, CH_4 and neopentane (2,2-dimethylpropane). Also, a combination band of tetramethylsilane vapor of the form $|(5,1)_{CH}\rangle$ has been observed and

assigned. Our results permit a detailed examination of the coupling of the CH stretching motions to normal modes, particularly CH bending modes.

II. EXPERIMENTAL

The pulsed photoacoustic spectrometer has been described in paper I.[10] The laser dyes used to span the various spectral regions investigated in this work were Oxazine-725, Rhodamine 640 and Coumarin 540A. The dye laser output pulses typically had the following characteristics: 1-30 mJ pulse energy, $\sim$5 ns pulsewidth and 0.6 cm^{-1} bandwidth. The wavelength ranges of the spectra were calibrated with emission lines from a Fe-Ne arc lamp by using a 0.5 m spectrometer.

Due caution was given to possible nonlinear effects by measuring the laser intensity dependence of the microphone signal amplitude for several molecules which was found to be linear in all cases over the range of our experiment. Also, the band shapes presented here were only weakly dependent on pressure and essentially independent (within the resolution of the system) over the pressure range of the experiment ($\sim$ 100 to $\sim$ 1385 torr).

The NPT and TMS spectra were digitized using a Houston instruments HIPAD digitizer which was interfaced to a PDP 11/03 based TERAK microcomputer. Spectra were fitted to sums of Lorentzian model functions by using a nonlinear least squares regression analysis.

The materials used in this study were: CHD_3 and CH_3D, Stohler Isotope Chemicals, 99% atom D; CH_2D_2, Merck Chemical, 99% atom D; CH_4, J. T. Baker, ultrapure; tetramethylsilane, Aldrich, 99.9+%; neopentane,

Pfaltz and Bauer. These materials were used without further purification, except for TMS which was vacuum distilled. Samples were introduced into the cell after the cell was evacuated to a pressure of < 1×10^{-6} torr by using a vacuum manifold.

III. RESULTS AND DISCUSSION

A. CHD_3

1. High-Energy Overtone Spectra

We were motivated to study the overtone spectroscopy of the deuteromethane series in part, as an attempt to identify various vibrational interactions which are significant for relatively small molecules at high vibrational energy. This series of molecules was chosen for the features of small size, high symmetry and no strong polarizations and for the fact that a relatively large amount of information on the low-energy spectroscopy and force field exists.[11a,12-21]

We begin with a consideration of the high CH stretching overtones of CHD_3. This molecule is taken as a model system for separating interactions in the high energy overtone region. We will be able to examine CH stretch-normal mode coupling in the absence of interactions between degenerate CH stretching states.

The question of whether the CH stretching overtones of CHD_3 are better described from a local or normal mode model is not addressed in this work.[22] It can be argued that the difference between the two models is not great for CHD_3. The question amounts to whether the CD stretch displacements can be neglected in comparison to the CH stretch.

Based on the relative number (3:1) and relative masses (2:1) of D to H, it can be shown that the relative amplitude (CD/CH) would be quite small for CHD_3 even in the normal mode states. For the purposes of this work no further consideration of this question is necessary. We now turn to the experimental results.

In Fig. 1, the CHD_3 stretching overtone spectra, which have been normalized for the laser intensity, are presented. The spectra are typically averages of only 3 or 4 scans each, and the signal to noise ratios are $\sim$ 100, 50, and 30 for the $\Delta\nu$ = 5,6, and 7 regions, respectively. The drop in S/N reflects somewhat the decrease in absorption strength (see paper I) with increasing CH stretching quantum number. Note the resolved rotational structure (described in paper I) which corresponds, primarily, to the $\Delta J = 0, \pm 1$ progressions for each vibrational band. Note also the presence of two main ro-vibrational band systems in the $\Delta\nu_{CH}$ = 5 and 6 regions and three bands in the $\Delta\nu_{CH}$ = 7 region.

With the observation of several bands near the CH stretching overtones, it is apparent that there is a mixing or Fermi-resonance phenomenon involved which is distributing oscillator strength into the nearby states from the "pure" CH stretching overtone. For CHD_3 there can be only one "pure" CH stretching state at a given quantum level. This state is the corresponding overtone of the well-known fundamental[12,13] at 2992 cm^{-1} which is of A_1 symmetry in the C_{3v} molecular point group. Thus, all overtones of this mode are of A_1 symmetry also. Since the potential energy coupling terms must be totally symmetric,[11b,23] the states involved in the Fermi-resonance must

likewise be of A_1 symmetry. From the point of view of assignment the problem is reduced to finding proper symmetry combination states or overtones in near resonance with the "pure" CH stretching overtone. It is reasonable to restrict the consideration to combination states which can be expected to couple with the overtone through low-order potential coupling terms.

We will denote the vibrational eigenstates of CHD_3 in an occupation number representation as $|\nu_1, \nu_2, \nu_3, \nu_4, \nu_5, \nu_6>$ where the quantum numbers are indexed in accord with Ref. 21. The CH stretch is labelled ν_1. Only excited modes will be indicated, for example: the νth quantum CH stretch level will be shown as $|\nu_1>$.

We expect to find the appropriate combination levels for coupling to $|\nu_1>$ in states of the form $|\nu_1 - 1, \nu_i, \nu_j>$ or $|\nu_1 - 1, \nu_i>$ with ν_i and ν_j being relatively small integers. The mixing of these states with $|\nu_1>$ would require coupling terms of order $1 + \nu_i + \nu_i$ or $1 + \nu_i$ such as $V_{1ij}^{(1+\nu_i+\nu_j)} \sim q_1 q_i^{\nu_i} q_j^{\nu_j}$ or $V_{1i}^{(1+\nu_i)} \sim q_1 q_i^{\nu_i}$ where q is the displacement coordinate in the harmonic oscillator basis. The total energy in the non-CH stretching modes of the combination band must make up approximately one quantum of CH stretch energy at the given ν_1 level. The expression for the vibrational energy of a system of oscillators which includes doubly degenerate modes is given by the equation[11c]

$$E = \sum_i \bar{\nu}_i (\nu_i + d_i/2) \sum_{\substack{i,j \\ i \geq j}} x_{ij} (\nu_i + d_i/2)(\nu_j + d_i/2) + \sum_{\substack{i,j \\ i \geq j}} g_{ij} \ell_i \ell_j \qquad (1)$$

Where $\bar{\nu}_i$ are harmonic frequencies, d_i are degeneracies, x_{ij} are anharmonic constants and the g_{ij} are vibrational angular momentum constants. The transition energy of an arbitrary "pure" overtone can be written (ignoring ℓ-type splitting as)

$$\Delta E_i = (\bar{\nu}_i + x_{ii}\, d_i + \frac{1}{2}\sum_{j\neq i} x_{ij}\, d_j)\nu_i + x_{ii}\nu_i^2. \qquad (2)$$

For the CHD_3 CH stretch this can be rewritten as

$$E_1 = A_1\nu_1 + B_1\nu_1^2. \qquad (3)$$

Where A_1 is the effective frequency and B_1 is the diagonal anharmonic constant. The energy mismatch, one CH quantum, to be made up by the non-CH stretch modes in the combination level must be approximately $A_1 + B_1\,(2\nu_1 - 1)$.

In Table I we list literature data for the wavenumbers of the band origins for the CHD_3 fundamentals and some overtones. In Table II the observed band origins for CHD_3 states observed in this study are presented. To help sort out the assignments we have used the Birge-Sponer plot (Fig. 2) for the CHD_3 $\tilde{\nu}_1$ overtones. The plot shows clearly that the higher energy band in the $\Delta\nu_1 = 5$ region falls very close to the extrapolated position of the best straight line fit (see Table III for the parameters) to the lower harmonics. This is consistent with our expectation that, in a weak coupling scheme, the highest intensity band should be the "pure" overtone. Here, the first order energies are not close enough for the levels to mix strongly. We

assign this band as the "pure" overtone $|5_1\rangle$. As for the other band, we have considered possible combination states and we find two A_1 states which are close to the required energy and couple to $|5_1\rangle$ through low-order terms. These states are $|4_1,2_5\rangle$ and $|4_1,1_5,1_6\rangle$ at 13,831 and 13,594 cm^{-1}, respectively, in zero-order (including diagonal anharmonicity), as calculated by using values in Table I. Modes $\tilde{\nu}_5$ and $\tilde{\nu}_6$ are both of e symmetry, however, the levels $|2_5\rangle$ and $|1_5,1_6\rangle$ split into A_1 and E sublevels of which the A_1 level may, with or without combination with the A_1 CH stretch overtones, interact with A_1 CH stretching levels. The spectra show (see Figure 1) that there is a third level at lower energy than the other levels involved in the Fermi resonance near $\Delta\nu_1 = 7$. We take the combination band near $\Delta\nu_1 = 5$ to be $|4_1,2_5\rangle$ which is the higher energy of the two combination bands. Note that this assignment suggests a large negative first-order shift of the combination band energy from the zero-order position (vide infra).

For the $\Delta\nu_1 = 6$ overtone region, two facts guide us in the assignment. First, we note again that the higher energy band lies closer to the extrapolation of the best fit line of the Birge-Sponer plot. Second, the shading of the Q branches is different for the two bands; the higher energy band is shaded to lower energy in the $\Delta\nu_1 = 5$ and 6 regions. This is taken as evidence that the higher energy bands correlate with the "pure" CH stretch and the lower energy bands correlate with combination states. However, the mixing is stronger at $\Delta\nu_1 = 6$, so the assignments here indicate only the parentage of the band. The higher energy band is therefore of $|6_1\rangle$ origin and the lower energy band is of $|5_1,2_5\rangle$ origin for the $\Delta\nu_1 = 6$ region.

In the $\Delta v_1 = 7$ region the situation is somewhat different. The band closest to the Birge-Sponer line is the center band. Also, the Q branch at higher energy is shaded to high energy, in analogy with the $|4_1,2_5\rangle$ and $|5_1,2_5\rangle$ bands. These observations suggest that the band at higher energy in this region is actually of $|6_1,2_5\rangle$ origin. The center band would be of $|7_1\rangle$ origin and the lower energy band could be of $|6_1,1_5,1_6\rangle$ origin. The assignment of the third band is tentative since other states of correct symmetry and small quantum number differences may exist near the required energy in the $\Delta v_1 = 7$ region. Some possibilities are $|6_1,2_3\rangle$ and $|6_1,2_6\rangle$. This assignment, if correct, suggests that the band with the highest peak intensity in the $\Delta v_{CH} = 7$ region is in fact a combination band with one less CH stretch quantum excited than in the "pure" overtone from which, presumably, oscillator strength is borrowed. We will return to a consideration of this point later, in the section on the analysis of the Fermi resonance.

The tuning and "crossover" of levels occur because of the larger anharmonic shift experienced by the "pure" overtone due to the larger CH stretch quantum number. As v_{CH} increases by one, the anharmonic shift of the "pure" overtone $|v_{CH}\rangle$ increases by one, the anharmonic shift of the "pure" overtone $|v_{CH}\rangle$ relative to a combination band of the form $|v_{CH} - 1, \{v_i\}\rangle$ increases by 2 Bv_{CH} (for a fixed $\{v_i\}$). Therefore, for a situation where at low v_{CH} the combination band is at lower energy than the overtone, there may be a crossing at higher v_{CH} of the combination and overtone states. Of course, this analysis neglects the possible off-diagonal anharmonic coupling of the modes, an effect which may introduce positive or negative relative shifts of the levels. The

tuning of the Fermi resonance between CH stretching states and combinations involving CH bending modes has been observed in the overtone spectroscopy of the halomethanes,[6,24] haloethanes,[25] and of some lower alkanes.[26] Before discussing the discrepancy between the zero-order and observed combination band positions we must consider the shifts due to the state mixing by Fermi resonance.

2. Analysis of the Fermi Resonance

We now attempt an analysis of the Fermi resonance of the "pure" CH stretching overtones with the CH stretch-bend combination. The approximation of treating only the purely vibrational interaction between the levels is made; that is, we ignore Coriolis coupling to nearby E states. It is expected that the Fermi interaction of the totally symmetric overtone and combination states will be dominant. We begin with the $\Delta v_1 = 5$ region.

Solution of the secular equation for the $|5_1\rangle$ and $|4_1,2_5\rangle$ levels gives for the perturbed energies[11b]

$$E_{\pm} = \bar{E}_{12} \pm \frac{1}{2} (4W_{12}^2 + \delta^2)^{1/2} \qquad (4)$$

where the subscripts are defined as $1 \equiv |5_1\rangle$ and $2 \equiv |4_1,2_5\rangle$ $\bar{E}_{12}$ is the average energy of the zero-order levels, W_{12} is the off-diagonal energy matrix element and $\delta = (E_1^0 - E_2^0)$ is the difference in the zero-order energies. We measure spectroscopically the $E_{\pm}$ values and the intensities of the bands. The ratio of the intensities gives directly the mixing coefficients for the two interacting states in the case of negligible zero-order combination band intensity. Unfortunately, the vibration-rotation bands that we have observed are overlapped thus

limiting the accuracy of the determined intensities. Another approach to determining the zero-order energies, interaction matrix elements and mixing coefficients can be taken.

The zero-order "pure" overtone energies can be obtained from the extrapolation of the Birge-Sponer line (see Table IV). This is possible provided that terms in the potential energy of higher order than quartic do not have an appreciable contribution in the range of the extrapolation. Linear fits of the Birge-Sponer plots have been reported for many molecules[2] and up to very high vibrational quantum numbers ($\Delta\nu_{CH} = 9$).[8] We will therefore assume the extrapolation to be valid for CHD_3, at least up to $\Delta\nu_{CH} = 7$. From the difference in the observed energy of the "pure" overtone and the extrapolated value one obtains the Fermi resonance shift. Since the shifts due to the resonance interaction are of equal magnitude for the two-level problem, we can use the shift (7.3 cm^{-1}) of the observed $|5_1\rangle$ energy from the zero-order calculated energy to correct the observed $|4_1,2_5\rangle$ energy. We are thereby able to obtain the zero-order energy for the combination band (see Table V). The off-diagonal matrix element W_{12}, which can be obtained from Eq. (3), can now be calculated and is found to be 30 cm^{-1}.

The wavefunctions for the mixed states[27] are

$$\Psi^+ = a|5_1\rangle + \sigma b|4_1,2_5\rangle$$
$$\Psi^- = -\sigma b|5_1\rangle + a|4_1,2_5\rangle \qquad (5)$$

where σ is the sign of W_{12} and $a^2 + b^2 = 1$. The expressions for the

coefficients are

$$a = \left(\frac{\Gamma + \delta}{2\Gamma}\right)^{1/2}$$
$$b = \left(\frac{\Gamma - \delta}{2\Gamma}\right)^{1/2} \qquad (6)$$

where $\Gamma = (4W_{12}^2 + \delta^2)^{\frac{1}{2}}$. By using Eqs. (4) and (5) it can be shown that

$$b^2 = \left|\frac{E_1^0 - E_+}{E_+ - E_-}\right| \qquad (7)$$

Thus the mixing coefficient can be obtained from a measurement of the level shift and the observed splitting.

The intensities of the transitions $|0\rangle \rightarrow \psi^+$ and $|0\rangle \rightarrow \psi^-$ are given by

$$I^+ \propto |\langle\psi^+|\mu_z|0\rangle|^2$$
$$I^- \propto |\langle\psi^-|\mu_z|2\rangle|^2 \qquad (8)$$

where μ_z is the component of the transition moment along the principal symmetry axis of the molecule. Expansion of the matrix elements gives

$$I^+ = a^2M_1^2 + b^2M_2^2 + 2\sigma abM_1M_2$$
$$I^- = b^2M_1^2 + a^2M_2^2 - 2\sigma abM_1M_2 \qquad (9)$$

where M_1 and M_2 are the zero-order transition matrix elements of the

"pure" overtone, $|5_1\rangle$, and the combination, $|4_1,2_5\rangle$, respectively. The transition moment operator is usually taken to be a single particle operator which means that the combination band would have nonzero-order intensity, i.e., M_2 would equal zero. If this is the case, then the ratio of the intensities is given by

$$I_{rel} = \frac{I_-}{I_+} = \frac{b^2}{a^2} \qquad (10)$$

Duncan, et al.[27] have discussed some interesting effects which can occur if $M_2 \neq 0$. The interference term can lead to an asymmetry in the intensity borrowing such that $I^+ \neq I^-$ at the precise point of resonance. Since a and b are taken to be positive the sense of the asymmetry is determined by the sign of the interference term.

For now we take $M_2 = 0$. This allows us to use the simple expressions above for the mixing coefficients to calculate the relative intensities from the Fermi-resonance shift and the observed splitting of the bands. By using the appropriate values from Tables IV and V one obtains $b^2 = 0.055$ and therefore $a^2 = 0.945$. The relative intensity was calculated, $I_{rel}^{calc} = 6 \pm 3\%$, and is somewhat lower than the observed value, $I_{rel}^{obs} = 18 \pm 8\%$, but agrees reasonably to the extent that the mixing is calculated to be fairly weak for this region. There are several factors which have been neglected and which may influence the calculated intensity, such as neglect of other levels which may be in weak resonance with the "pure" overtone, vibration-rotation interaction, or non-zero transition moment (M_2) of the combination band which could result, for example, from mixing with the $|4_1\rangle$ level or electrical

anharmonicity.

Using the same method as above for the $\Delta v_1 = 6$ region, we obtain $|W_{12}| = 35\ cm^{-1}$, $a^2 = 0.66$ and $b^2 = 0.34$. The observed relative intensity is in good agreement with the calculated value, $I_{rel}^{obs} = 55 \pm 10\%$ and $I_{rel}^{calc} = 52 \pm 10\%$. Here the $|6_1\rangle - |5_1,2_5\rangle$ mixing apparently dominates the relative intensity. Clearly there is strong mixing of the pure overtone and the combination band in this region. This leads, of course, to delocalization of the energy in the various modes involved (v_1 and v_5 in the present case). However, since the combination state involves a large number of CH stretching quanta relative to bending quanta (5:2) and since the relative energy of a CH stretch to CH bend quantum is about two, much of the energy ($\sim$ 80%) of the state is in the CH stretching coordinate. So, in spite of the sizeable state mixing, much of the vibrational energy remains in the CH stretching mode in the perturbed levels.

In the $\Delta v_1 = 7$ region (Figure 1c) the Fermi resonance is more complicated due to the presence of at least one more sizeable band than in the $\Delta v_1 = 5$ or 6 regions. The situation is complicated further due to severe overlapping of the band systems which results in a highly congested spectrum. It is not possible to estimate the relative band intensities with certainty without recourse to fitting the spectrum with a model. We will not pursue the analysis as such; rather we wish to qualitatively explain the spectrum in terms of the assignment given above.

The standard treatment of the three-level resonance problem involves solution of a 3 x 3 secular determinant for the perturbed

energies and for the mixed state wavefunctions. In the present case, implementation of this procedure is prevented due to a lack of knowledge of the various parameters.

We now define the abbreviations for zero-order states and interaction matrix elements in this region. The subscripts below will refer to zero order states as follows: $1 \equiv |7_1\rangle$, $2 \equiv |6_1,2_5\rangle$ and $3 \equiv |6_1,1_5,1_6\rangle$. For example, E_1^0 denotes the unperturbed energy of the $|7_1\rangle$ state and W_{13} is the interaction matrix element between $|7_1\rangle$ and $|6_1,1_5,1_6\rangle$. The only parameters which may be accurately calculated are E_1^0 and $|W_{12}|$. This leaves the problem undetermined since we have four unknowns E_2^0, E_3^0, W_{13} and W_{23} and only three equations relating them. We resort to another level of approximation in order to explain the spectrum.

The assignment given earlier associates a combination band with the highest peak intensity feature (high energy Q band) in the $\nu_1 = 7$ region. Although the relative integrated intensities may differ substantially from the relative Q band peak heights we take them to be proportional for the sake of illustration. Thus, the observed relative intensities are approximately 0.15: 0.35: 0.50 for I_3: I_1: I_2, respectively, where the subscripts refer to the perturbed levels of indicated parentage. One explanation for this intensity distribution would be as follows: the $|7_1\rangle$ and $|6_1,2_5\rangle$ states are in very close resonance in zero-order and mix strongly giving roughly equal intensities in the perturbed states. The $|6_1,1_5,1_6\rangle$ state, being closer to the $|7_1\rangle$ than the $|6_1,2_5\rangle$ perturbed levels, now interacts with the perturbed overtone $|7_1\rangle$ and oscillator strength is distributed from the

perturbed $|7_1\rangle$ level into $|6_1,1_5,1_6\rangle$, the mixing being less than the $|7_1\rangle$ - $|6_1,2_5\rangle$ mixing. This model explains qualitatively why the sum of the peak heights of $|7_1\rangle$ and $|6_1,1_5,1_6\rangle$ levels is about that of the $|6_1,2_5\rangle$ level. Even if there is a non-zero interaction between the $|6_1,2_5\rangle$ levels the conclusion of the above argument will hold qualitatively as long as

$$\left|\frac{W_{13}^2}{\Delta E^\circ_{13}}\right| >> \left|\frac{W_{23}^2}{\Delta E^\circ_{23}}\right| \tag{11}$$

One can now perform a simple numerical analysis of the three level resonance. First, the $|6_1,1_5,1_6\rangle$ level is ignored; we take $W_{13} = W_{23} = 0$, and the resulting 2 x 2 Fermi resonance is analyzed as before. We take the E_1^0 value to be that from the extrapolation of the Birge-Sponer plot. From this approximation we obtain $|W_{12}| \sim 30$ cm^{-1}. The combination state has crossed over to higher energy, in zero order, so now ψ^+ goes over into $|6_1,2_5\rangle$ as $W_{12} \to 0$. We write the mixed state wavefunctions as

$$\begin{aligned} \psi^+ &= a|6_1,2_5\rangle + \sigma b|7_1\rangle \\ \psi^- &= -\sigma b|6_1,2_5\rangle + a|7_1\rangle \end{aligned} \tag{12}$$

As before, we calculate the coefficients and get $a^2 = 0.53$ and $b^2 = 0.47$, indicating an almost equal mixture. If we allow for interaction with level 3, then assumptions about the values of the parameters are necessary to perform a numerical analysis. By a consideration of

various approximations we find that $W_{13} \approx W_{12}$ if W_{23} is ignored. We also find that the amplitude of level 3 is smaller than the other bands and that the $|6_1,1_5,1_6\rangle - |7_1\rangle$ mixing is weaker than the $|6_1,2_5\rangle - |7_1\rangle$ mixing. Further calculations, possibly involving exact diagonalization and least-squares fitting of the spectrum, are required to obtain more precise information.

The values of E_{corr}, defined as E_{obs} + FRS, (Fermi resonance shift) for the $|\nu_1,2_5\rangle$ state have been obtained and are given in Table V. According to first-order perturbation theory, one expects for a combination band $|\nu_1,\nu_5\rangle$ a shift from the zero-order energy of the form

$$\Delta E_{15}^{(1)} = \nu_1 \nu_5 x_{15} \qquad (13)$$

where x_{15} is an off-diagonal anharmonic constant. In Table V we list the observed shifts which were determined from the differences in the Fermi resonance corrected energy and the energy calculated from the parameters of Tables I and III. Using the shift of $|4_1,2_5\rangle$ to determine the constant x_{15} we obtain -19.5 ± 3 cm^{-1}. This value is then scaled according to Eq. 14 for $|5_1,2_5\rangle$ and $|6_1,2_5\rangle$, and the results are listed in Table V under $\Delta E_{calc}^{(1)}$. The errors are within $\sim$15% and we take this as reasonable, since the approach was the simplest possible one. Note that the x_{15} value (-19.5 ± 3 cm^{-1}) determined here is in good agreement with the anharmonic constant of Gray and Robiette: $x_{15} = -17.8$ cm^{-1}.[21]

One of the most important results of this section is the observation of a strong Fermi resonance at quite high energy in this very simple, single CH oscillator molecule, CHD_3. The interaction of

the CH stretching overtones with normal CH bending modes is sufficiently large as to strongly affect the spectra. The diagonal CH stretching anharmonicity is sufficiently large for us to find situations of tuning of near resonance and strong mixing for the high overtones.

The very strong mixing at $\Delta v_{CH} = 6$ and the congested overlapping bands in the $\Delta v_{CH} = 7$ region have been rationalized using a fairly large coupling of the CH stretch primarily to the CH bending and CD_3 asymmetric bending modes. This strong coupling and overlapping has important dynamical implications. It is clear that bending vibrations will be very important in the relaxation of the CH stretch and must be included in a proper theoretical study of the dynamics of CHD_3.

3. Comparison with the Results of the Rotational Analysis

In Paper I[10] we presented the rotational B' constants derived from a combination sum analysis of the rotational structure of bands in the $\Delta v_{CH} = 5,6$ and 7 regions of CHD_3. The constants derived for the $|5_1\rangle$, $|6_1\rangle$, $|4_1,2_5\rangle$. $|5_1,2_5\rangle$ and $|6_1,2_5\rangle$ levels were all found to be larger than expected in the simplest model for the Δv_{CH} dependence of these constants, involving non-interacting states.

A model for the constants involving a simple two-level Fermi resonance was discussed and it was concluded that this model also could not explain the observed rotational constants. This is in contrast with the relative success of the two-level Fermi resonance model used in this work to analyze the spectra for $\Delta v_{CH} = 5$ and 6. Here we have used the Fermi-resonance shifts to determine the mixing coefficients and relative intensities of the Fermi dyads, with reasonable agreement between observation and analysis resulting. For the $\Delta v_{CH} = 7$ region, three

bands are apparent in the spectrum and the observed spectrum is rationalized in terms of a three-level Fermi resonance.

The inability of the simple Fermi resonance model to explain the rotational constants was rationalized by an argument that there are three or more interacting levels which are important for each region and these states mix to an extent which affects rotational constants, but that the "weak coupling" states do not individually acquire significant enough intensity to be observed directly. It is clear that this mixing requires involvement of states with higher B' values than B" values, since the observed perturbations are to higher B'. Thus, combinations involving high excitation of ν_5 (CH bending) become likely candidates for this type of coupling since it is known that the α_5^B value is negative, i.e., that B' increases with increasing ν_5.

We have calculated a vibrational state map for CHD_3 using the anharmonic constants derived by Gray and Robiette.[21] The anharmonic constants were determined from a fit to previously known spectroscopic data of many isotopic methanes of a force field including quadratic and cubic potential terms and a diagonal quartic term for the CH stretching coordinate. The vibrational states were generated by using an exact state counting algorithm which includes a symmetry restriction.[28] Only those states with a totally symmetric direct product representation were mapped. ℓ-type doubling was ignored. For states with overtones of e modes excited this approximation will still be reasonable since these states must couple to $|\nu_1\rangle$ or $|\nu_1,2_5\rangle_{A_1}$ which are both, by necessity, = 0 states. For a Fermi-resonance we have the selection rule that ℓ = 0 so we are interested in the lowest energy (ℓ = 0) A_1 component of a

particular manifold of ℓ states originating from a given vibrational state.

The energies of the unperturbed states generated agree reasonably well with the unperturbed energies of the states observed in this work, the errors being $\lesssim 50$ cm^{-1}. Also, the close resonance and tuning of the zero-order energies of the $|\nu_1\rangle$ and $|\nu_1,2_5\rangle$ states are observed in the calculated energies as well as the "cross-over"of the $|6_1,2_5\rangle$ state to higher energy than the $|7_1\rangle$ state. We believe therefore, that the anharmonic constants are reasonable and will adequately serve our purposes here.

The presence of states with highly excited CH bending (ν_5) character in the vicinity of the spectroscopically observed states is apparent from our calculation. In particular, states of the form $|(\nu - 2)_{CH}, 4_5\rangle$ (two less CH quanta) appear at ~ 300 cm^{-1} or less from the "pure overtone" in the $\nu_{CH} = 5$ region and these states move into very close resonance with $|\nu_{CH}\rangle$ at $\nu_{CH} = 7$. Many other states are generated in the proximity of the spectroscopic states, but we feel that to be reasonably important the states must be able to couple with the "pure" overtone or "strong coupling" combinations [$|(\nu - 1)_{CH}, 2_5\rangle$] via low order coupling terms and this, of course, implies low numbers of quanta to be exchanged. We note, however, that "branched" interactions, e.g., $|(\nu_{CH})\rangle \leftrightarrow |(\nu - 1)_{CH}, 2_5\rangle \leftrightarrow |(\nu - 2)_{CH}, 4_5\rangle \leftrightarrow |(\nu - 3)_{CH}, 6_6\rangle \leftrightarrow$ ..., can lead to mixing of states with very high rotational constants through terms which are of cubic order.

It is also possible that combination states of E symmetry mix with the "pure" overtone or combination ($|\nu - 1_{CH}, 2_5\rangle$) via

vibrational-rotational interactions. In each manifold of states arising from combinations with overtones of e-modes, there will be states of E symmetry which will possibly be able to couple with $|\nu_{CH}\rangle$ or $|\nu_{CH} - 1, 2_5\rangle$.

We have given a plausible qualitative explanation of the perturbed rotational constants observed for high overtones of CHD_3. However, the need for new quantitative theoretical calculations is strongly indicated by our experimental results and preliminary calculations.

4. Comparison with other CH-Containing Saturated Molecules

Combination bands of the form $|\nu_{CH}, 2_{bend}\rangle$ have been observed in the CH stretching overtone spectra of $CHCl_3$ and $CHBr_3$,[24] some lower alkanes,[26] haloethanes,[25] and dihalomethanes.[6] As shown by Fang and Swofford[24] the intensity of the combination band may be very large as a result of the Fermi resonance with a nearby "pure" CH stretching overtone. They have analyzed the first order shift of the combination band and obtained large negative anharmonic interaction constants: x_c (CH str, bend) = -31 ± 3 cm^{-1} ($CHCl_3$); -24 ± 5 ($CHBr_3$). Interestingly, the same interaction constant obtained in this work for CD_3H (x_{15} = -19.5 ± 3 cm^{-1}) is somewhat smaller but very comparable to the trihalomethane anharmonic constants. Similar values have been obtained for other molecules in the studies mentioned above.

Mørtensen et al.[6] have performed a theoretical analysis of the anharmonic coupling of the CH stretch and bending motions based on an effective G-matrix for the bending motion which accounts for the change in the effective mass for the bending motion when the CH stretch is

excited. However, this analysis predicted a decrease in bending frequency with the number of CH stretch quanta which was larger than that observed. This indicates, as they point out, that potential energy coupling is probably important also. From our analysis of the Fermi resonance in CDH_3 we find fairly large interaction matrix elements for the CH stretch-bend interaction and this interaction results largely from anharmaonic potential energy coupling. This result emphasizes the importance of both kinetic and potential energy coupling terms in the theoretical description of the CH stretch-bend interaction in the high energy region.

B. Other Deuterated Methanes

We have also obtained the $\Delta\nu = 6$ CH stretching overtone spectra (see Figure 3) for other gaseous deuteromethanes: CH_2D_2, CH_3D, and CH_4. The spectrum of CH_4 (Figure 3c) in this region has been obtained previously.[29,30] Our spectrum is in excellent agreement with the previous low resolution work, providing an independent check of our methodology.

The CH_2D_2 molecule is a very interesting one because of the different possible types of coupling. There exists a possibility for purely CH stretching resonance and near-resonance interactions between the identical CH bond modes in addition to interactions between the CH stretch and other lower frequency modes, as in the case of CHD_3. CH_2D_2 can serve as a test of the applicability of the local mode model in the high energy region. The spectrum presented in Figure 3a is quite simple; there exist basically two vibrational bands. The main band is

broadened relative to CHD_3 and the rotational structure is washed out into simple P, Q, and R bands. This congestion is expected since the molecule is an asymmetric top with near degeneracy in the moment of inertia: the rotational structure is complex, resulting in severe overlapping of the individual vibrational-rotational levels. The other vibrational band is weaker and without well-defined rotational structure. As for the assignment, these are two general possibilities: either the states are, in local mode language, the symmetric and antisymmetric combinations of the $|6,0\rangle$ states, where the two occupation numbers refer to the two local CH stretches, or one state is a "pure" local mode overtone, that is a superposition of the $|6,0\rangle_{\pm}$ states, and the other state is some local-normal combination band. Without a complete study of the lower vibrational overtones it is not possible to give a definite conclusion of this assignment. Some information is available from other studies which makes one possibility much more reasonable. First of all, the problem of the overtone spectroscopy and theory for two identical coupled X-H oscillators which share a common X atom has been addressed for other systems, for example for H_2O[4,5,31-33] and the dihalomethanes.[6,24] In the theoretical treatments, the local mode picture has been successfully used to describe the vibrational states of the two stretching oscillator system ranging from low ($\Delta\nu$ = 1,2) to higher energy ($\Delta\nu \geq 3$). This picture uses, as a basis, the properly symmetrized combinations of local bond stretching functions. The splitting of these symmetric and antisymmetric pure stretching states results primarily from direct coupling of the oscillators for $\Delta\nu$ = 1 and through mixing with higher energy vibrational configurations

(symmetrized local-local combinations) for $\Delta\nu \geq 2$. Since for higher energy states there is very weak direct first order coupling and since the splitting of symmetrized local-local combinations from the symmetrized overtone increase with increasing ν, (due to the large bond anharmonicity), it is found that the net splitting of the local mode doublets decreases with increasing ν under particular conditions (magnitude of interbond coupling < bond anharmonicity) thus resulting in increased localization of the vibrational energy with increasing ν.

The splitting of the fundamentals, $|1,0\rangle_{\pm}$ gives twice the interaction energy (X_{12}) of the CH oscillators, as is found by diagonalizing the appropriate 2 x 2 energy matrix. The CH stretching fundamentals of CH_2D_2 have been studied previously.[34] The energy of the $|1,0\rangle_{\pm}$ states were found to be 2975.5 cm^{-1} ($|1,0\rangle_{+}$) and 3012 cm^{-1} ($|1,0\rangle_{-}$). The splitting is 36.5 cm^{-1} and therefore the interbond coupling energy is x_{12} = 18.2 cm^{-1}. To estimate the bond anharmonicity we use the average energy of the $|1,0\rangle_{\pm}$ states (2993.7 cm^{-1}) and the observed value of the higher intensity transition in the $\Delta\nu_{CH} = 6$ region (16238 cm^{-1}) along with the simple Birge-Sponer relationship: $\Delta E = A\nu + B\nu^2$. We find that A $\sim$ 3052 cm^{-1} and that B, the bond anharmonicity is $\sim$ -58 cm^{-1}. Thus, for CH_2D_2 we see that $|X_{12}| < |B|$ and we would expect the splitting of $|\nu,0\rangle_{\pm}$ states to decrease with increasing ν. The states observed in the $\nu = 6$ region are split by 114 cm^{-1}, which is much larger than the 36.5 cm^{-1} fundamental splitting. On this basis it is much more reasonable to assign the higher energy band as due to unresolved absorption to $|6,0\rangle_{\pm}$ and the weaker lower energy band to a combination band of the form $|5,\{\nu_i\}\rangle$, where $\{\nu_i\}$ refers to a set of quanta in

non-CH stretching modes. We can now put an upper limit on the splitting of the $|6,0\rangle_+$ and $|6,0\rangle_-$ states of $<10\ cm^{-1}$.

Since symmetric (A_1) and antisymemtric (B_1) overtone states are allowed in electric dipole absorption for CH_2D_2, then combination states of A_1 or B_1 symmetry can mix via Fermi resonance with the corresponding overtone of the same symmetry. Several possible combination states exist which have correct symmetry, apporoximately correct energy and can mix with $|6_{CH}\rangle$ via low order terms and include $|5_{CH},2_9\rangle$ and $|5_{CH},1_3 + 1_4\rangle$. Accurate calculations of the energies are required to make a definite assignment.

The spectra of gaseous CH_3D and CH_4 are shown in Figures 3b and 3c are apparently much more congested than the spectra of CH_2D_2 and CHD_3 at the same quantum level. For CH_3D, a feature at longer wavelength than the main band peak can be seen. It is possible that this feature is a combination band similar to the longer wavelength band in the CH_2D_2 spectrum, but suffers greater overlap with the main band. The small band at shorter wavelength is probably the R branch of the main vibrational band.

The CH_3D overtone spectrum will be comprised primarily of A_1 and E symmetry-adapted combinations of the local model basis states $|\nu,0,0\rangle$, $|0,\nu,0\rangle$, and $|0,0,\nu\rangle$ where the occupation numbers refer to the three CH stretches. However, since the CH_3D $\Delta\nu_{CH} = 6$ spectrum is rather congested, in contrast to the CH_2D_2 spectrum, it is not possible to resolve these states at room temperature or to put a meaningful upper limit on their splitting. Therefore, we resort to the local model label for assignment purposes. The main band is identified as $|6_{CH}\rangle$ and some

possible combination states are $|5_{CH},2_3\rangle$, $|5_{CH},1_3,1_6\rangle$ and $|5_{CH},1_5,1_6\rangle$, again using the mode numbering of ref. 21.

The CH_4 = 6 spectrum (Figure 3c) is the most congested spectrum obtained in this study of some isotopic methanes. The low resolution spectrum obtained here does not allow identification of the number of band systems that are present. At higher resolution it is found that the band is made up of resolvable features,[29,30] but no identification of the various bands was given. From our studies of various deuteromethanes at $\Delta\nu_{CH}$ = 6, we conclude that the spectrum is not only rotationally congested but is vibrationally congested as well, probably involving two and possibly more band systems, the pure stretching overtone $|6_{CH}\rangle$ and combinations built of $|5_{CH}\rangle$, for example $|5_{CH},2_4\rangle$. However, the complete mechanism which results in the observed congested spectrum is still an unresolved issue.

C. $\Delta\nu_{CH}$ = 6 Overtone Spectra Neopentane

The $\Delta\nu_{CH}$ = 6 overtone spectrum of gaseous NPT is shown in Figure 4. The presence of several bands is clearly indicated in the spectrum. In order to determine the parameters (positions, heights and GWHM) of the various bands and to obtain information on the shapes of these bands, we have analyzed the spectra by using a non-linear least-squares regression. The spectra were fit to sums of Lorentzian functions and a flat baseline. The best fit values of the parameters were used to generate the components and computed function which are plotted with the experimental spectrum in Figure 4.

The best fit bandshape parameters are listed in Table VI along with a summary of some parameters of the $\Delta\nu_{CH}$ = 6 spectra of the other

molecules studied in this work. Reasonably good fits to the spectra were obtained using Lorentzian model functions, as is apparent from the agreement of the computed spectrum with experimental one in Figure 4. The parameters of the smaller peaks in the spectra are quite uncertain in some cases. The main interest in this work, however, is in the dominant peaks and these are resolved with reasonable precision from the bandshape analysis. The neopentane spectrum has been resolved by least-squares fitting into one main band at 15756 cm^{-1} and three other bands, each with less than 20% of the intensity of the main band.

As for the origin of the smaller bands in the NPT spectrum. the possibility of inequivalence splitting due to conformationally different CHs can be ruled out. The high molecular symmetry (T_d) is preserved even if one considers the structure of the methyl groups, for the lowest energy conformer. In other words, the methyl groups have identical environments, each with the three-fold axes about the C-C bonds preserved in the equilibrium geometry. Therefore, all hydrogens must be equivalent.

If one considers long range (i.e., intermethyl) CH coupling negligible, then the spectrum of NPT can be analyzed in terms of four equivalent, independent methyl groups, as has been done previously for TMS.[3] The description of the spectra then follows as explained above for CHD_3. The overtone transitions are dominated by A_1 and E combinations of the three local mode basis functions ($|\nu,0,0\rangle$, $|0,\nu,0\rangle$ and $|0,0,\nu\rangle$). However, the results obtained in this work for CH_2D_2 provide strong empirical evidence that the splitting of the symmetry adapted states $|6,0\rangle_{\pm}$ is less than 10 cm^{-1}. Since the splitting of the

bands in the NPT spectrum are > 50 cm^{-1}, it is very unlikely that the various bands represent the A_1 and E symmetry adapted states. Any splitting of these states is probably obscured due to the fairly large bandwidths (> 50 cm^{-1}) displayed by the main bands. Local-local combination bands, which involve quanta distributed in two or more CH stretches (e.g. |5,1,0>) can be ruled out as possibilities because they would fall outside the range of the scans presented (the shift of |5,1,0> from |6,0,0> would be 600 cm^{-1}. Therefore, it is argued that the overtone band is due to unresolved transitions to $|6,0,0\rangle_{A_1}$ and $|6,0,0\rangle_{E}$ and that the other bands are due to combinations of $|5,0,0\rangle_{A_1,E}$ and lower energy normal modes which are in Fermi-resonance with the "pure" overtones as described above for some of the deuteromethanes.

The assignment of the "pure" overtone in the NPT spectrum is straightforward if we associate this transition with the strongest band. The band at 15756 cm^{-1} is assigned as $|6_{CH}\rangle$. The observed band position agrees quite well with that predicted (15750 cm^{-1}) from the results of a previous study[35] of the lower overtones ($\Delta\nu_{CH}$ = 3-5) of gas phase NPT.

The assignments of the combinations are not as simple because of the large number of possibilities due to the relatively high number of vibrational degrees of freedom. Restricting the consideration to combinations which would require low numbers of quanta to be exchanged in mixing with $|6_{CH}\rangle$ allows some possible states to be identified. We have chosen combination states which are built on $|5_{CH}\rangle$ and have A_1 direct product representations for the normal mode components. These states would have no symmetry restrictions for coupling with $|6_{CH}\rangle$. Using the frequencies given by Snyder and Schachtsneider,[36] we find some

likely candidates for the assignments. These are indicated in Table VI. The normal modes are numbered in analogy with ref. 37: $\tilde{\nu}_2$ (a_1, 1368 cm^{-1}) is a symmetric CH_3 bend, $\tilde{\nu}_{14}$ (t_2, 1361 cm^{-1}) is a symmetric CH_3 bend, $\tilde{\nu}_{15}$ (t_2, 923 cm^{-1}) is a mixture of C-C stretch and CH_3 rock and $\tilde{\nu}_{16}$ (t_2, 1253 cm^{-1}) is a mixture of C-C stretch, CH_3 rock and symmetric CH bend.[36] These assignments are tentative and it should be noted that sizeable first-order anharmonic shifts of the combination bands are implied for each. the assignment suggested here is different from the assignment of the combinations given previously for the lower overtones.[35] In the previous work bands shifted from the pure overtone to higher and lower energy by $\sim$120 cm^{-1} were assigned to a torsional combination ($|\nu_{CH},1_\tau\rangle \longleftarrow |0_{CH},0_\tau\rangle$) and a torsional hot band ($|\nu_{CH},0_\tau\rangle \longleftarrow |0_{CH},1_\tau\rangle$), respectively. It is unlikely that bands shifted by 120 cm^{-1} from the "pure" overtone would be torsional sidebands since the torsional frequencies of NPT have been determined to be significantly higher from IR spectroscopy[38] (A_1, 221 cm^{-1} and T_1, 281 cm^{-1}), and inelastic neutron scattering[39] (A_2, 211 cm^{-1} and T_1, 276 cm^{-1}) and these results are in reasonable agreement. As these torsions are the lowest frequency normal modes of NPT one must then consider combinations built on lower CH stretching quanta for a reasonable assignment of the combinationals. However, it is conceivable that in our NPT spectrum the band at 15985 cm^{-1} is a torsional combination (229 cm^{-1} shift from $|6_{CH}\rangle$).

We have already mentioned that Lorentzian bandshape functions give a reasonable fit to the observed NPT $\Delta\nu_{CH} = 6$ spectrum. This can be taken as some evidence of homogeneous broadening of the bands in the

spectrum, as has been argued extensively in the literature. Further evidence for homogeneous broadening comes from the observation of the splitting ($\sim$ 25 cm^{-1}) of the OP and RS branches of the fundamental CH stretching bands.[40] This splitting is clearly much smaller than the observed widths ($\sim$ 100 cm^{-1}) of the main bands, suggesting that the inhomogeneous broadening due to rotational structure is negligible.

The bandwidths of the lower overtones ($\Delta\nu_{CH}$ = 3-5) of NPT vapor have been measured by Henry and Mohammadi.[35] These authors found values of the widths to be: 52 cm^{-1}, $\Delta\nu_{CH}$ = 3; 62 cm^{-1}, $\Delta\nu_{CH}$ = 4 and 64 cm^{-1}; $\Delta\nu_{CH}$ = 5. Their results would seem to indicate a possible saturation of the bandwidth for higher values of $\Delta\nu_{CH}$.[41] The results of our work suggest that this is not the case for the range which has been investigated ($\Delta\nu$ = 3-6). It is quite possible that the trend is nearly monotonically increasing linewidth with $\Delta\nu_{CH}$ over the range studied thus far.

The gas phase neopentane overtone bandwidths even at $\Delta\nu_{CH}$ = 3, are typically broader than the $\Delta\nu_{CH}$ = 5 overtone bandwidths for the methyl CHs of 1,2,4,5-tetramethylbenzene (durene) observed recently[7] at low temperature but are comparable to the durene methyl bandwidths at room temperature. In that work the effect of temperature on the durene methyl overtone bandwidths was qualitatively interpreted in light of recent related work on methyl group fundamentals.[42-44] The dependence was ascribed to torsional-dephasing due to the CH stretch frequency dependence on a thermal distribution of or population fluctuations in torsional modes of the methyl group. This other work provides an indication that the room temperature NPT overtone bandwidths may be

strongly influenced by dephasing processes rather than population relaxation. If that is the case then the observed bandwidth is determined by the total rate of dephasing[45] ($1/T_2$) which, for a two level system where the lower level is the ground state, is given by $(1/T_2) = (1/T'_2) + (1/2T_1)$, where T_2' is the pure dephasing time and T_1 is the population relaxation time of the excited level. Consequently the population relaxation time might be quite long relative to the one inferred from the bandwidth.

The question of overtone relaxation of molecules with hindered to free internal rotation of CH containing groups is clearly quite an interesting problem and deserves further experimental and theoretical investigation.

From measurements of the bandwidths of some rovibrational levels of CHD_3, a lower limit on the relaxation times of the highly excited states $\Delta v_{CH} = 5,6$ of this molecule can be extracted. For these levels a lower limit on the T_1 relaxation time of 5 ps was obtained.[10] Of course, this estimate neglects pure dephasing, but this can be rationalized since the self-broadening coefficient for some methane CH stretching overtones have been determined[29,30,46-49] to be 0.086 cm^{-1}/atm. Thus, at the pressures of our experiment collisional processes give a much smaller width than the resolution limited ones actually measured. Furthermore, for CHD_3 there are no internal rotations or very low frequency modes which might introduce fluctuations[42-44] in the CH stretch frequency. The inferred population relaxation time lower limit (5 ps) is long in comparison with those obtained from many previous studies of polyatomic molecules. Since the

value is only a lower limit the actual relaxation time could be much longer, perhaps approaching the collision-induced or even the radiative decay time, in which case the spectral linewidths would be Doppler limited. This conclusion is consistent with the discussion in Sec. 5.1 in Paper I. In contrast to what would be inferred from bandwidths of other molecules such as NPT, the CHD_3 bandwidths indicate that the excited states persist for a timescale that may be useful for influencing unimolecular or bimolecular reactions involving X-H bond breakage.

D. Combination Band in the $\Delta v_{CH} = 6$ Spectral Region of TMS

Early in our experimental work we observed absorption bands of TMS vapor. Later, we assigned the bands as originating from local mode-local mode combination bands, but we performed no further studies on this molecule. Since no experimental work on the high energy overtone spectroscopy of gas phase TMS has been previously reported, we describe here our observations. In Figure 5 the absorption spectrum of TMS vapor over the range of 16150-16580 cm^{-1} is presented. This spectrum has been analyzed as above for NPT by using a least-squares analysis with Lorentzian model bandshape functions. The results of this analysis are included in Table VI. The spectrum is seen to be comprised of two main bands of almost equal intensity and several minor bands. By comparison of the band position with previous liquid phase work[3] and with work on gas to liquid shifts of NPT overtones,[35] we conclude that the main bands have largely local-mode local-mode combination band $|(5,1)_{CH}\rangle$ character. Five CH stretching quanta are in one oscillator

and another oscillator on the same methyl group is simultaneously excited with one quantum. Burberry and Albrecht[3] have calculated the splitting of the symmetrized $|(5,1)_{CH}\rangle$ states (A_1, E) to be ~ 2 cm^{-1}, and it is therefore unlikely that the observed splitting has that origin. We tentatively assign the lower energy main band as $|(5,1)_{CH}\rangle$ and the higher energy one as a local-normal combination built on either $|5_{CH}\rangle$ or $|6_{CH}\rangle$.

IV. Conclusions

We now summarize the conclusions reached in this work.

1) The high energy overtone spectra ($\Delta\nu_{CH}$ = 5,6 and 7) of CHD_3 are strongly affected by Fermi-Resonance of the "pure" overtone $|\nu_{CH}\rangle$ with combinations $|\nu_{CH} - 1,2_5\rangle$ and $|\nu_{CH} - 1,1_5,1_6\rangle$. The spectra are reasonably well analyzed using degenerate perturbation theory. This analysis yields values for some of the interaction matrix elements and first order energies of the combination bands. There are large first-order shifts of the combination bands which also result from interactions of the CH stretch and bending vibrations. The shift is roughly in agreement with the scaling with ν_{CH} given by first order perturbation theory. Very congested spectra are obtained for the ν_{CH} = 7 region which indicate that in this region there is extensive vibrational mixing.

2) The fair success of the simple analysis of the CHD_3 overtone spectra in terms of Fermi resonances is in contrast with the failure of such an approach to describe the derived rotational constants (Paper I). This discrepancy is rationalized in terms of interactions with other weakly coupled combinations of high rotational B' constant. Preliminary

calculations support the possibility that such combinations involve high excitation of the ν_5 bending vibration and two or more quanta less in the CH stretch.

3) A lower limit of 5 ps for the population relaxation time has been obtained from the CHD_3 bandwidths. This indicates that the population relaxation is very slow for this small polyatomic molecule and that pumping of overtones of such small molecules may be useful, for example in enhancing bimolecular reactions such as hydrogen abstraction via collisions with scavengers.

4) The spectrum of CH_2D_2 in the region around $\nu_{CH} = 6$ indicates two bands which are assigned in analogy with the bands of CHD_3. There is no splitting observed of the $|6_{CH}\rangle_{\pm}$ states. This observation allows an upper limit (determined by the width of the Q branch) of the splitting of ~ 10 cm^{-1} to be established. This result is in agreement with the results of other work (vide supra) which indicate similar small splittings of the symmetrized local mode states for several two CH oscillator molecules.

5) Comparison of the $\nu_{CH} = 6$ spectra of CHD_3, CH_2D_2, CH_3D and CH_4 indicate increasing spectral congestion with increasing numbers of hydrogens. Rotational and vibrational congestion have been implicated, however, further work is required to identify the actual mechanism of congestion.

6) The $\nu_{CH} = 6$ spectrum of NPT is analyzed by least-squares fitting to Lorentzian bandshapes and yields a width of 107 ± 3 cm^{-1} for the $|6_{CH}\rangle$ state. The bands are argued to be homogeneously broadened, however dephasing processes induced by torsional motions of the methyl

groups may be making a substantial contribution so the width does not necessarily give the lifetime. Smaller bands in the spectrum are tentatively assigned as combinations of the form $|5_{CH}, \{\nu_i\}>$ with $\{\nu_i\}$ referring to various normal modes such as CH_3 bending or possibly modes involving C-C stretching.

This study of high overtone spectra of small and medium sized methyl containing molecules in the gas phase has yielded some interesting results. Further theoretical and experimental work should benefit from this base of information.

REFERENCES

1. B. R. Henry, Acc. Chem. Res., **10**, 207 (1977).
2. For reviews see:
   a) B. R. Henry, Vib. Spectra. Struct., **10**, 269 (1981).
   b) M. L. Sage and J. Jortner, Adv. Chem. Phys., **47**, 293 (1981).
   c) H. L. Fang and R. L. Swofford, Adv. in Laser Spectroscopy, Vol. I, Ed. B. A. Garetz and J. R. Lombardi, Heyden & Son, Ltd., Philadelphia, (1982).
3. M. S. Burberry and A. C. Albrecht, J. Chem. Phys., **71**, 4631 (1979).
4. H. S. Moller and O. Sonnich Mørtensen, Chem. Phys. Lett., **66**, 539 (1979).
5. R. T. Lawton and M. S. Child, Mol. Phys., **40**, 773 (1980).
6. O. Sonnich Mørtensen, B. R. Henry and M. Ali Mohammadi, J. Chem. Phys., **75**, 4800 (1981).
7. J.W. Perry and A. H. Zewail, J. Phys. Chem., **85**, 933 (1981); ibid, **86**, 5197 (1982).
8. K. V. Reddy, D. F. Heller and M. J. Berry, J. Chem. Phys., **76**, 2814 (1982).
9. J. W. Perry and A. H. Zewail, J. Chem. Phys. **70**, 582 (1979); Chem. Phys. Lett., **65**, 31 (1979).
10. D. J. Moll, J. W. Perry, A. Kuppermann and A. H. Zewail, J. Chem. Phys., submitted.
11. G. Herzberg, Infrared and Raman Spectra, Van Nostrand, Princeton, 1945. a) p. 306, b) p. 215, c) p. 210.
12. W.S. Benedict, K. Morikawa, R. S. Barnes and H. S. Taylor, J. Chem. Phys., **5**, 1 (1937).

13. D. G. Rea and H. W. Thompson, Trans. Faraday Soc., **52**, 1304 (1956).

14. T. A. Wiggins, E. R. Shull, Jean. M. Bennett and D. H. Rank, J. Chem. Phys., **21**, 1940 (1953).

15. L. F. H. Bovey, J. Chem. Phys., **21**, 830 (1953).

16. H. C. Allen, Jr. and K.E. Plyler, J. Res. Nat. Bur. Stand. Sect. A, **63A** (2), 145 (1959).

17. H. W. Kattenberg and S. Broderson, J. Mol. Spectrosc., **59**, 126 (1976).

18. D. E. Jennings and W. E. Blass, J. Mol. Spectrosc., **55**, 445 (1975).

19. J. K. Wilmhurst and H. J. Bernstein, Can. J. Chem., **35**, 226 (1957).

20. J. Dupre-Maquaire, J. Dupre and G. Tarrago, J. Mol. Spectrosc., **96**, 63 (1981).

21. D. L. Gray and A. G. Robiette, Mol. Phys., **37**(6), 1901 (1979).

22. The CHD_3 molecule is a special case in that the CH stretch internal coordinate is directed along the principal symmetry axis of the molecule, therefore the CH stretch coordinate is totally symmetric for either a local or normal mode model. The state symmetries and selection rules for C_3v will hold for either model.

23. E. B. Wilson, J. Decius and P. Cross, "Molecular Vibrations", McGraw-Hill, Co., New York (1955), p. 197.

24. H. L. Fang and R. L. Swofford, J. Chem. Phys., **72**, 6382 (1980).

25. B. R. Henry and M. Ali Mohammadi, Chem. Phys., **55**, 385 (1981).

26. H. L. Fang and R. L. Swofford, J. Chem. Phys., **73**, 2607 (1980).

27. J. L. Duncan, D. Ellis and I. J. Wright, Mol. Phys., **20**, 673 (1971).

28. J. W. Perry and A. H. Zewail, to be published.

29. G. Stella, J. Gelfand and Wm. Hayden Smith, Chem. Phys. Lett., **39**, 146 (1976).

30. J. Gelfand, W. Hermina and Wm. Hayden Smith, Chem. Phys. Lett., **65**, 201 (1979).

31. R. Wallace, Chem. Phys., **11**, 189 (1975).

32. M. L. Elert, P. R. Stannard and W. M. Gelbart, J. Chem. Phys., **67**, 5395 (1977).

33. A. A. Ovchinnikov and N. S. Erikman, Opt. Spectrosc., **34**, 690 (1973); ibid., **34**, 887 (1973).

34. J. C. Deroche and G. Guelachvilli, J. Mol. Spectrosc., **56**, 76 (1975).

35. B. R. Henry and M. Ali Mohammadi, Chem. Phys. Lett., **75**, 99 (1980).

36. R. G. Snyder and J. H. Schachtsneider, Spectrochimica Acta., **21**, 169 (1965).

37. K. Shimizu and H. Murata, J. Mol. Spectrosc., **5**, 44 (1960).

38. J. R. Durig, S. M. Craven and J. Bragin, J. Chem. Phys., **52** 2046 (1970).

39. C. I. Ratcliffe and T. C. Waddington, J. Chem. Soc. Farad. Trans. II, **72**, 1821 (1976).

40. S. Sportouch, C. Lacoste and R. Gaufres, J. Mol. Struct., **9**, 119 (1971).

41. We have attempted to estimate the bandwidths of the NPT CH overtones reported in ref. 35 from the figures given in that publication. Whereas we obtained values in good agreement with the reported ones for $\Delta\nu_{CH} = 3$ and 4, it was found that the value for $\Delta\nu_{CH} = 5$ is 95 ± 20 cm^{-1}, depending on the choice of the baseline. In our computer fitting of the $\Delta\nu_{CH} = 6$ bands, we employed fits using four bands, but the converged fits consistently gave one main band and several smaller ones. In ref. 35 the authors report that three bands were used to fit the spectrum. It is possible that a fit using several bands each making large contributions could explain the discrepancy in the estimated and reported widths. The relative areas of the components are not given in ref. 35, so it is not possible to reach a conclusion on this. In any case, they also give a value, said to be obtained directly from the spectrum, of 64 cm^{-1}. We feel that there is some problem with this value, or with the spectrum, and that more information is required to resolve this matter.

42. S. Marks, P. A. Cornelius and C. B. Harris, J. Chem. Phys., **73**, 3069 (1980).

43. D. Cavagnat and J. Lascombe, J. Chem. Phys., **76**, 4336 (1982).

44. R. A. MacPhail, R. G. Snyder and H. L. Strauss, J. Chem. Phys., **77**, 1118 (1982).

45. M. J. Burns, W.-K. Liu and A. H. Zewail, in Spectroscopy and Excitation Dynamics of Condensed Matters, series in Modern Problems in Condensed Matter Sciences, Vol. 4, eds., V. M. Agranovich and R. M. Hochstrasser (North-Holland Publishing Co., Amsterdam-New York-Oxford, 1983), p. 301.

46. J. Margolis, J. Quant. Spectrosc. Radiat. Transfer, **11**, 69 (1971).

47. P. Varansi, J. Quant. Spectrosc. Radiat. Transfer, **11**, 1711 (1971).

48. L. Darnton and J. Margolis, J. Quant. Spectros. Radiat. Transfer, **13**, 969 (1973).

49. G. Kramer and C. O. Weiss, Z. Physik, **271**, 311 (1974).

TABLE I - Fundamental and overtone states for CHD_3

State	Symmetry	ΔE^a	Ref.
$\|1_1\rangle$	A_1	2,992.2	12,13
$\|1_2\rangle$	A_1	2,142.6	18
$\|1_3\rangle$	A_1	$\sim$ 1,003	19
$\|1_4\rangle$	E	2,250.9	17
$\|1_5\rangle$	E	1,292.4992	20
$\|1_6\rangle$	E	$\sim$ 1,036	19
$\|2_1\rangle$	A_1	5,865.02	14
$\|3_1\rangle$	A_1	8,623.31	15
$\|4_1\rangle$	A_1	11,266.9	15
$\|2_5\rangle_E$	E	2,592,62	16
$\|2_5\rangle_A$	A_1	2,564.6	16

a) Band origins given in vacuum wavenumbers.

TABLE II - States observed for CHD_3 in this work

$\Delta\nu_1$ Region	ΔE[a]	Assignment[b]
5	13,801.1 (1.0)	$\|5_1\rangle$
	13,668.1 (1.0)	$\|4_1, 2_5\rangle$
6	16,230.1 (1.0)	$\|6_1\rangle$
	16,156.4 (1.0)	$\|5_1, 2_5\rangle$
7	18,532.0 (1.0)	$\|6_1, 2_5\rangle$
	18,473.0 (2.0)[c]	$\|7_1\rangle$
	18,352.4 (1.0)[c]	$\|6_1, 1_5, 1_6\rangle$

a) Q branch origins in vacuum wavenumbers, see paper I.
b) See text for discussion, only parentage is indicated by assignment.
c) Q branch peak position given instead of Q branch origin.

TABLE III - Least squares parameters[a] of linear fits to the Birge-Sponer plot for CHD_3CH stretching harmonics

Fit 1:[b]	$A_1 = 3050.1 \pm 0.9$
	$B_1 = -58.5 \pm 0.3$
	$cR = -0.99997$
	$^{d}S_{y.x} = 0.7$
Fit 2:[e]	$A_1 = 3048.2 \pm 0.2$
	$B_1 = -57.9 \pm 0.1$
	$R = -1.00000$
	$S_{y.x} = 0.1$
Fit 3:[f]	$A_1 = 3049.9 \pm 2.2$
	$B_1 = -58.2 \pm 0.5$
	$R = -0.9998$
	$S_{y.x} = 2.6$

a) All parameters except the correlation coefficient in cm^{-1}.

b) Fit of 4 points, $E|1_1>$ through $E|4_1>$.

c) Linear correlation coefficient.

d) Standard error in a calculated E/ν.

e) Fit of 3 points, $E|2_1>$ through $E|4_1>$.

f) Fit of 7 points, $E|1_1>$ through $E|7_1>$.

TABLE IV - Observed and calculated energies for CHD_3 CH stretch overtones.

State	ΔE_{obs}[a]	ΔE_{calc}[a,b]	Dev.
$\|1_1\rangle$	2,992.24	2,990.34	1.9
$\|2_1\rangle$	5,865.02	5,864.90	0.12
$\|3_1\rangle$	8,623.31	8,623.09	-0.37
$\|4_1\rangle$	11,266.9	11,266.68	0.22
$\|5_1\rangle$	13,801.2	13,793.90	7.3[c]
$\|6_1\rangle$	16,230.1	16,205.34	24.8[c]
$\|7_1\rangle$	18,473.0	18,501.00	-28.0[c]

a) Units are in vacuum wavenumbers.
b) Calcualted using parameters from fit 2 of Table III.
c) These values are taken as Fermi resonance shifts.

TABLE V - Energies of CHD_3 $|\nu_1, 2_5\rangle$ CH stretch-bend combinations

State	ΔE_{obs}	ΔE_{corr}[a]	ΔE_{calc}[b]	$\Delta E^{(1)}_{obs}$[c]	$\Delta E^{(1)}_{calc}$
$\|4_1,2_5\rangle$	13,668	13,676	13,821	-156	-155
$\|4_1,2_5\rangle$	16,156	16,181	16,359	-177	-195
$\|6_1,2_5\rangle$	18,532	18,501	18,770	-269	-234

a) Fermi resonance corrected wavenumbers.
b) Calculated using parameters from fit 2 of Table II and values from Table I.
c) Value defined as $\Delta E_{corr} - \Delta E_{calc}$.
d) Estimated from a numerical analysis of the 3-level Fermi resonance analysis.

TABLE VI. Parameters of bands observed in $\Delta\upsilon_{CH}$=6 Spectral Region.

Molecule	ΔE[a]	FWHM[a]	A_{rel}	Assignment
CHD_3	16,230.1 (1.0)[b]	<1	1.00	$\|6_1\rangle$
	16,156.4 (1.0)		1.55	$\|5_1 2_5\rangle$
CH_2D_2	16,238 (5)	~20	---	$\|6_{CH}\rangle$ ±
	16,124 (5)			$\|5_{CH} 2_9\rangle$ or $\|5_{CH}, 1_3 1_4\rangle$
CH_3D	16,226 (10)	---	---	$\|6_{CH}\rangle$ A_1/E
	16,161 (10)			$\|5_{CH}, 2_3\rangle$ or $\|5_{CH}, 1_3 1_6\rangle$
CH_4	16,179 (10)	---	---	$\|6_{CH}\rangle$
	16,137 (10)			$\|5_{CH} 2_4\rangle$
NPT	15,985 (20)[c]	95 (70)[c]	0.05 (0.05)[c]	$\|5_{CH}, 2_{14}\rangle$ or $\|5_{CH} 2_2\rangle$
	15,810 (4)	42 (12)	0.09 (0.05)	$\|5_{CH}, 2_{16}\rangle$
	15,756 (3)	107 (3)	1.00 (0.10)	$\|6_{CH}\rangle$
	15,637 (10)	101 (20)	0.19 (0.08)	$\|5_{CH}, 1_{14}, 1_{15}\rangle$
TMS	16,559 (5)	37 (17)	0.10 (0.05)	LM-NM comb.
	16,468 (3)	59 (7)	0.96 (0.10)	LM-NM comb.
	16,412 (3)	48 (6)	1.00 (0.10)	$\|5_{CH} 1_{CH'}\rangle$
	16,361 (5)	23 (2)	0.07 (0.02)	?
	16,205 (20)	65 (60)	0.10 (0.10)	?

[a]Values given in cm^{-1}.

[b]Errors given are 2 standard deviations.

[c]Errors given are 3 standard deviations.

Figure 1. Pulsed photoacoustic CH-stretching overtone spectra of CHD_3. All spectra in this work are of samples at a temperature of 25°C and have been normalized for laser power. The vertical scales are in arbitrary units and vary from spectrum to spectrum. The vertical lines in the spectra mark the first-order positions of the levels and the arrows indicate the Fermi resonance shifts.

a) Spectrum of $\Delta v_{CH} = 5$ region. The sample pressure was 370 torr. The spectrum is an average of two scans.

b) Spectrum of $\Delta v_{CH} = 6$ region. The sample pressure was 370 torr. The spectrum is an average of three scans.

c) Spectrum of $\Delta v_{CH} = 7$ region. The sample pressure ws 1385 torr. The spectrum is an average of four scans. On this spectrum only the first-order position of the "pure" overtone $|7_1\rangle$ is indicated.

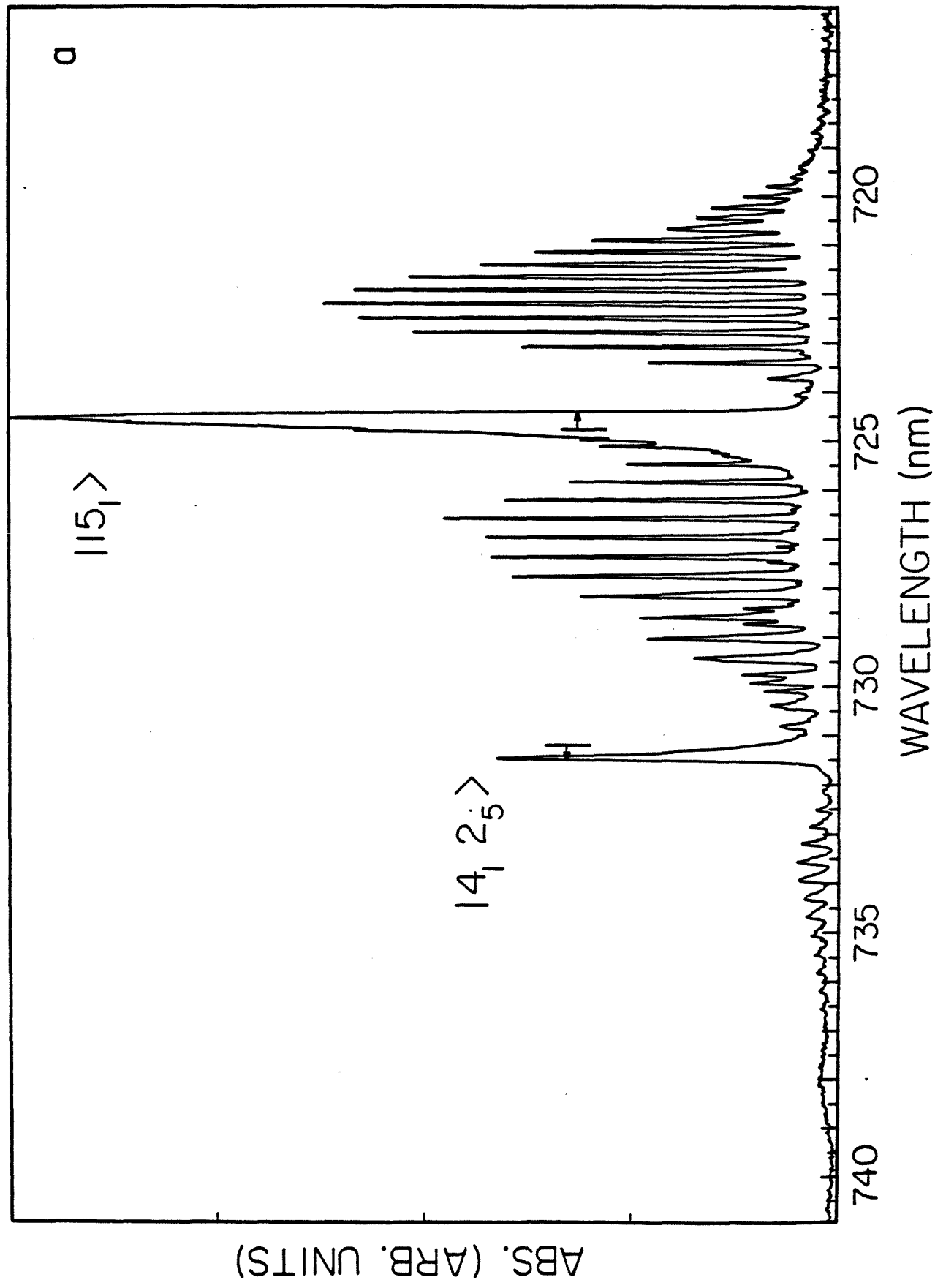
a
11^5_1
$14_1\,2_5$
740
735
730
725
720
WAVELENGTH (nm)
ABS. (ARB. UNITS)

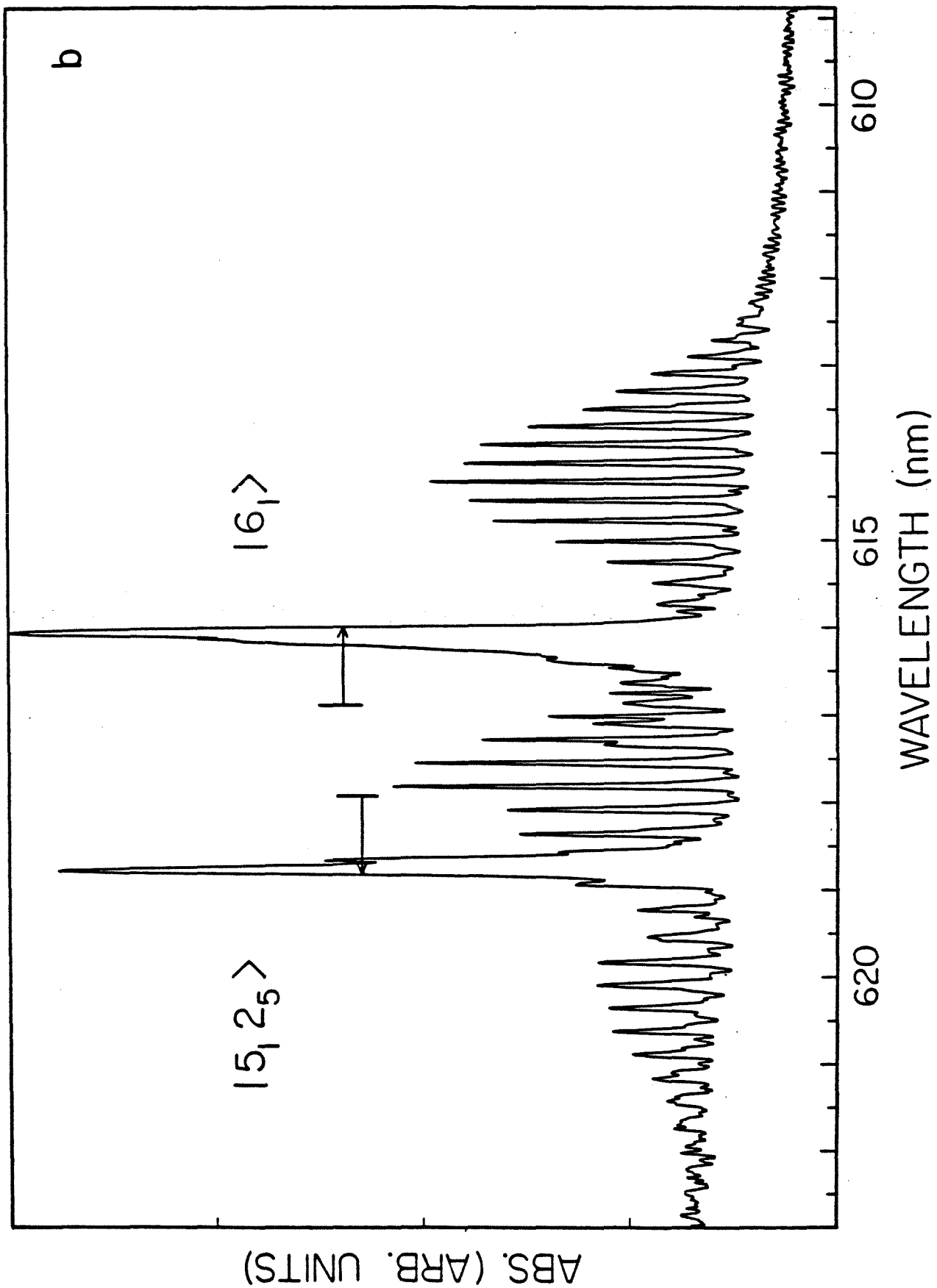
b
16_1
$15_1 2_5$
620
615
610
WAVELENGTH (nm)
ABS. (ARB. UNITS)

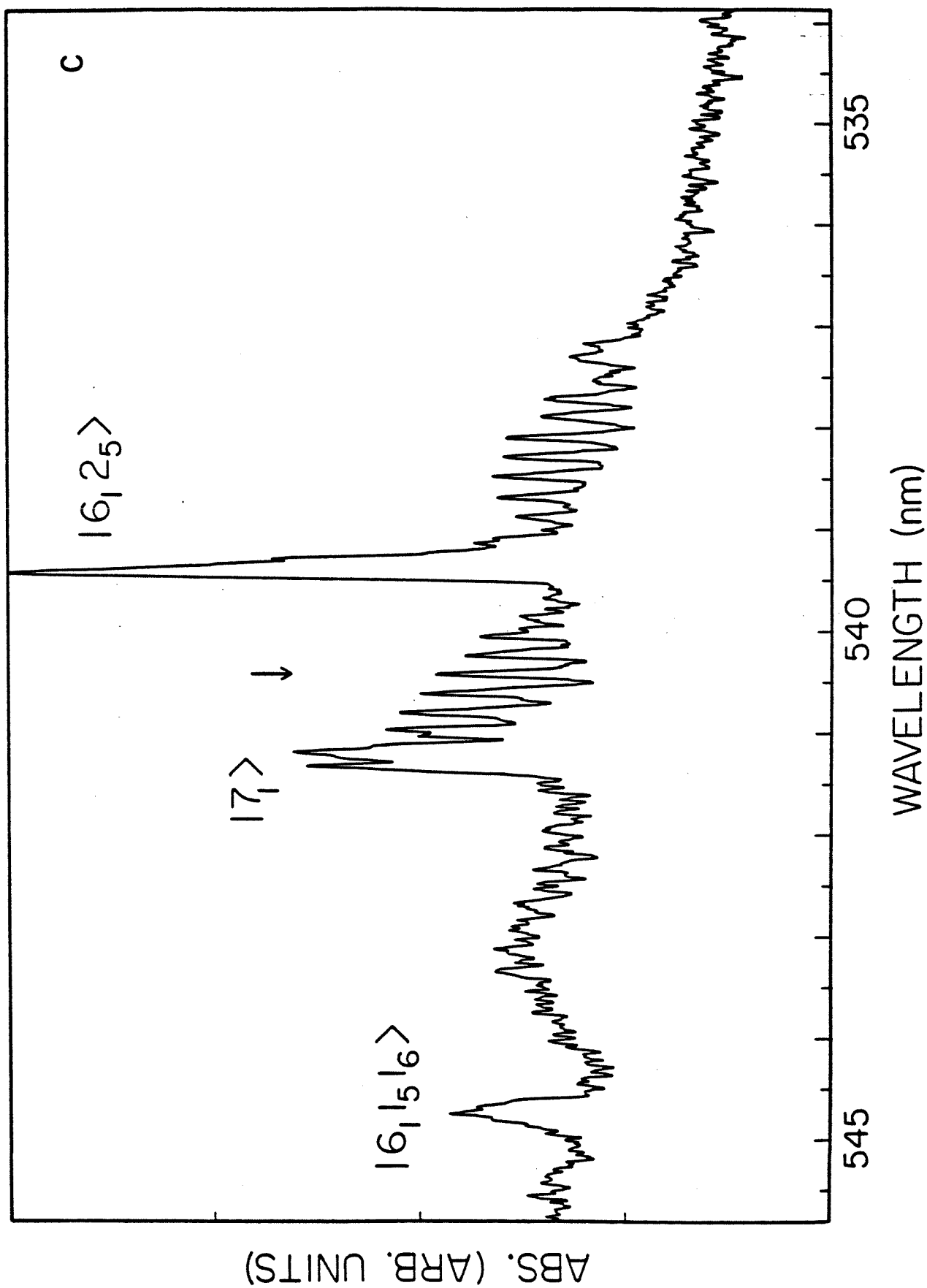
c
$16_1 2_5$
17_1
$16_1 1_5 1_6$
545
540
535
WAVELENGTH (nm)
ABS. (ARB. UNITS)

Figure 2. Birge-Sponer plot ($\Delta E/\nu$ vs. ν) for CHD_3 CH stretching fundamental and overtones. The symbols are defined as follows: ● , our data, "pure" overtone or fundamental; ◙ , previous data; ◉ , our data, combination bands.

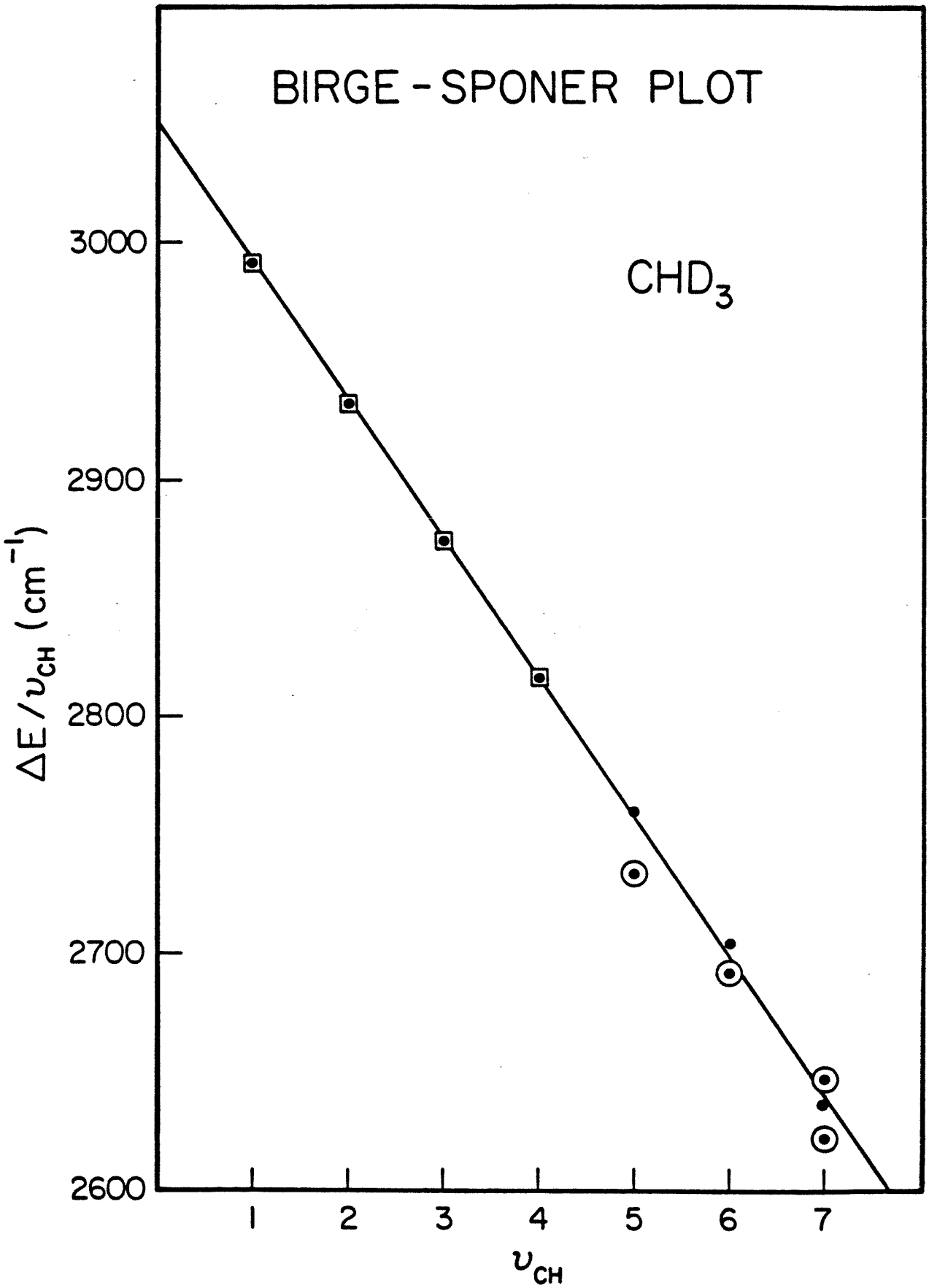
BIRGE - SPONER PLOT
CHD3
3000
2900
2800
2700
2600
ΔE / υCH (cm-1)
1
2
3
4
5
6
7
υCH

Figure 3. Pulsed photoacoustic CH stretching overtone spectra of a) CH_2D_2, b) CH_3D and c) CH_4 vapors in the $\Delta\nu_{CH} = 6$ region.

a) The sample pressure was 330 torr. The spectrum is an average of four scans.

b) The sample pressure was 370 torr. The spectrum is an average of five scans.

c) The sample pressure was 300 torr. The spectrum is an average of five scans. All sample temperatures were 25°C.

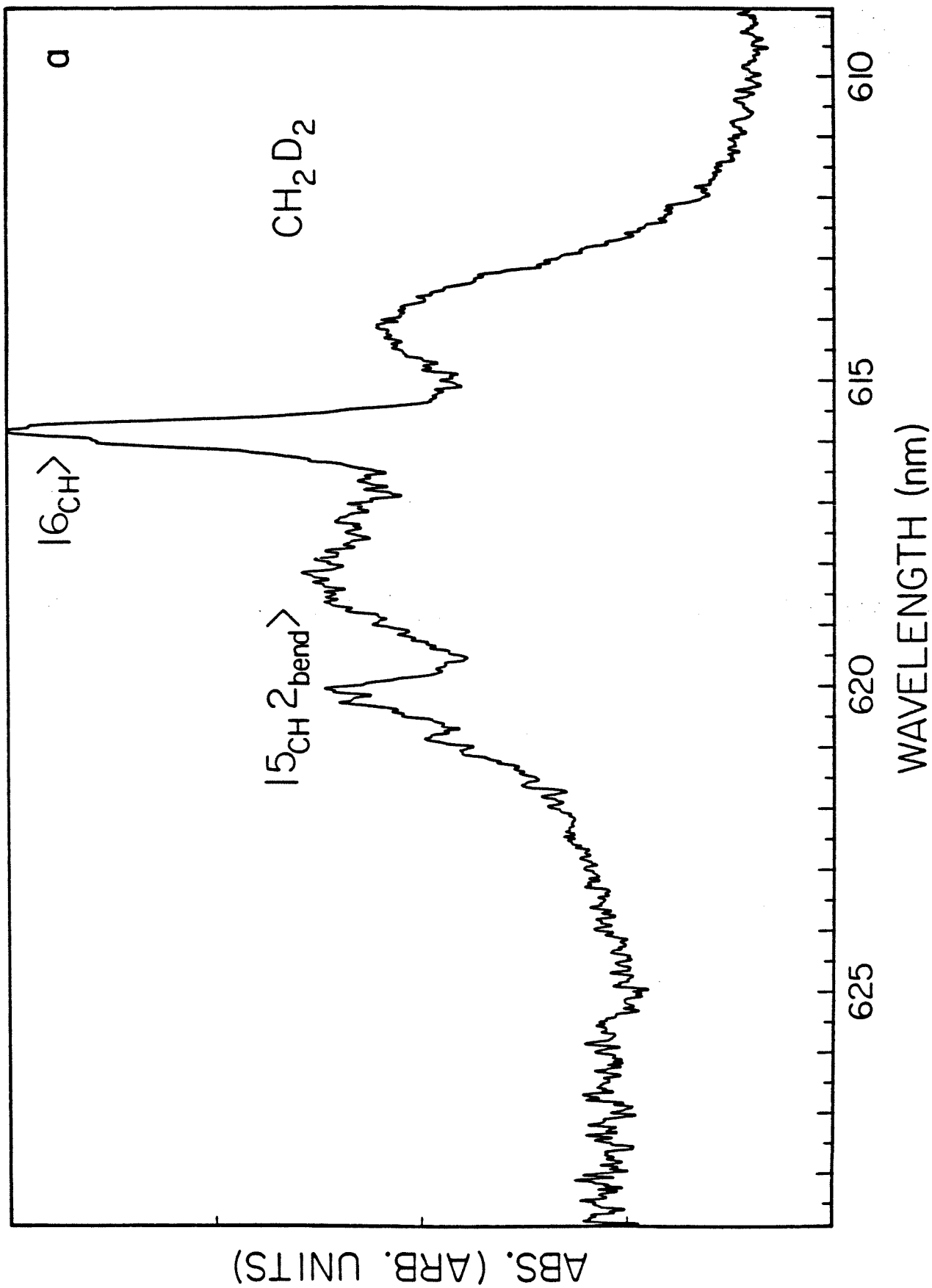
a
CH_2D_2
$|6_{CH}\rangle$
$|5_{CH}2_{bend}\rangle$
610
615
620
625
WAVELENGTH (nm)
ABS. (ARB. UNITS)

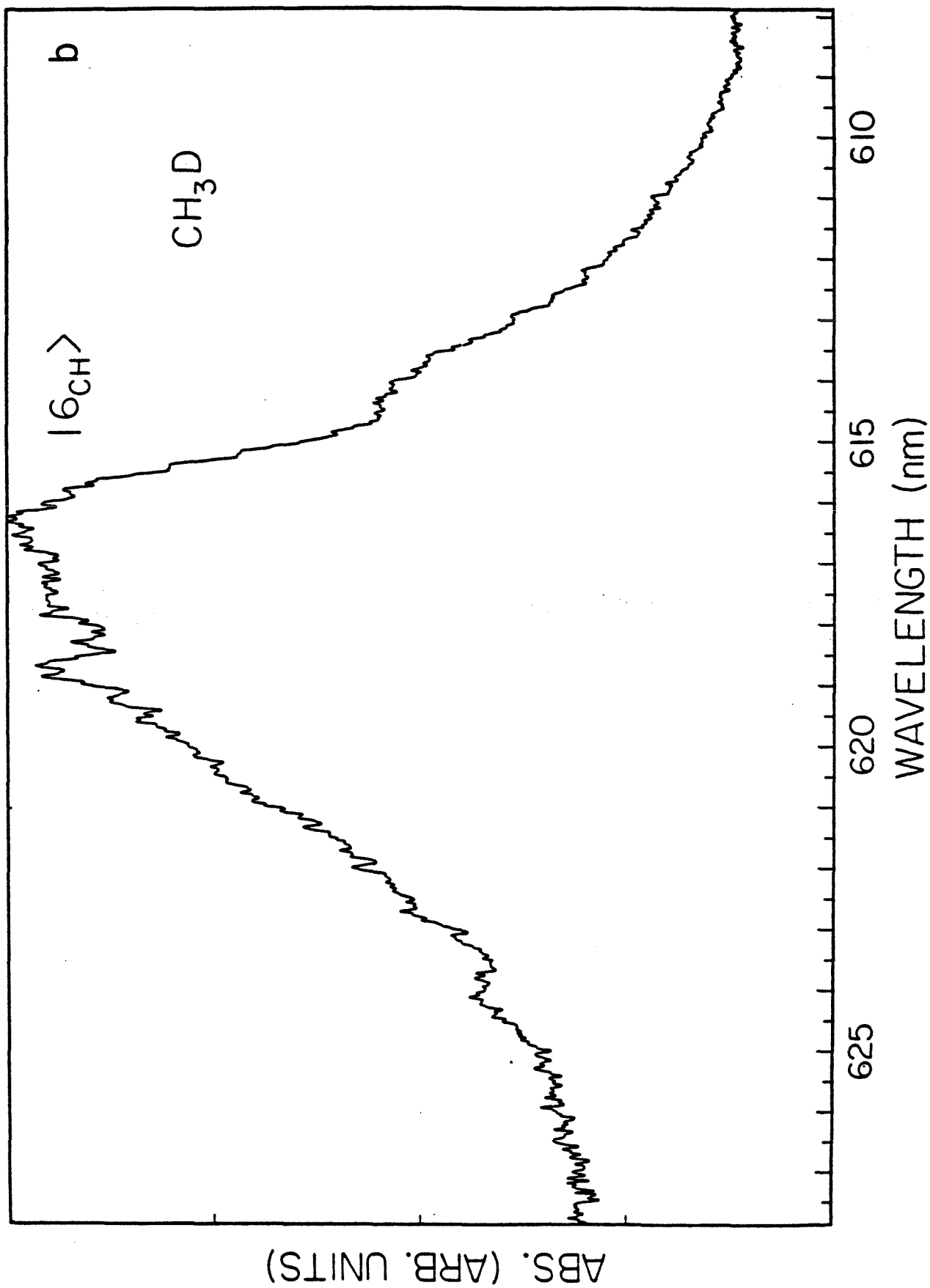
b
CH_3D
$|6_{CH}\rangle$
625
620
615
610
WAVELENGTH (nm)
ABS. (ARB. UNITS)

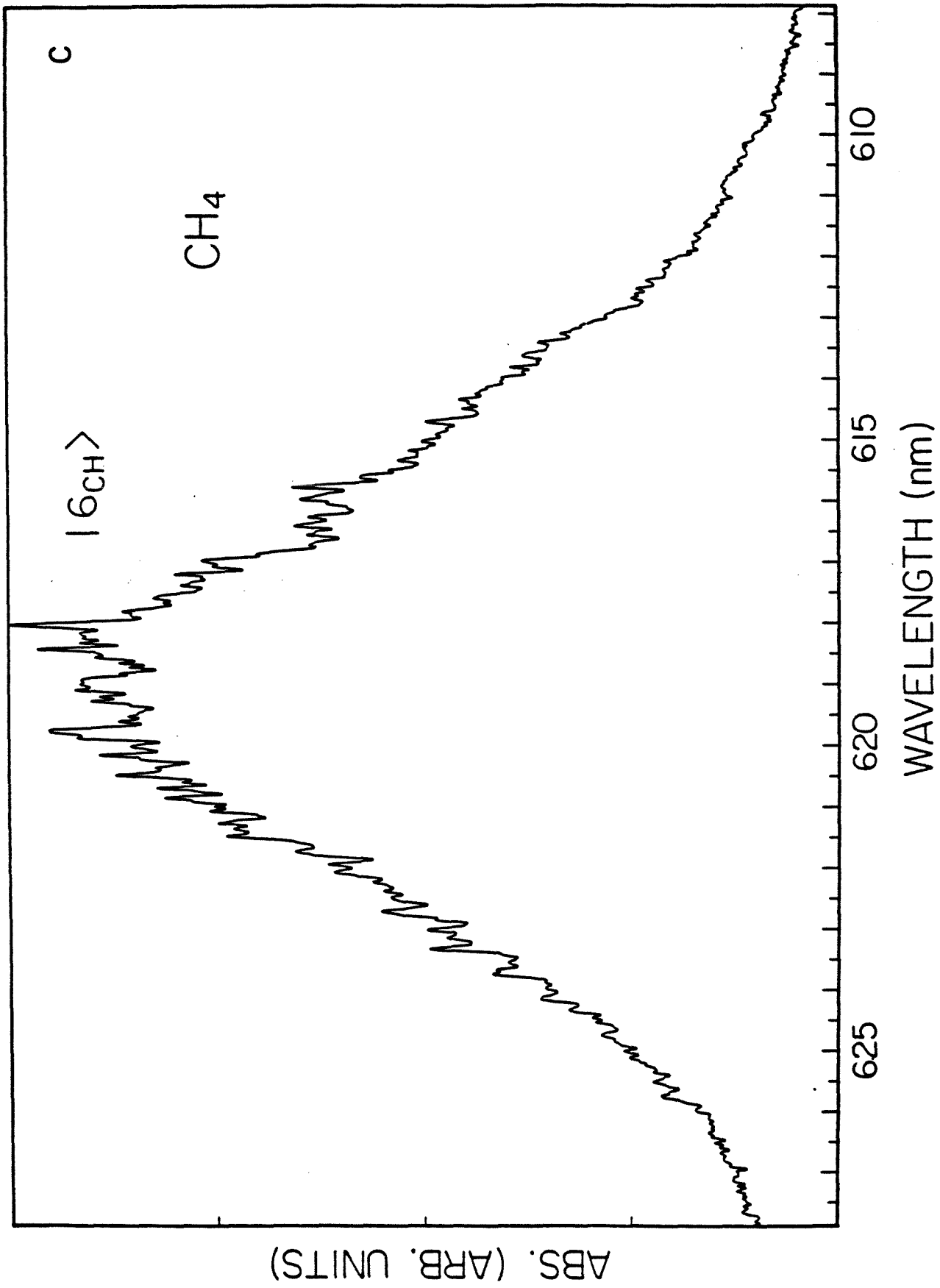
c
CH4
16CH>
ABS. (ARB. UNITS)
625
620
615
610
WAVELENGTH (nm)

Figure 4. Pulsed photoacoustic CH stretching overtone spectrum of neopentane vapor in the $\Delta\nu_{CH} = 6$ region. The sample pressure was 760 torr and the temperature was 25°C. The spectrum is an average of three scans. The points are the experimental data and the smooth curve is a sum of the Lorentzian components and baseline.

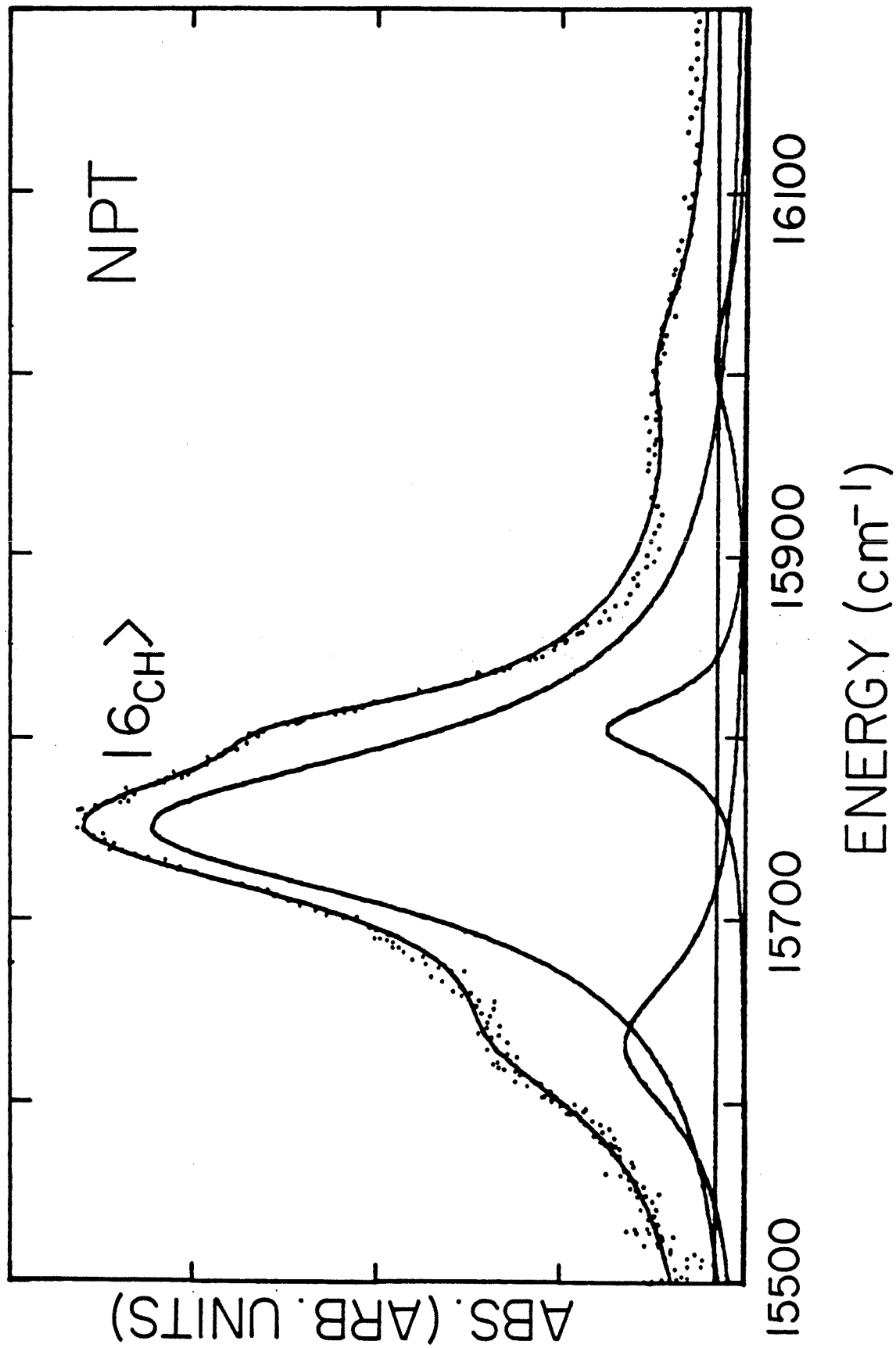
NPT
16_{CH}
ABS. (ARB. UNITS)
15500
15700
15900
16100
ENERGY (cm^{-1})

Figure 5. Pulsed photoacoustic spectrum of tetramethylsilane vapor in the region of the |5,1> CH stretching combination band. The sample pressure was 100 torr and the temperature was 25°C. The spectrum is an average of three scans. The points are the experimental data and the smooth curve is a sum of the Lorentzian components and baseline.

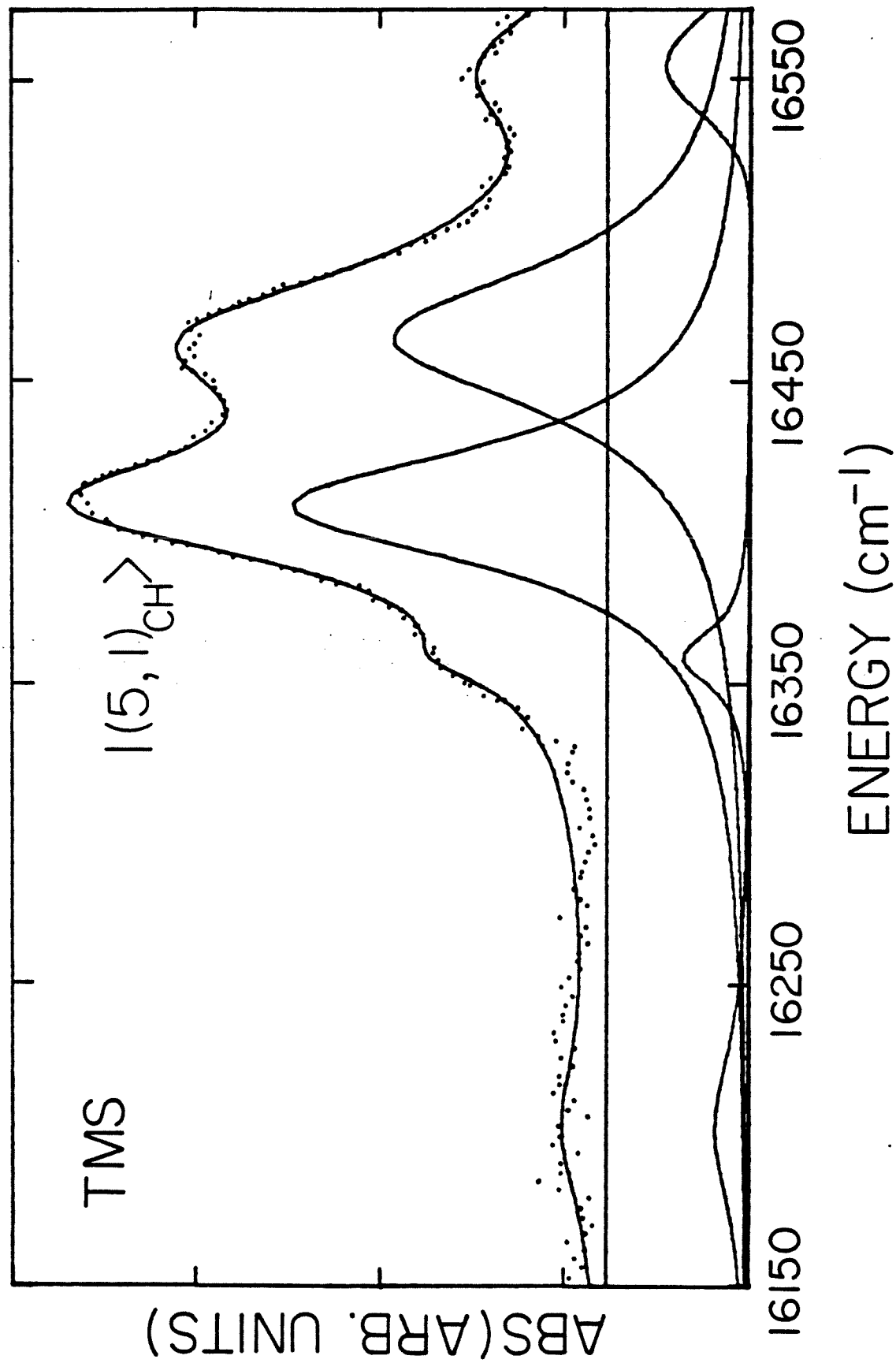
TMS
$|(5,1)_{CH}\rangle$
ABS(ARB. UNITS)
16150
16250
16350
16450
16550
ENERGY (cm^{-1})

Chapter VI

xsecond Pump-Probe Multiphoton Ionization of lated Molecules: A New Method for the Study of Ultrafast Intramolecular Processes

ABSTRACT

Picosecond time-resolved multiphoton ionization spectroscopy of isolated trans-stilbene and aniline is reported. Nonexponential decay of trans-stilbene is observed and evidence for collisionless vibrational energy redistribution is presented. The results are modelled using a population rate equation analysis of the time-delayed multiphoton ionization process. The rate of IVR is found to be about 0.5 * 1012s-1at 296K. Also, the excess energy dependence of the isomerization rate is determined for total vibrational energy of 2000 to 4500 cm-1; comparisons with calculated thermally averaged rates and rates of jet-cooled molecules are made.

This chapter is based on a recent paper by J.W. Perry, N.F. Scherer and A.H. Zewail (Chem. Phys. Lett., in press, Dec. 1983).

I. INTRODUCTION

This chapter reports new results from an experiment designed to directly measure the rate of intramolecular vibrational-energy redistribution (IVR) and/or coherence decay in isolated molecules with varying amounts of excess vibrational energy. Time-resolved fluorescence experiments with picosecond excitation of jet-ccoled anthracene molecules have been reported[1,2] for low to moderate excess energies (typically 0-2000 cm^{-1}) and from these studies it was shown that at low excess (< 2000 cm^{-1}) IVR is restricted to certain modes on the timescale of hundreds of picoseconds. At higher energy, however, IVR is expected to be faster and no direct time domain measurements of this fast IVR have been reported for isolated large molecules. For these reasons we develop the method of picosecond pump-probe multiphoton ionization as a direct probe of IVR. Furthermore, with intense picosecond pulses we can explore the importance of coherence effects in the multiphoton processes and learn about the various relevant timescales. The time resolution of our apparatus is about 2 ps and the peak power of the pulse can be up to about 10^4 gigawatts/cm^2.

The idea of the experiment can be described as follows. A picosecond pulse excites molecules into vibrational levels of S_1. Because of IVR (rate constant k), some molecules will redistribute the vibrational energy into a new distribution of states thus yielding a set of vibrationally-equilibrated levels (see Figure 1). A probe pulse ionizes the molecules from $|S_1v'\rangle$ and $|S_1\{\ell\}\rangle$ by resonant (or nonresonant) multiphoton absorption. Because $|S_1v'\rangle$ and the redistributed levels are ionized by the probe, the ion current signal

(i) may display a biexponential behavior in the delay time between the pump and probe pulses. Details of the transient behavior will depend on ratios of ionization cross-sections of $|S_1 v'\rangle$ and $|S_1\{\ell\}\rangle$ and on the relative depletion rates. Hence, k and k_ℓ can be measured directly. The time resolution of our amplified picosecond pulses allows us to observe the IVR even if k^{-1} is about 0.5 ps.

The experiments presented here are for isolated trans-stilbene and aniline. Stilbene was chosen since several photophysical studies of the isolated molecule have been performed. First, the pioneering work of Greene et al.[3] has shown that the S_1 lifetime can be measured under collision free conditions (low pressure vapor). Second, the spectra and isomerization rates of the jet-cooled molecules have been obtained by Syage et al.[4] using picosecond excitation and fluorescence detection. Finally, more recently, the yield yield has also been obtained by Amirav and Jortner[5] and by Zwier et al.[6] from measurements of excitation and absorption spectra of jets. The experiments of Syage et al.[4] have suggested that the IVR is faster than the measured isomerization rates above the barrier for isomerization (1200 cm^{-1}). This was based on the excess energy dependence of the rates and the spectra. The biexponential picosecond transients reported here confirm the earlier suggestions of fast IVR and show the effect of excess vibrational energy in the isolated stilbene on isomerization rates in a range not studied previously.

II. EXPERIMENTAL

a) Laser System

The laser system consisted of an amplified synchronously-pumped mode-locked dye laser, shown in Figure 2. An actively mode-locked Ar ion laser (Spectra Physics Model 171) operating on the 5145 Å line produced a train of $\sim$ 120 ps pulses at a repetition rate of $\sim$ 82 MHz. These pulses were used to synchronously pump a R6G dye laser which was equipped with a wedge filter tuning element. The bandwidth of the dye laser was $\sim$ 8 Å and the pulse width was typically $\sim$ 3 ps as determined by second harmonic generation (SHG) autocorrelation measurements (described below).

The dye laser pulses were amplified by using a three-stage flowing dye cell amplifier (Quanta Ray PDA 1) which employed spatial filters between the amplifying cells, thus allowing wavelength tunability of the amplified pulses. The amplifier dye cells were pumped at 20 Hz using the second harmonic of a Q-switch Nd:YAG laser (Quanta Ray DCR-2) equipped with a pulse shortening modification. The firing of the Nd:YAG Q-Switch was synchronized to the laser pulses via the Ar^+ laser mode locker RF driver signal. A variable delay was provided in the synchronization electronics allowing adjustment of the Q-Switch trigger pulse to ensure coincidence of Nd:YAG and dye laser pulses at the amplifier dye cells. Solutions of Kiton red, R-640 or DCM dyes were used in the amplifier. This allowed tuning from 575 nm to 627 nm, with good output pulse energy (0.25 mJ to > 0.5 mJ).

The amplified pulses were also characterized using the SHG

method. A comparison of typical autocorrelation functions of the dye laser and amplified system pulses is shown in Figure 3. The best fit theoretical curves are obtained using a model function for the autocorrelation which includes a pulse envelope and a coherence width contribution shown as

$$G(\tau) = \frac{\langle I(t+\tau)I(t)\rangle}{\langle I^2(t)\rangle} = G_p(\tau)\ [1 + G_N(\tau)]$$

where $G(\tau)$ is the observed autocorrelation function, I is the intensity; $G_p(\tau)$ is the pulse envelope autocorrelation and $G_N(\tau)$ is the autocorrelation of the noise process. The modelling of the pulses from the mode-locked dye laser has been described previously.[7] Also the dye laser cavity length dependence of the pulse widths[7] and the pulse fluctuations[8] have been investigated. From a streak camera study[8] of the mode-locked dye laser pulses evidence has been obtained which suggests that the individual pulse envelopes vary quite significantly from pulse to pulse at the cavity length corresponding to the smallest autocorrelation width. This instability was found to decrease with a slightly lengthed cavity ($\sim$ 10 μ). At the cavity length corresponding to the shortest pulses we have observed enhanced noise modulation of the dye laser intensity. The modulation is decreased with a slight (several micion) cavity length increase. Thus, for reason of increased stability we normally chose to generate the dye laser with the cavity length set somewhat lengthened from the shortest pulse position. For the data shown in Figure 3 the cavity length detuning was about $\sim$ 5 μ. At this setting the parameters in Table I were obtained from the least-squares

fits using Lorentzian functions for the pulse envelope and noice process shapes.

Table I
Autocorrelation Analysis of Dye Laser and Amplified System Pulses.

	t_p[a]	t_c[b]	R[c]
dye laser	3.0 ± 0.1	0.52 ± 0.03	0.70 ± 0.05
amp. sys.[d]	3.1 ± 0.15	0.52 ± 0.07	0.64 ± 0.07

a) pulse envelope width
b) coherence width (width of G_N)
c) amplitude of noise contribution to autocorrelation function (discussed in Ref. 7).
d) measured at a gain of $\sim 10^5$.

We measured the dependence of the amplified system autocorrelation function on the gain in the amplifier. These results are shown in Figure 4. From these results it is clear that there is only a slight broadening of the pulse widths with higher gain. Also there is evidently no great change in the pulse shape at higher gain.

b) Picosecond MPI Method

A schematic of part of the experimental apparatus is shown in Figure 5. The amplified visible laser beam was collimated and split into two equal intensity beams. One beam was passed through a fixed arm of a Michelson interferometer and was frequency doubled using a KDP crystal. The other beam was passed through a variable delay arm of the interferometer. The UV and visible beams were recombined collinearly using a dichroic mirror and were focused into the photoionization cell

(quartz cell with Brewster angle windows and Ni wire electrodes) using a 50 cm lens. To perform the UV pump-UV probe experiments the visible beams, after passing through the interferometer, were made parallel but not collinear and were separately frequency doubled then focused to a common spot as above. The signal was optimized by carefully adjusting the appropriate mirror to maximize the overlap of the beams in the sample. Typically, the background ionization signal due to the visible beam alone was negligible (< 0.1%) whereas the UV-induced background was more significant (10-30%).

The electrodes were biased at 100 V. Ion current was detected using a charge sensitive preamplifier (Ortec Model 109 PC), whose output pulse was integrated using a boxcar averager (Princeton Applied Research Model 162 with dual 164 integrators and digital storage). The boxcar was triggered with a pulse from a photodiode which was excited by the laser pulse. The integrated ionization signal was normalized for variation in the UV power. The normalized signal was digitized using a voltage-to-frequency converter. A multichannel analyzer, whose channel advance was synchronized to the translator delay time scan, was used to acquire and average the signal as the delay time between the UV and visible pulses was varied. Data were transferred to a PDP 11/23 microcomputer with which data analysis was performed.

c) Samples and Temperature Regulation

Trans-stilbene (Aldrich 99%+) was purified by recrystallization. Several milligrams of the material was introduced into the cell which was then evacuated to a pressure of $\sim 10^{-6}$ torr. Aniline (Aldrich, 99%+) was used as obtained. The liquid was introduced into cell and

then several freeze-pump-thaw cycles were performed.

The vapor pressure of the sample was controlled by either immersing the side arm in an appropriate coolant (ice baths or liquid nitrogen) or placing the entire cell in a "home" - built oven which was heated with a stream of hot nitrogen gas. The nitrogen was heated by flowing the gas over a hot nichrome wire coil. The heater coil was located outside the oven $\sim$ 1 foot from the cell to minimize electrical interference. Regulation of the cell temperature was to $\pm$ 0.2°C and the main body of the cell was $\sim$ 10°C warmer than the side arm.

d) Pulse Diagnostic Measurements

The pulses from the synchronously-pumped dye laser and the dye-laser amplifier were monitored routinely using SHG autocorrelation methods. The high repetition rate of the dye laser (82 MHz) allows one to make measurements at a rate which can provide "real-time" visual inspection of the autocorrelation function on an oscilliscope. These measurements were made with a rapid scanning (10 Hz) autocorrelator. This type of measurement was used to perform cavity-length tuning of the dye laser. In order to make quantitative measurements of the autocorrelation functions a different method was employed which allowed convenient electronic data acquisition and processing. The two methods are described below.

A schematic of the rapid scanning autocorrelator is shown in Figure 6a. A portion of the dye laser output is split into two beams. The beams are directed through a Michelson interferometer similar to that described above. The two beams are made noncollinear and parallel and are focussed to a common spot in a nonlinear crystal ($LiIO_3$). The

phase-matched second harmonic was detected along the bisector of the visible beams using a photomultiplier.

The variable delay arm of the interferometer is comprised of a corner cube which was mounted on a B & K instruments Model 4810 "minishaker" (vibration exciter). When driven with an appropriate ac waveform the shaker will produce a vibratory motion of the corner cube. This motion causes a variation of the optical path in the variable arm of the interferometer and thus a variation in the delay time between the two pulses.

The shaker was driven with a sine wave from a variable phase oscillator (General Radio Model 1305-A) which was amplified by an audo amplifier. A fixed phase output from the oscillator was used to drive the horizontal axis of an oscilloscope. The phase of the shaker driver signal was adjusted to compensate for the phase difference of the vibratory motion and the oscilloscope reference signal thus providing a smooth display on the oscilloscope.

The other method used to make autocorrelation measurements is similar to that described above except that the delay time is varied using a slowly scanning translator and the processing of the photomultiplier signal was different. In this case one of the beams is chopped with a mechanical blade chopper and the photomultiplier signal is phase sensitively detected using a lock-in amplifier. The lock-in output signal is digitized with a voltage to frequency converter and then accumulated as a function of the delay time using a multichannel analyzer. The channel address of the MCA is advanced as the translator is stepped by the controller.

For measurements of the amplified dye laser pulses the slow scanning system was used with a different method of signal processing. A schematic of this arrangement is shown in Figure 6b. The pulsed signal from the PMT was amplified and then integrated using a boxcar averager which was triggered by a photodiode pulse. The output of the boxcar was processed and the translator and MCA were scanned as above.

Typical dye laser autocorrelations are shown in Figure 3.

III. RESULTS

Figure 7 displays the trans-stilbene vapor MPI transient for excitation at 2976A and probing at 5952A for "long" and "short" time ranges. In these measurements, the UV pulse excites molecules to a nonequilibrium distribution of vibrational levels in S_1. When subjected to an intense visible pulse, these molecules are photoionized. Since the ionization potential of trans-stilbene is 7.7 eV[9], two visible photons are required. The ionization efficiency is quite high due to a resonant intermediate (S_4) which is strongly electric dipole-coupled to S_1[10]. Alternatively, in another type of experiment the intermediate is by-passed by using a UV probing pulse.

The decay of the MPI signal is Figure 7 is clearly nonexponential. Approximating the decay as biexponential and using a Gaussian pulse convolution, we have obtained the two time constants using nonlinear least-squares regression analysis. For the transient in Figure 7, τ_1 = 2 ps and $\tau_2 = 120 \pm 10$ ps, and the fast component accounts for about 70% of the total signal amplitude.

Several results which are pertinent to the origin and systematics of the MPI decays are listed below.

A) The MPI signal is extremely sensitive to the overlap of the UV and visible beams.

B) The MPI signal was reduced to < 5% of the 296K value by immersing the sample bulb in liquid nitrogen. As expected, the signal increased as the temperature was increased to about 360K. The longer lifetime of the decay was decreased slightly (15%) at the higher temperature relative to room temperature for excitation close to the electronic origin.

C) The background signal, which is due almost entirely to the UV alone, is typically between 10% and 30% of the peak signal.

D) The integrated ion signal varies linearly with the UV pulse energy over the range of 0.1 to 2 μJ/pulse (see Figure 8a). However the delay time response was independent of the UV pulse energy. We used this low UV power range to insure the linearity of the number of molecules excited to S_1.

E) The integrated ion signal did not vary linearly with the visible pulse energy but was close to linear above about 100 μJ/pulse and up to 200 μJ/pulse, with a higher than linear dependence below about 100 μJ/pulse, (see Figure 8b). This indicates saturation behavior at higher power. The fraction of the amplitude which decayed by the fast component varied close to linearly with the visible pulse energy above about 100 μJ/pulse for excitation at 2975 Å (see Figure 8c). The longer lifetime component of the decay varied relatively little, decreasing by 20% with increasing visible pulse energy over the range studied.

F) Nonexponential decay with similar characteristics as described above (where pump and probe polarizations are parallel) are

observed when both the UV and visible beams were depolarized. This shows that the observed response is not due to anisotropy effects.

G) In the experiment where UV pulses were used to pump and probe a symmetric response about zero delay time with fast and slow decay components was observed. This experiment shows that the observed nonexponential decay is not due to the presence of the S_4 intermediate in the UV-visible pump-probe experiment.

H) In a separate experiment, measurements were performed on aniline vapor with the sample bulb held at 273K. An MPI signal due to UV and visible excitation was easily obtained. When exciting the S_1 origin, the $6a_1^1$, or the 12_1^1 levels[11] of S_1 with the UV and probing with the visible, the MPI signal rose with instrument response (2 ps) and remained flat over several hundred picoseconds (see Figure 9). This observation eliminates the possibility of a coherent enhancement of the ion signal near zero time delay. It is also consistent with the expectation that IVR in aniline is relatively slow, as will be discussed later.

Finally, we have measured the dependence of the trans-stilbene MPI decays on the excitation energy. These results are summarized in Figure 10. The nonexponential decay was observed at all excitation energies studied. The short decay time constant was found not to vary within our resolution over the range studied. In contrast, the longer decay constant varied from 400 ± 50 ps at λ_{uv} = 3100 Å to 66 ± 6 ps at λ_{uv} = 2876 Å. These results will also be discussed later.

IV. DISCUSSION

A. Intramolecular Vibrational-Energy Redistribution (IVR)

IVR in polyatomic molecules under collisionless conditions has been the subject of extensive theoretical and experimental investigation (for example: references 12-23) investigation. The bulk of the experimental information available on IVR within the first excited singlet state of polyatomic molecules is based on spectral information, for example the resolved fluorescence spectra of molecules subsequent to vibronic excitation. Direct time domain measurements of IVR have only recently been reported for isolated large molecules[1,2]. In this section, we will briefly review the concepts and phenomenology involved in collisionless IVR of large molecules, following quite closely the description by Freed and Nitzan[15].

The starting point is the partitioning of the full molecular Hamiltonian as follows:

$$H^M = H_o + W$$

where H_o is the zero-order molecular Hamiltonian and W is the interaction energy due to the coupling of various zero-order states. The total Hamiltonian is:

$$H = H^M + H^R + H^{MR}$$

where H^R is the radiation field Hamiltonian and H^{MR} is due to the interaction of the molecules and the light field. We denote the

eigenfunctions of the zero-order vibrational part of the molecular Hamiltonian in an occupation number representation in a basis set of normal modes, although other bases are possible and may be convenient. It is useful here, from a spectroscopist's point of view, to separate the vibrational modes into two groups: one optically active group (modes denoted by a) and an inactive group (modes denoted by b for both). The optically active modes correspond to these which are observed as progressions on the electronic absorption spectra and for molecules with some degree of symmetry they are primarily the totally symmetric modes. The zero order vibronic levels are written as products of electronic and vibrational wavefunctions, for example $|S_0, \{V_{a_i}\}, \{V_{b_i}\}\rangle$ and $|S_1, \{V_{a_i}\}, \{V_{b_i}\}\rangle$ where S_0 and S_1 are the ground and first excited singlet electronic wavefunctions.

The coupling term W is viewed as being responsible for non-radiative transitions between different a modes and different b modes as well as between a and b modes within an electronic state. Physically this coupling term is due to vibrational anharmonicity and also to vibration-rotation interaction. The effect of vibration-rotation coupling on the vibrational redistribution has been shown theoretically to be significant.[23]

We turn attention now to the S_1 state. It is important to consider the nature of the true (or exact) molecular eigenstates. These states are superpositions of the zero-order levels:

$$\Psi(S_1,n) = \sum_{V_a,V_b} C_{V_a,V_b} |S_1, V_a, V_b\rangle$$

Excitation of a molecule by a narrowband laser of appropriate frequency will cause a transition from $|S_0,0,0\rangle$ to a $\Psi(S_1,n)$ state (if these states are spaced in energy by an amount larger than the bandwidth). Specifically, this state would be of the form

$$\Psi(S_1,n) = C_{n;V_a,0}|S_1,V_a,0\rangle + \sum_{V_a',V_b'} C_{n;V_a',V_b'}|S_1,V_a',V_b'\rangle$$

which has a contribution of a particular optically active zero-order state. In the weak coupling limit ($|W|<$ energy spacing of $\Psi(S_1,n)$) each $\Psi(S_1,n)$ correlates with a single optically active state. If the excitation bandwidth (say from a short pulse laser) spans all the $\Psi(S_1,n)$ with a component of $|S_1,V_a,0\rangle$ and if the bandwidth is narrow enough to avoid other $|S_1,V_a,0\rangle$ states then the probability of a $|S_1,V_a,0\rangle$ is unity. This is due to the completeness of the eigenstates. This non-stationary state evolves in time. In the statistical limit, the probability of the initial state decays exponentially with a rate constant k given by

$$k = \frac{2\pi}{h}|\langle W\rangle|^2\rho$$

where ρ is the density of states and $\langle W\rangle$ is the average coupling matrix element. This process is the intramolecular vibrational redistribution process. The relaxation proceeds in a way which conserves the total vibrational energy of the molecules in the S_1 electronic state. It should be emphasized that the evolution is strongly dependent on the way in which the system is excited and that the description given above

corresponds to one limiting case.

Since our experimental measurements were carried out with room temperature vapors, we must consider the effects of the initial thermal distribution of population.[19] The equilibrium probability distribution of molecules in the ground electronic state is described by

$$N(E)dE = \rho(E)\exp(-E/kT)dE/Q$$

which gives the number of molecules N(E) with energies between E and E+dE, $\rho(E)$ is the density of states and Q is the vibrational partition function ($Q = \int_0^\infty \rho(E)\exp(-E/kT)dE$). One consequence of this thermal distribution of population (say at $\sim$ 300 K) is that, for a large molecule like stilbene, the probability of molecules being in the ground vibrational state is extremely low. This is due to the fact that the density of states is a rapidly growing function whose value is very low for low energy. The probability reaches a maximum at quite high energy ($\sim$ 2000 cm^{-1}). Another consequence of the thermal distribution is that the absorption spectra are severely congested. This is due to the superposition of the many progressions originating from the populated vibrational levels in the ground electronic. In the case of trans-stilbene vapor the room temperature absorption spectrum $S_1 \leftarrow S_0$ is in fact essentially continuous with little well defined structure.[3] The details of the population distribution of the molecules in the electronically excited state depends on the exact excitation energy. However, it is expected that for the situation of stilbene at room temperature that much of the thermal energy of ground state will be

transferred to the excited state and that the envelope of the excited state population distribution will be quite similar to that of the ground state. The primary difference being that amplitudes of the optically active levels will be somewhat enhanced relative to other levels due to favorable Franck-Condon factors. The probability distributions are shown in Figure 11; we have approximated the initial excited state distribution by equating it with the form of the ground state distribution.

The excited state population distribution has an important influence on the dynamics. The increased width of the distribution due to the thermal energy of the ground state leads to relaxation on a shorter time scale than would be found in the absence of this congestion. Qualitatively, this introduces a rate of Γ/h into the decay where Γ is the width of the distribution. For stilbene at room temperature the width of the distribution is about 2000 cm^{-1} and therefore the relaxation time (rapid initial dephasing) would be $\sim$ 2.5 fs. This relaxation is very fast (essentially instantaneous) on the timescale of our experiment so this decay is not observed. On the longer timescale of our experiment it is still possible to observe the effects due to the decay of the various zero-order states as discussed above. The observed relaxation is averaged over the initial distribution of excited states. Thus in effect we measure the thermally averaged IVR rate which is given by:

$$\langle k \rangle_T = \sum_i P_i(T) k_i .$$

In the continuum limit this expression becomes

$$\langle k \rangle_T = \int_0^E P_i(E,T)\, k_i(E)\, dE$$

where $P_i(E,T)$ is the normalized initial probability distribution and k_i is the statistical limit IVR rate for the i^{th} zero-order state. The system evolves to a quasi-equilibrated vibrational distribution in the S_1 state due to this relaxation. If indeed the system were to reach a completely thermalized distribution then the final probability distribution, for excitation 4000 cm^{-1} above the S_1 (0,0) energy, would appear as the dashed curve in Figure 11. The extent to which the final distribution differs from the initial one depends on the excess vibrational energy of excitation: $E_x = E_{exc} - E_{0,0}$.

B. Equation Analysis Population Rate

In previous time-resolved MPI experiments with nanosecond pulses a kinetic scheme for the populations was invoked.[24,25] This treatment neglects off-diagonal terms for the density matrix equations and has been shown[26] to be a suitable description of MPI processes under certain experimental conditions. Ackerhalt and Eberly[26] showed for a ladder excitation scheme where the final state is an ionization or a dissociation continuum that a rate equation description becomes valid for describing excited state populations providing that the radiative pumping rate (σ I) increases for each step up the ladder.

On the picosecond timescale this might not be an adequate description simply because at very high laser intensities population pulsations (Rabi cycling) can occur in this very short time domain.

Furthermore, the coherence properties (dephasing times) of the intermediates may influence the MPI transients even if the Rabi frequency is relatively small. For trans-stilbene the cross sections for the $S_1 \leftarrow S_0$ and $S_4 \leftarrow S_1$[10] transitions are $\sigma_{01} = 4 \times 10^{-17}$ cm^2 and $\sigma_{14} \gtrsim 2 \times 10^{-15}$ cm^2 at the corresponding wavelength maxima. Also the visible (probe) intensity was always much higher (> 25 times) than the UV intensity, thus the pumping rate for $S_4 \leftarrow S_1$ was higher than for $S_1 \leftarrow S_0$. However, the cross section for the $S_{i,e} \leftarrow S_4$ step is not known. We therefore tentatively assume the validity of the rate equation analysis in order to describe the important effects which depend on light intensities and populations. Considering the scheme depicted in Figure 1, we shall consider two simple cases; one where there is no IVR (single manifold case), and in the other, IVR takes place between an initially excited optically active set of vibrational states and a vibrationally equilibrated distribution of states in S_1 (two manifold case).

(1) Single Manifold Case

Here, we consider the single photon excitation of molecules to $|S_1,v'>$, where v' refers to a set of initially excited modes, by a UV pump pulse. The system is then probed at a time t_o by a visible or UV pulse which excites the molecules to the ionization continuum. The ion current is detected as a function of t_o. (The kinetics are developed more fully in the Appendix). The UV pulse produces $N_1(o) = \sigma_{01} I_1 N_0$ and this population evolves freely after the UV pulse according to $N_1(t) = \sigma_{01} I_1 N_0 e^{-k_s t}$. At time t_0, a UV pulse probes the $N_1(t)$ population, giving an ion current that decays

exponentially by k_s. For visible pulse probing, the population of the intermediate (in this case, the S_4 electronic state) is given by:

$$N_4(t_0) = \frac{\sigma_{14} I_2}{(\sigma_{4i} I_2 + k_4)} N_1(t_0).$$

assuming a steady state for N_4 is achieved during the pulse. The ion current is then simply: $i = cst.\exp(-k_s t_0)$, again showing the single exponential behavior.[25b].

We considered the possible sources of complications of the decay in the single manifold case. Inclusion of stimulated emission processes into the kinetic analysis was considered. In the $|S_1v'\rangle \leftarrow |Gv''\rangle$ transition only a small fraction (< 20%) of the ground state molecules are excited per pulse under the conditions of our experiment, therefore stimulated emission was justifiably neglected. Stimulated emission for $|S_1v'\rangle \leftarrow |S_4\rangle$ is probably more significant since $\sigma_{14} I_2\, t \gg 1$. However, inclusion of this process in the simple kinetic scheme described above merely scales down the steady-state (S_4) population and does not introduce a biexponential delay time dependence of the ion current. Finally, we consider the role of coherence of the intermediate level $|S_1v'\rangle$ on the decay. Noting that the pulse area of the UV pulse is rather small ($< 0.2\,\pi$), we neglect population pulsations between $|Gv''\rangle$ and $|S_1v'\rangle$. More on this will be discussed later.

(2) Two-manifold Case

As a simplified scheme which allows discussion of the effects of IVR on the pump-probe MPI experiment by using a kinetic analysis, we introduce the two-manifold scheme shown in Figure 1. The

MPI process is visualized as follows. As above, the UV pulse excites molecules to $|S_1,v'>$. In the free evolution of this state, vibrational energy is redistributed to the equilibrated distribution $|S_1\{\ell\}>$. It is from these states that molecules are able to undergo configurational change which leads to isomerization, indicated by the rate k_ℓ. Now the probe pulse (UV or visible) will excite molecules at time delay t_0 from both manifolds to the ionization continuum. The relative contribution to the ion signal of the initial and redistributed manifold depends, in general, on the rate of IVR (k) and the relative effective cross-section for ionization out of $|S_1v'>$ and $|S_1\{\ell\}>$. We show this using a kinetic analysis. The population of $|S_1v'>$ evolves freely after the UV pulse as $N_1 = \sigma_{10}I_1N_0e^{-k_1t}$ where $k_1 = k + k_s$. This population feeds the $|S_1\{\ell\}>$ states and the population of these states is given by $N_\ell = \frac{\sigma_{01}I_1N_0k}{(k_1-k_\ell)}$ $[e^{-k_\ell t} - e^{-k_1t}]$. The probe pulse at time t_0 samples $N_1(t_0)$ and $N(t_0)$ and produces ion current of the form:

$$i = (\alpha - \beta)e^{-k_1t_0} + \beta e^{-k_\ell t_0}$$

where α and β are intensity dependent coefficients for visible probing. For UV probing, the ratio, R, of the fast to the slow components is simply $[(\sigma_{1i}/\sigma_{\ell i})(\frac{k_1-k_\ell}{k}) - 1]$. For visible probing the situation is different. We have used the steady state approximation for the S_4 resonant intermediate for both manifolds and have included the stimulated emission rates from both intermediates. Within this level of approximation, it is seen that we obtain the same form of the ion signal but with a different ratio R that is power dependent.

IVR (k) is expected to be much faster than the isomerization (k_ℓ). So, in this limit, the ratio is

$$R = \frac{((\sigma_{4'i} + \sigma_{\ell 4'})\, I_2 + k_{4'})}{((\sigma_{4i} + \sigma_{14})\, I_2 + k_4)} \left(\frac{\sigma_{14}\, \sigma_{4i}}{\sigma_{\ell 4'}\, \sigma_{4'i}}\right) - 1 ,$$

where primes refer to the $\{\ell\}$ manifold. In the case where the relaxation rate k_4 is competitive with or larger than the stimulated rate, the ratio could show some intensity dependence. For visible probing experiments, we have observed an essentially linear dependence of the ratio on I_2 which would suggest that $(\sigma_{41} + \sigma_{14}) I_2 \lesssim k_4$. Also note that if the stimulated and spontaneous rates and cross-sections for the levels in both manifolds are equal, then the ratio R goes to zero.

The results of the above kinetic analysis are consistent with the experimental observations made thus far for visible or UV probing. The effects of IVR have been modelled in this context. The physical basis of such a model is that the initially excited distribution of states has a different effective cross section for probing than the equilibrated distribution of vibrational levels. This is possible if the effective vibrational overlaps with the intermediate and/or final states changes as a result of IVR. It should be emphasized that in this very simple model, the continuous process of IVR has been approximated by an initial and an equilibrated distribution with an effective rate for equilibration. This is reasonable only for the case of statistical limit relaxation. At room temperature, the absorption spectrum of t-stilbene is essentially structureless,[3] indicating that a large number of states can be excited at all excess energies. In a free-jet

expansion, the dispersed fluorescence is very broad (hot vapor type) when the excess energy exceeds the barrier energy for isomerization. Furthermore, the lifetimes become independent of the mode excited at about the same energy. Therefore, for this excitation of the cold beam IVR is thought to be fast, especially above the barrier threshold ($\sim$ 1200 cm^{-1}).[4] Our results here, obtained by using UV pumping and UV or visible probing, indicate that the IVR lifetime at bulb temperature is $\simeq$ 2 ps. The average thermal energy of the molecule at 296°K is about 2000 cm^{-1}. This average energy is certainly larger than the barrier height and therefore we expect the IVR to be fast. The fast rates in the energy range studied here were observed at different excess energies and this is due either to a limited time resolution or to a saturation of the IVR rate in this range. This last point will be examined further in future study.

For aniline in a bulb, the dispersed fluorescence[11] is discrete for excitation into the $6a^1$ (E_x = 492) and 12^1 (E_x = 953) levels of S_1. Consequently, we expect IVR to be relatively slow. As mentioned before, the aniline picosecond MPI transient (not shown) did not shown the biexponential behavior; the signal remained flat over several hundred picoseconds, consistent with the expected lack of IVR on this time scale. We are currently examining higher energy regions where IVR may become faster.

The coherence of the level excited or the laser field may influence the ionization probability. Since we are in the small pulse area limit for the pump pulse, vide supra, coherent population pulsation can be ignored. The dephasing of the level could lead to a decrease in

the ion signal. This would arise out of the spreading of the initially excited wavepacket. We note that at the very low pressure (< 10^{-4} torr) of samples in our experiment, collisional effects can safely be ignored on the picosecond time scale. Therefore, the principal process which could lead to dephasing on this timescale is the intramolecular redistribution process which has been modelled above. Dephasing due to inhomogeneous preparation of levels is expected to be on the time scale of shorter than 0.5 ps and would not be seen in these experiments. As for the coherence of the laser pulse, we have established that the coherence time of the pulse is $\sim$ 0.5 ps (from auotcorrelation measurement) which is markedly shorter than the pulse width and the apparent width of the early part of the decay (fast component). The absence of this fast component in aniline taken under similar conditions supports this conclusion.

C. Excess Energy Dependence of Isomerization

From the kinetic analysis of the MPI delay time decays presented above we find that for trans-stilbene the long decay component gives the rate of isomerization from vibrationally equilibrated molecules in S_1, similar to the measurement of triplet state lifetimes by nanosecond time-resolved MPI.[25b-d] In Figure 4 are shown representative decays at the highest and lowest excitation energies used in this study. Also shown is a summary of the decay rates obtained from various works along with a plot of calculated thermally-averaged decay rates versus excess energy.

In order to compare the results from experiments performed under widely differing conditions, we use the upper abscissa which is the

total vibrational energy of the excited molecules: $E_{total} = E_x + \langle E_v \rangle_T$, where E_x is the excess vibrational energy ($E_x = E_{exc} - E_{0,0}$) and $\langle E_v \rangle_T$ is the average vibrational energy at temperature T. The average energies for the temperature of the various experiments were calculated using the frequencies of Warshel.[27]

The good qualitative agreement of the results shown in Figure 4 from quite different and independent experiments is noted. It is interesting that the rates determined for the free-jet (isolated molecules at very low temperature) are in very good agreement with the results from this study at the same total energy. This agreement gives support to the idea that at the higher excitation energies ($\geq$ 1200 cm^{-1}) of jet-cooled molecules collisionless IVR serves to produce essentially vibrationally equilibrated molecules prior to isomerization. The direct observation in this study of fast IVR of molecules with a total vibrational energy of $\geq$ 2000 cm^{-1} is consistent with the above conclusion.

We performed a calculation of the thermally averaged decay rates for comparison with the results obtained at room temperature or higher temperature. The thermally averaged rates are given by[28]

$$k(T,E_x) = \frac{1}{Q} \int_0^\infty k(E + E_x)\rho(E)e^{-E/k_bT} dE.$$

where Q is the vibrational partition function, $k(E + E_x)$ is the low temperature (jet) isomerization rate evaluated at the total vibrational energy and $\rho(E)$ is the vibrational density of states. To evaluate the $\rho(E)$ we have used the frequencies[27] as above, arranged into seven

groups. The values of $\rho(E)$ were determined by using a direct counting method for $E < 10{,}000\ cm^{-1}$ and by using the Whitten-Rabinovitch approximation for higher energies. The values of $k(E_x)$ were obtained from the free-jet results of Syage et al.[4] and the functional form was taken to be $k(E_x) = A \exp(-B/E_x)$ where A and B are constants. $k(E_x)$ is the total rate minus the radiative rate.[4] We make the assumption that this equation can be extrapolated to the energies needed to perform the averaging and calculate the rates in Figure 4. The data of this work and of Greene et al.[3] can be compared to the calculated curve and they should be referenced to the lower abscissa. We find the agreement of the calculated and experimental rates to be reasonable since only independent information was used with no adjustment to fit the data. The small deviations (< 25%) of the calculated rates compared to our experimental data may be due to a breakdown of the validity of the extrapolation of the $k(E_x)$ function which was used. Alternatively, it is possible that the density-of-states function was not sufficiently accurate.

If the calculated curve were scaled to agree with our data, the points of Greene et al.[3] would deviate from the calculated curve by about equal and opposite amounts. Therefore, it is possible that the very close agreement of the highest energy value[3] with the calculated value is fortuitous. In any case, the main purpose of the calculation has been served in that it confirms the idea that the longer decay component observed is the isomerization rate. It should be mentioned that these isomerization rates for trans-stilbene at all excess energies studied are smaller than that of cis-stilbene in a bulb also obtained by

UV-visible MPI.[15,16] This is rationalized as due to a low or absent barrier for the cis-stilbene isomerization.

V. CONCLUSIONS

The principal conclusions of this work are:

1. Picosecond time-resolved MPI as a technique for probing IVR in isolated molecules has been demonstrated. In this work the method is applied to stilbene and aniline. Nonexponential decay behavior yields the collisionless IVR and isomerization (for stilbene) rates; the time constant for the former is $\sim$2 ps. In aniline, only a long lifetime of the prepared state was observed.

2. The isomerization time was found to vary from 400 ps to 66 ps with total excess vibrational energy over the range of 2000 to about 4500 cm^{-1}. These measurements extend the experimentally determined rates into a range not investigated previously in the time domain. The data of this work are in reasonable agreement with the results of experiments performed under different conditions (jets and bulbs). The calculated thermally-averaged rates are in fairly good agreement with our measurements.

APPENDIX TO CHAPTER VI

Kinetic Models for Excited State Dynamics

In this section kinetic models are developed which are relevant to the excited state dynamics of stilbene in the picosecond pump-probe MPI experiments. First, expressions are derived for the delay time dependence of the excited state populations and the ion current for UV-UV and UV-VIS experiments in the case where only a single type of vibrational state (or distribution) is involved. Then, the populations and ion current are determined, again for UV and VIS probing, for the case where the vibrational redistribution process populates other states and thus a new distribution is formed.

A schematic which depicts the first kinetic model to be considered is shown in Figure 12a. This is the case of sequential two-photon ionization by UV pulses. The differential equations for the populations are:

$$\frac{dN_o}{dt} = - \sigma_{01} I(t) N_0 + (\sigma_{01} I(t) + \gamma_{01}) N_1$$

$$\frac{dN_1}{dt} = \sigma_{01} I(t) N_0 - (\sigma_{1i} I(t) + \sigma_{01} I(t) + \gamma) N_1$$

$$\frac{dN_i}{dt} = \sigma_{1i} I(t) N_1$$

where $I(t)$ is the pulse intensity time envelope, $\gamma = \gamma_{01} + \gamma_1$ and the initial condition is $N_0(0) = N_0^0$; $N_1(0) = N_i(0) = 0$. $I(t)$ is taken as a square pulse with amplitude I which starts at $t = 0$ and has duration Δt. In the steady state approximation for the intermediate one obtains

$$N_1 = \frac{\sigma_{01} I}{(\sigma_{1i} + \sigma_{01}) I + \gamma} \; N_0$$

and

$$N_0 = N_0^0 \cdot \exp[-\Gamma t]$$

where $\Gamma = \sigma_{01} I \left[1 - \frac{\sigma_{01} I + \gamma_{01}}{(\sigma_{01} + \sigma_{1i}) I + \gamma} \right]$.

The ion current is given by

$$\frac{dN_i}{dt} = \sigma_{1i} I N_1 = \frac{\sigma_{01} \sigma_{1i} I^2 N_0^0}{(\sigma_{1i} + \sigma_{01}) I + \gamma} \; e^{-\Gamma t}.$$

From this expression it can be seen that for $(\sigma_{1i} + \sigma_{01})I << \gamma$ the ion current is proportional to I^2 (low power limit) and for $(\sigma_{1i} + \sigma_{01})I >> \gamma$ the ion current is proportional to I (high power limit) which shows a saturation like effect at high intensity.

Consider now excitation of the system by two identical UV pulses with a variable time delay (t_0) between them. As $\tau \to \infty$ the system relaxes completely in between the pulses so the ion current which results is due to the sum of the contributions from both pulses and this is just twice the contribution from one pulse. When the pulses are overlapped in time the intensity is doubled. In the low intensity limit the ion signal is then increased by a factor of four and therefore there is an increase over the $t_0 = \infty$ value by a factor of 2. This change in the ion signal decays with the field free decay rates to the $t_0 = \infty$ value as t_0 is increased; thus the intermediate state lifetime may be obtained. Of course, since the pulses are identical the ion signal is symmetric about zero delay time: the signal is given by

$$i = c \cdot e^{-\gamma|t_o|}$$

We now analyze a slightly different case where different frequencies, one specific to each transition, are used in the time-resolved pump-probe ionization. In this case we will ignore the stimulated and spontaneous downward relaxation connecting S_0 and S_1; we allow only for a loss of population out of S_1. The rate equations become

$$\frac{dN_0}{dt} = - \sigma_{01} I_1(t) N_0$$

$$\frac{dN_1}{dt} = \sigma_{01} I_1(t) N_0 - (\sigma_{1i} I_2(t-t_0) + \gamma) N_1$$

$$\frac{dN_i}{dt} = \sigma_{1i} I_2(t-t_0) N_1$$

where $I_1(t)$ is the pump pulse and $I_2(t-t_0)$ is the probe pulse at time t_0. The system is subject to the same initial condition as before, except evaluated at $t = -\infty$. This system of differential equations can be solved directly. The populations of S_0 and S_1 are given as

$$N_0(t) = N_0^0 \exp[-\sigma_{01} \int_{-\infty}^{t} I_1(t')dt']$$

$$N_1(t) = \exp[-\int_{-\infty}^{t} P(t')dt'] \int_{-\infty}^{t} Q(t') \exp[\int_{-\infty}^{t} P(t'')dt'']dt'$$

where $P(t) = \sigma_{1i} I_2(t-t_0) + \gamma$

and $Q(t) = \sigma_{01} N_0 I_1(t) \exp[-\sigma_{01} \int_{\infty}^{t} I_1(t')dt']$.

These equations contains effects due to depletion of populations and the pulse shapes. The total ion current as a function of the delay time is

$$N_i = \sigma_{1i} \int_{-\infty}^{\infty} I_2(t-t_0) N_1(t)dt.$$

To see the limiting form we used the δ-function pulse approximation and obtained

$$N_i = \sigma_{1i} I_2 N_1(t_0)$$

$$N_1(t_0) = \sigma_{01} I_1 N_0^{(-\infty)} e^{-\sigma_{01} I_i} e^{-\gamma t_0}$$

We see that indeed the ion signal decays as a single exponential with increasing delay time, t_0, by the rate of population loss from the intermediate.

The rate equations for the UV pump and VIS probe are now analyzed. The appropriate schematic is shown in Figure 12b.

The level structure now includes a second intermediate state. However, the transitions $S_4 \leftarrow S_1$ and $S_i \leftarrow S_4$ occur only during the VIS probing pulse and we show below that the delay time (between UV) and VIS pulses) dependence of the ion signal shows a

decay determined by the rate of population loss from S_1. The differential equations for this case are analogous to those given above (sequential transitions with loss) and are not written out here. The solutions show the same form as above and those for S_1 and S_4 are:

$$N_1(t) = \exp[-\int_{\infty}^{t} P(t')dt'] \int_{\infty}^{t} Q(t')\exp[\int_{\infty}^{t} P(t'')dt'']dt'$$

where $P(t) = \sigma_{14}I_2(t-t_0) + \gamma_1$

and $Q(t) = \sigma_{01}I_1(t)N_0 \exp[-\sigma_{01}\int_{\infty}^{t} I_1(t')dt']$

and

$$N_4(t) = \exp[-\int_{\infty}^{t} R(t')dt'] \int_{\infty}^{t} \delta(t') \exp[\int_{\infty}^{t} R(t'')dt'']dt'$$

where $R(t) = \sigma_{4i}I_2(t-t_0) + \gamma_4$

and $\delta(t) = \sigma_{14}I_2(t-t_0)N_1(t)$.

Again using the δ-function pulse approximation we obtain:

$$N_1(t) = \sigma_{01}N_0I_1e^{-\sigma_{01}I_1} e^{-\gamma_1 t}$$

$$N_4(t) = \sigma_{01}\sigma_{14}N_0I_1I_2e^{-\sigma_{01}I_1} e^{-\gamma_1 t_0} e^{-\gamma_4(t-t_0)}.$$

The solution for the ion current is also of the same form as above except it now involves $N_4(t)$ instead of $N_1(t)$.

Integrating the ion current equation gives:

$$N_i = \sigma_{01}\sigma_{14}\sigma_{4i}N_0I_1I_2^2e^{-\sigma_{01}I_1} e^{-\gamma_1 t_0},$$

which shows the expected form of exponential decay in delay-time by the rate of loss of population from S_1. As discussed earlier, the effects of IVR will be dependent on the time-evolution of the Franck-Condon overlap integrals as a result of the evolution of S_1 vibrational population. The cross-sections in the equation above for the ion current are proportional to the corresponding Franck-Condon factors and therefore the time dependence due to the IVR could be incorporated here. However, we will model the effects in a very simple way by using a kinetic scheme which treats IVR process in terms of an initial distribution of states and a final distribution (equilibrated) with an effective time independent rate constant for transfer and with different cross-section for each distribution.

We now consider the rate equations for the UV pump-UV probe (time-delayed resonant two-photon ionization) experiment. This scheme is as shown in Figure 1 except the probes are one-photon ionizations The equations will be solved in the <u>low</u> population depletion approximation. The differential equations are:

$$\frac{dN_1}{dt} = \sigma_{01} I_1(t) N_0 = k_1 N_1$$

$$\frac{dN_\ell}{dt} = kN_1 - k_\ell N_\ell$$

$$\frac{dN_i}{dt} = \sigma_{1i} I_2(t-t_0) N_1 = \sigma_{\ell i} (I_2(t-t_0) N_\ell$$

subject to the initial conditions $N_0(-\infty) = N_0$, $N_1(-\infty)$, $N_\ell(-\infty)$, $N_i(-\infty) = 0$. These equations may be solved by standard methods and the solutions are

$$N_1(t) = \sigma_{01} N_0 \int_{-\infty}^{t} I_1(t') e^{-k_1(t-t')} dt'$$

$$N_\ell(t) = k \cdot \sigma_{01} N_0 \int_{-\infty}^{t} e^{-k_\ell(t-t'')} \int_{-\infty}^{t} I_i(t') e^{-k_\ell(t''-t')} dt' dt''$$

and

$$N_i(t_0) = \sigma_{1i} \int_{-\infty}^{\infty} I_2(t - t_0) \cdot N_1(t) dt + \sigma_{\ell i} \int_{\infty}^{\infty} I_2(t-t_0) N_\ell(t) dt.$$

By using the δ-function pulse approximation, the expression for the ion current becomes

$$N_i(t_0) = \sigma_{1i}\sigma_{01} N_0 I_i I_2 e^{-k_1 t_0} + \frac{\sigma_{\ell i} k \sigma_{01} N_0}{k_1 - k_\ell} \left[e^{-k_\ell t_0} - e^{-k_1 t_0} \right]$$

which can be rewritten as:

$$N_i(t_0) = (\alpha - \beta) e^{-k_1 t_0} + \beta e^{-k_\ell t_0}$$

where $\alpha = \sigma_{01}\sigma_{1i} N_0 I_1 I_2$ and $\beta = \dfrac{\sigma_{01}\sigma_{\ell i} N_0 I_1 I_2 k}{k_1 - k_\ell}$

Defining the ratio R as $(\alpha-\beta)/\beta$ gives

$$R = \frac{\sigma_{1i}}{\sigma_{\ell i}} \quad \frac{k_1 - k_\ell}{k} - 1.$$

Note that for $k_1 > k_\ell$ and $\sigma_{1i} > \sigma_{\ell i}$, R is positive and thus the ion signal shows a biexponential delay-time dependence. In the present case k_1 is dominated by the rate of IVR and is expected to be larger than the rate of isomerization k_ℓ. Also, the effective ionization cross-section of the initial states (σ_{1i}) is expected to be larger than that of the final states ($\sigma_{\ell i}$) because of the higher weighting of the optically active states in the initial distribution.

To extend the analysis to the UV pump VIS probe experiment (see Figure 1) we proceed at a similar level of approximation as above. The rate equations for this case are

$$\frac{dN_1}{dt} = \sigma_{01} I_1(t) N_0 - (k_1 + \sigma_{14} I_2(t-t_0)) N_1$$

$$\frac{dN_\ell}{dt} = kN_1 - (k + \sigma_{4'i} I_2(t-t_0)) N_\ell$$

$$\frac{dN_4}{dt} = \sigma_{14} I_2(t-t_0) N_1 - (k_4 + \sigma_{4i} I_2(t-t_0)) N_4$$

$$\frac{dN_{4'}}{dt} = \sigma_{4'} I_2(t-t_0) N_\ell - (k_{4'} + \sigma_{4'i} I_2(t-t_0)) N_{4'}$$

$$\frac{dN_i}{dt} = \sigma_{4i} I_2(t-t_0) N_4 + \sigma_{4'i} I_2(t-t_0) N_{4'}$$

where the initial conditions are as before (i.e. equal to zero for all intermediates and ion states), N_4 refers to the population of S_4 and the primes refer to the vibrationally relaxed states. Because of the high pumping rate of the $S_4 \leftarrow S_1$ transitions we invoke the

steady state approximation for the N_4 and $N_{4'}$ populations. This gives:

$$N_4(t) = \frac{\sigma_{14} I_2(t-t_0) N_1}{(\sigma_{4i} I_2(t-t_0) + k_4)}$$

and

$$N_{4'}(t) = \frac{\sigma_{\ell 4'} I_2(t-t_0)}{(\sigma_{4'i} I_2(t-t_0) + k_{4'})} N_\ell$$

If we are in the low depletion limit for N_1 and N_ℓ then the solutions for N_1 and N_ℓ are the same as given above. Substituting these expressions into the ones for N_4 and $N_{4'}$, the expression for the ion current becomes

$$\frac{dN_i(t_0)}{dt} = \frac{\sigma_{4i}\sigma_{14} I_2^2(t-t_0)}{(\sigma_{4i} I_2(t-t_0) + k_4)} N_1 + \frac{\sigma_{4'i}\sigma_{\ell 4'} I_2^2(t-t_0)}{(\sigma_{4'i} I_2(t-t_0) + k_{4'})} N_\ell$$

In the square pulse approximation for $I_2(t-t_0)$ this expression reduces to a form which can easily be integrated and with the δ-function pulse approximation for $I_1(t)$ we get

$$N_1(t) = \frac{\sigma_{4i}\sigma_{14}\sigma_{01} I_2^2 I_1 N_0}{(\sigma_{4i} I_2 + k_4)} \int_{t_0}^{t_0+\Delta t} e^{-k_1 t}\, dt.$$

$$+ \frac{\sigma_{4'i}\sigma_{\ell 4'}\sigma_{01} I_2^2 I_1 N_0 k}{(\sigma_{4'i} I_2 + k_{4'})(k_1 - k_\ell)} \int_{t_0}^{t_0+\Delta t} (e^{-k_\ell t} - e^{-k_1 t})\, dt.$$

Assuming no relaxation during the pulse we get

$$N_i(t_0) = (\alpha - \beta)e^{-k_1} + \beta e^{-k_\ell t_0}$$

where $$\alpha = \frac{\sigma_{4i}\sigma_{14}\sigma_{01}I_1I_2^2\Delta tN_0}{(\sigma_{4i}I_2 + k_4)}$$

and $$\beta = \frac{\sigma_{4'i}\sigma_{\ell 4'}\sigma_{01}I_1I_2^2\Delta tN_o k}{(\sigma_{4'i}I_2+k_{4'})(k_1-k_\ell)} \quad .$$

The ratio R becomes:

$$R = \frac{(\sigma_{4'i}I_2 + k_{4'})}{(\sigma_{4i}I_2 + k_4)} \left(\frac{k_1 - k}{k}\right)\left(\frac{\sigma_{4i}\sigma_{14}}{\sigma_{4'i}\sigma_{\ell 4'}}\right) - 1.$$

We see once again the possiblity for observing biexponential decay and in this case the ratio may show some intensity dependence depending on the system parameters.

REFERENCES

1. W. R. Lambert, P. M. Felker and A. H. Zewail, J. Chem. Phys. **75** 5958 (1981).
2. P. M. Felker and A. H. Zewail, Chem. Phys. Lett., to be published.
3. B. I. Greene, R. M. Hochstrasser and R. B. Weisman, Chem. Phys. **48**, 289 (1980).
4. J. A. Syage, W. R. Lambert, P. M. Felker, A. H. Zewail and R. M. Hochstrasser, Chem. Phys. Lett. **88**, 266 (1982).
5. A. Amirav and J. Jortner, Chem. Phys. Lett. **75**, 295 (1983).
6. T. S. Zwier, E. Carrasquillo and D. H. Levy, J. Chem. Phys. **78**, 5493 (1983).
7. D. P. Millar and A. H. Zewail, Chem. Phys. **72**, 381 (1982); D. P. Millar, Ph.D. Thesis, California Institute of Technology (1982).
8. S. L. Shapiro, R. R. Cavanagh and J. C. Stephenson, Opt. Lett. **6**, 470 (1981).
9. J. P. Maier and D. W. Turner, J. Chem. Soc. Faraday Trans. **269**, 196 (1973).
10. K. Yoshihara, A. Namiki, M. Sumitani and N. Nakashima, J. Chem. Phys., **71**, 2892 (1979).
11. D. A. Chernoff and S. A. Rice, J. Chem. Phys. **70**, 2511 (1979).
12. P. Avouvis, W. M. Gelbart and M. A. El-Sayed, Chem. Rev. **77**, 793 (1977).
13. W. Rhodes, "Radiationless Transitions," ed. S. H. Lin, 219-258 (1980), Academic Press, New York.

14. S. H. Lin, "Radiationless Transitions," ed. S. H. Lin, 363-422 (1980), Academic Press, New York.

15. K. F. Freed and A. Nitzan, J. Chem. Phys. **73**, 4765 (1980).

16. P. R. Stannard and W. M. Gelbart, J. Phys. Chem. **85**, 3592 (1981).

17. W. Rhodes, J. Phys. Chem. **87**, 30 (1983).

18. J. D. McDonald, Ann. Rev. Phys. Chem. **30**, 29 (1979).

19. R. P. H. Rettschnick, "Radiationless Transitions," ed. S. H. Lin, 185-218 (1980), Academic Press, New York.

20. A. Zewail, W. Lambert, P. Felker, J. Perry and W. Warren, J. Phys. Chem **86**, 1184 (1982).

21. C. S. Parmenter, J. Phys. Chem. **86**, 1735 (1982).

22. R. E. Smalley, J. Phys. Chem. **86**, 3504 (1982).

23. S. H. Lin, Z. Xing-Gvo, Q. Zhi-Dng, L. Xing-Wen and H. Eyring, Proc. Natl. Acad. Sci. USA **79**, 1356 (1982).

24. E. W. Schlag and H. J. Neusser, Acc. Chem. Res. **16**, 355 (1983).

25. a) S. V. Andreyev, V. A. Antonov, I. N. Knyazev and V. S. Letokhov, Chem. Phys. Lett. **45**, 166 (1977); b) D. H. Parker and M. El-Sayed, Chem. Phys. **42**, 379 (1979); c) D. S. Zakheim and P. M. Johnson, Chem. Phys. **46**, 263 (1980); P. M. Johnson, Acc. Chem. Res. **13**, 20 (1980); C. E. Otis, J. L. Knee and P. M. Johnson, J. Phys. Chem. **87**, 2232 (1983); d) T. G. Dietz, M. A. Duncan and R. E. Smalley, J. Chem. Phys. **76**, 1227 (1982).

26. J. R. Ackerhalt and J. H. Eberly, Phys. Rev. A **14**, 1705 (1976).

27. A. Warshel, J. Chem. Phys. **62**, 214 (1975).

28. L. R. Khundkar, R. A. Marcus and A. H. Zewail, J. Phys. Chem. **87**, 2473 (1983).

29. B. I. Greene and R. C. Farrow, J. Chem. Phys. 78, 3336 (1983).

30. In ref. 15, the t-stilbene response was reported to be flat over 10 ps. This is consistent with our relatively low power results. However, as we emphasized in section 4A, the ratio (R) for UV pumping-visible probing is dependent on the visible intensity. Note that in our UV pumping-UV probing experiments we again observe the biexponential behavior which mimics the relatively high power UV pumping-visible probing behavior.

Figure 1: Schematic showing the level structure, optical transitions and decay rates relevant to the UV-VIS picosecond pump-probe MPI experiment. Stimulated emission processes, discussed in text, have not been indicated on this figure.

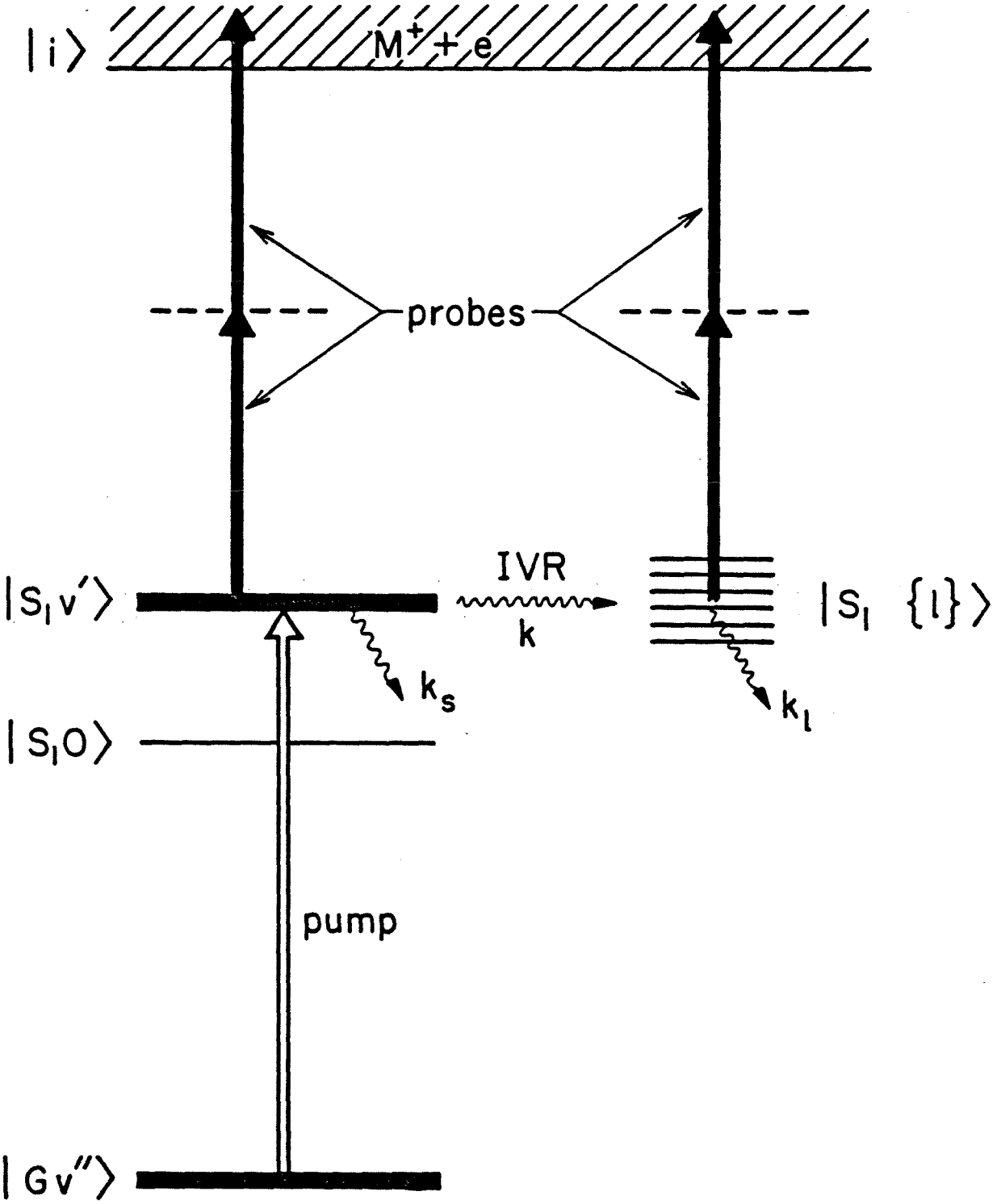
|i⟩
M+ + e
probes
IVR
k
|S1 v'⟩
|S1 {l}⟩
ks
kl
|S1 0⟩
pump
|G v''⟩

Figure 2: Schematic diagram of the amplified picosecond pulse laser system. Abbreviations used are: RF, radiofrequency; DC, dye cell; SF, spatial filter pinhole; CL, cylindrical lens; BD, beam dump for 1.064 m radiation. Typical pulse parameters at various stages in the system are indicated.

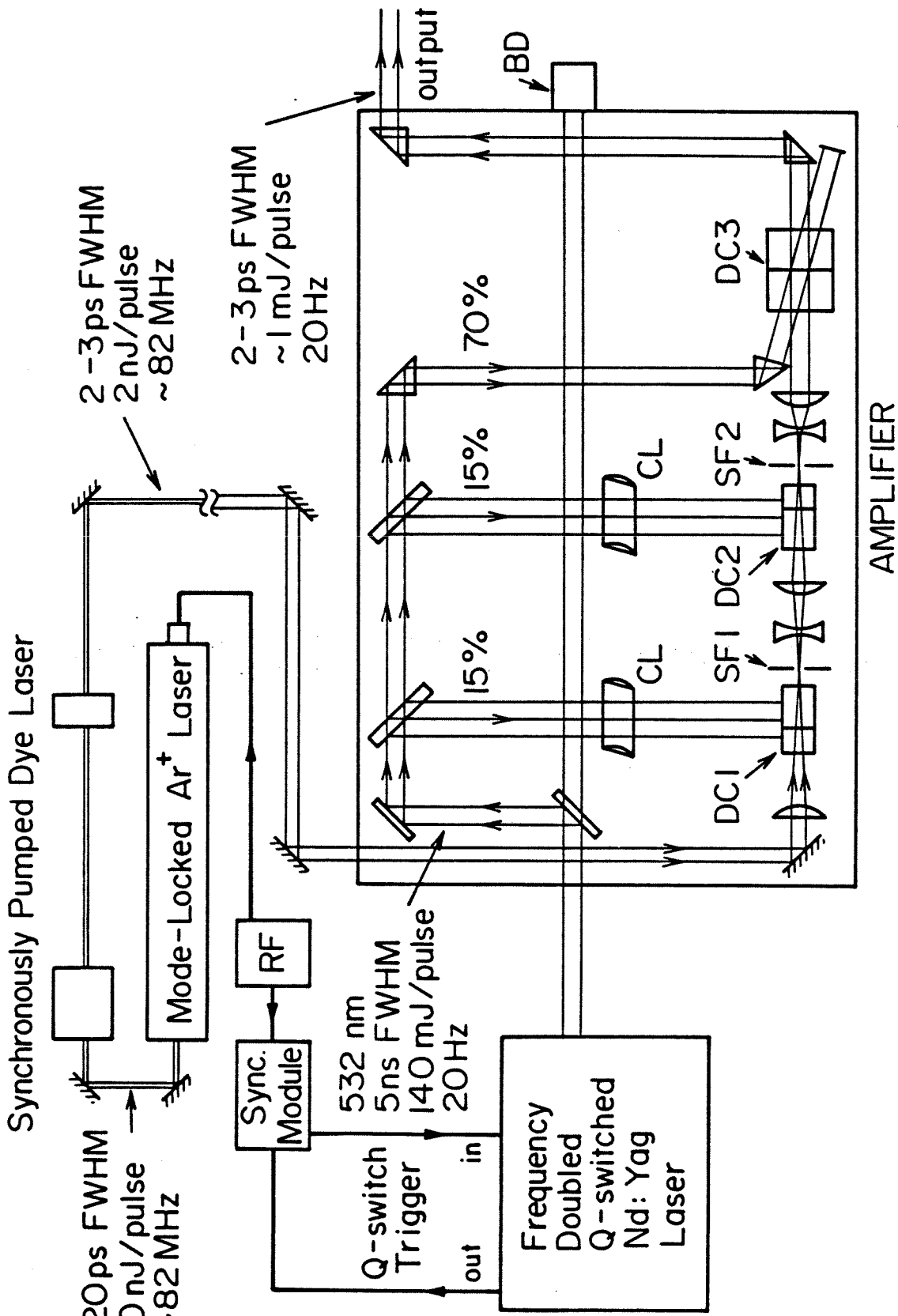
Synchronously Pumped Dye Laser
120ps FWHM
10nJ/pulse
~82MHz
2-3ps FWHM
2nJ/pulse
~82MHz
Mode-Locked Ar+ Laser
RF
Sync. Module
532 nm
5ns FWHM
140mJ/pulse
20Hz
Q-switch Trigger
out
in
Frequency Doubled Q-switched Nd:Yag Laser
2-3ps FWHM
~1mJ/pulse
20Hz
output
BD
70%
15%
15%
CL
CL
DC3
SF2
DC2
SF1
DC1
AMPLIFIER

Figure 3: Autocorrelation traces of picosecond pulses from: A, mode-locked dye laser and B, amplified system. The intensity is the second-harmonic intensity. The points are the experimental data and the smooth curves are the best fit calculated functions. The calculated curves were obtained using Lorentzian model functions for the pulse envelope and noise process autocorrelation functions. The fits are fairly good, but not perfect because the actual pulse shape undergoes a change from Lorentzian to Gaussian in the range of the cavity length detuning used here ($\sim +5\,\mu m$). The laser amplifier gain was $\sim 2 \times 10^5$ for B.

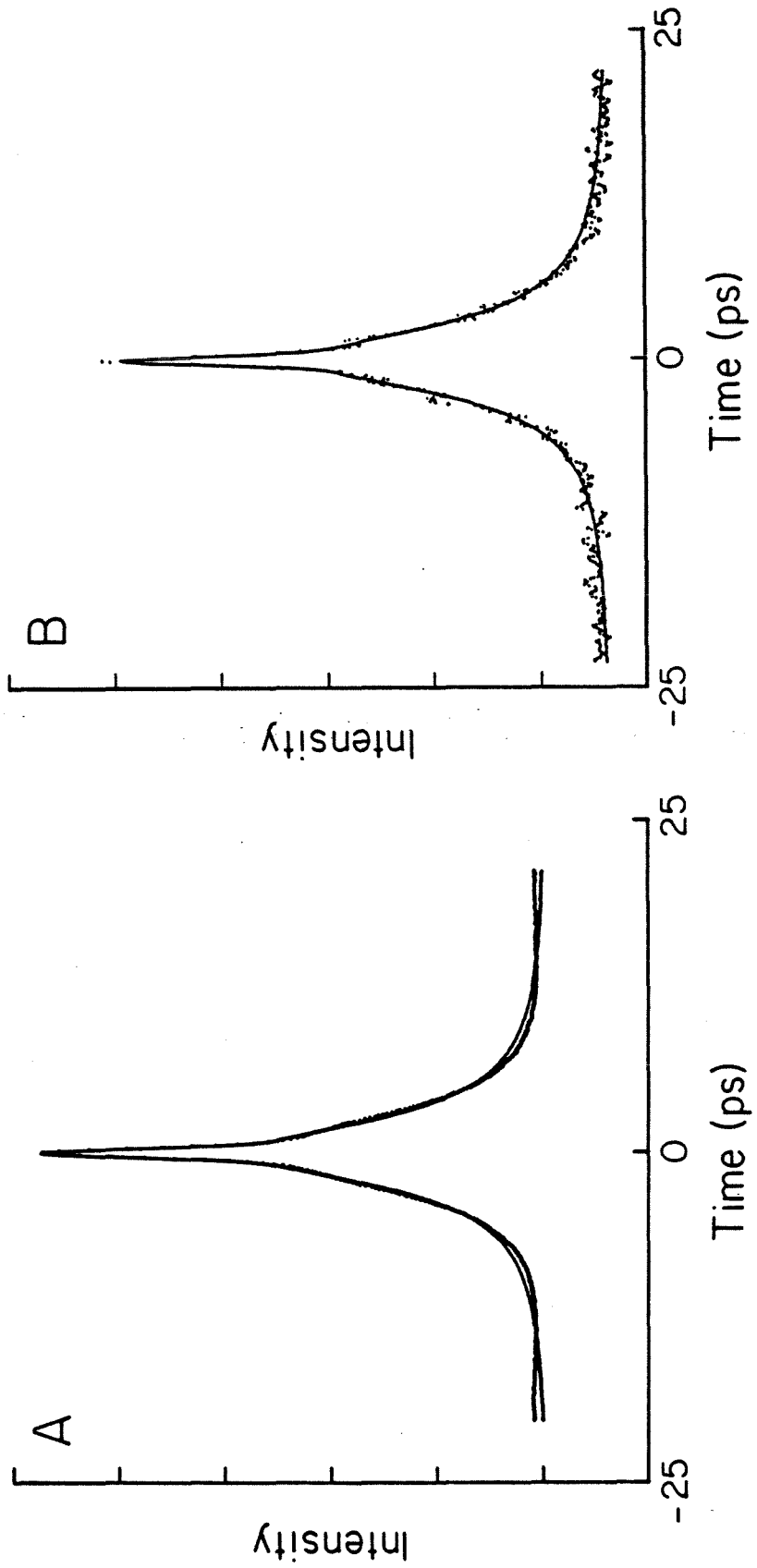
A
B
Intensity
Intensity
-25
0
25
Time (ps)
-25
0
25
Time (ps)

Figure 4: Dependence of laser pulse width and coherence time on net amplified power (proportional to amplifier gain). Pulse parameters obtained by analysis of autocorrelation functions of laser pulses. Note the essentially constant pulse width (broadened only slightly at higher gain, 18 mW $\sim$ 10^6 gain) and coherence time.

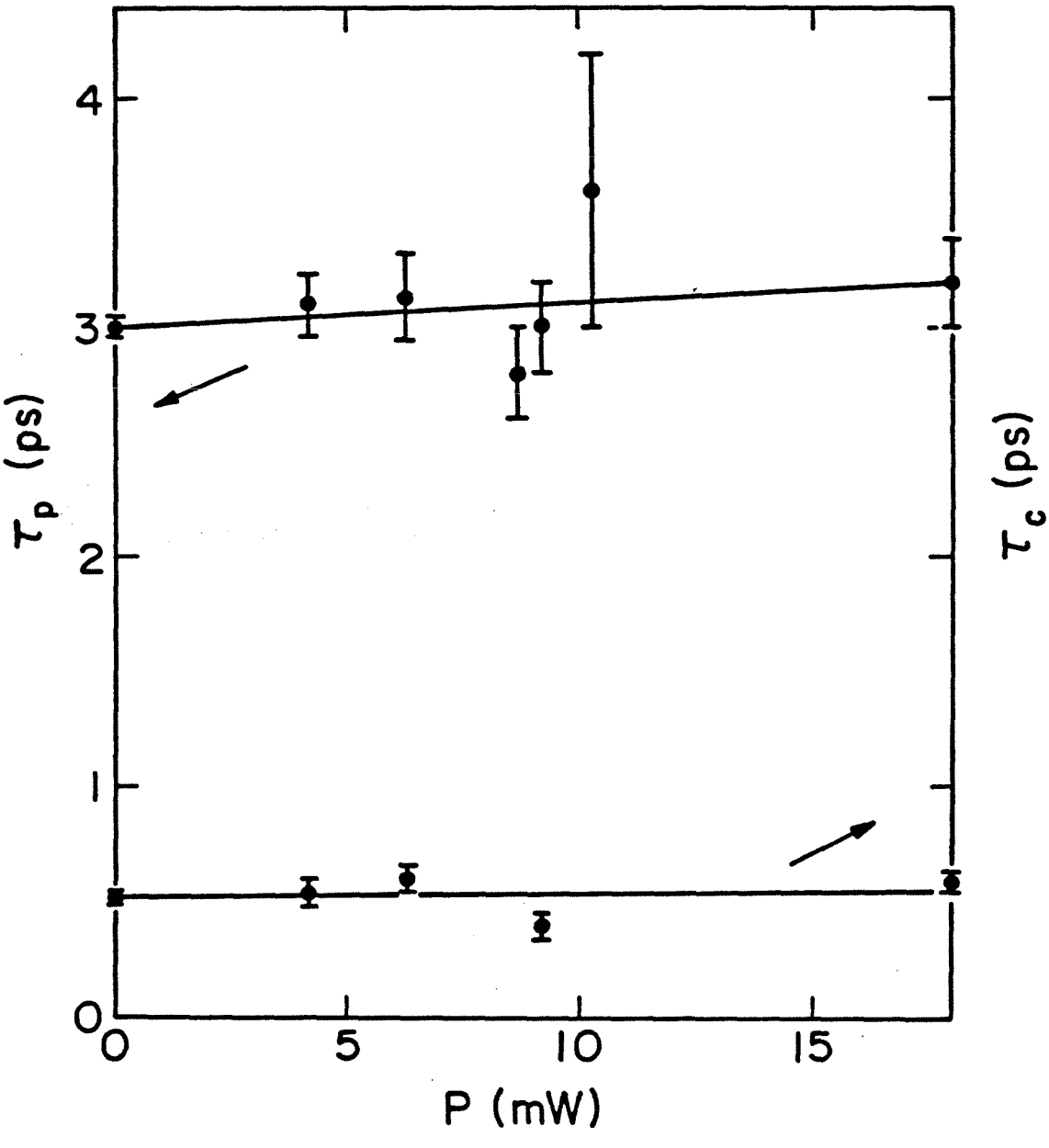
4
3
2
1
0
0
5
10
15
P (mW)
τ_p (ps)
τ_c (ps)

Figure 5: Schematic diagram showing the experimental arrangement for the picosecond MPI experiment for UV pump-visible probe. For UV pump-UV probe, a slightly different arrangement was used (see text). Abbreviations used are: BS, beam splitter; F, filter; KDP, potassium dihydrogen phosphate crystal; ST, scanning translator; DM, dichroic mirror; PM, photomultiplier; PD, photodiode; L, lens; PIC, photoionization cell; CSPA, charge sensitive preamplifier; BVS, bias voltage supply; PA, preamplifier; BA, boxcar averager; VFC, voltage-to-frequency converter; MCA, multichannel analyzer; SMC, stepping motor controller; TP, Tektronix plotter (TK-4662).

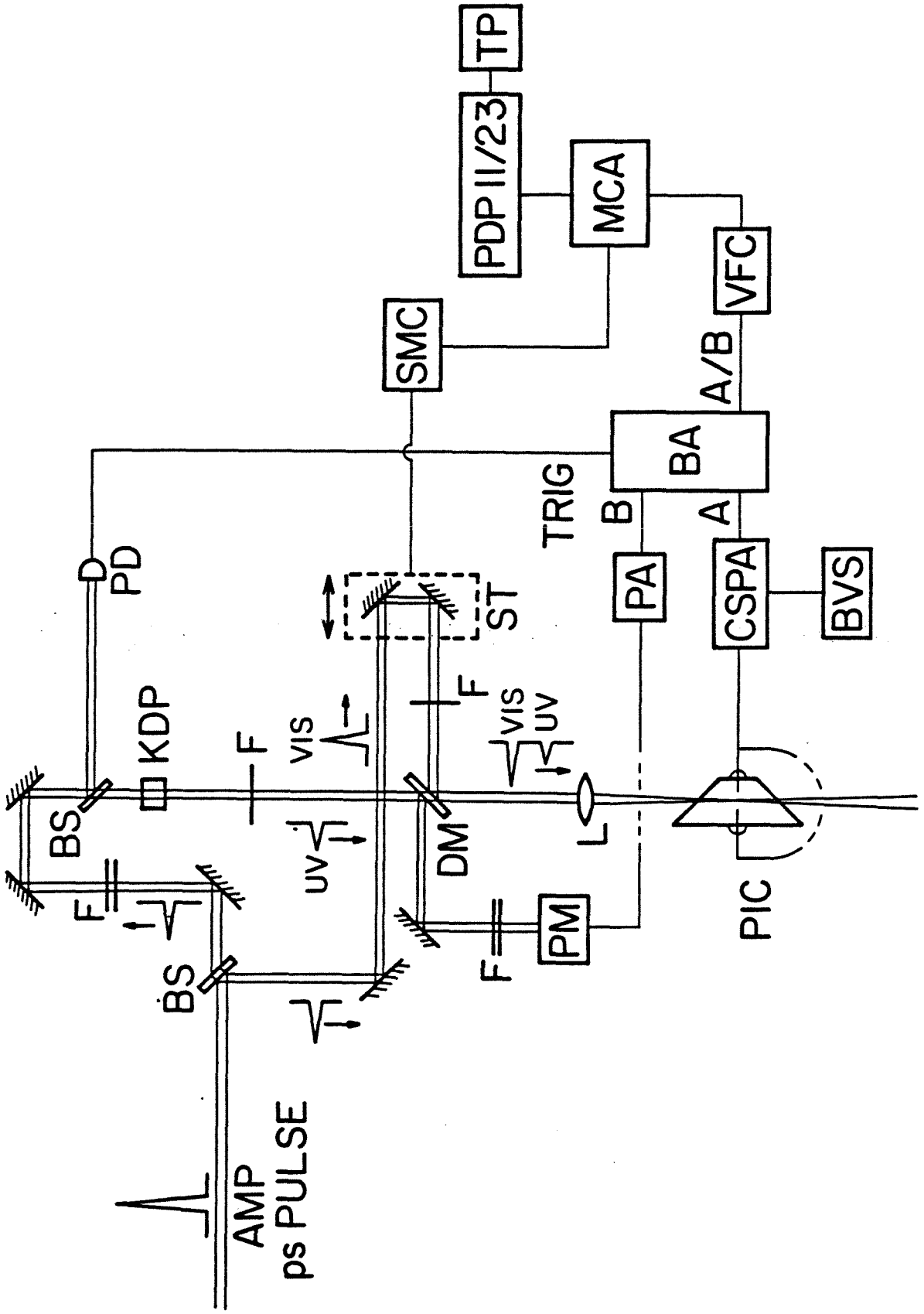
TP
PDP 11/23
MCA
VFC
SMC
A/B
BA
TRIG
B
A
PA
CSPA
BVS
D
PD
ST
F
VIS
UV
KDP
F
BS
DM
L
PIC
F
PM
BS
AMP
ps PULSE

Figure 6A: Schematic diagram of "real-time" autocorrelator. Abbreviations used are: BS, beam splitter; RP, right angle prism; CC, corner cube; S, shaker; L, lens; FDC, frequency doubling crystal ($LiIO_3$ or KDP); ID, iris diaphragm; F, filter; PMT, photomultiplier tube; HV, high voltage power supply; OS, oscilloscope; OSC, variable phase oscillator; AMP, audio amplifier.

B: Schematic diagram of "slow"-scanning autocorrelator. Abbreviations used are: PD, photodiode; ST, scanning translator; others as in Figure 6a or Figure 5.

A

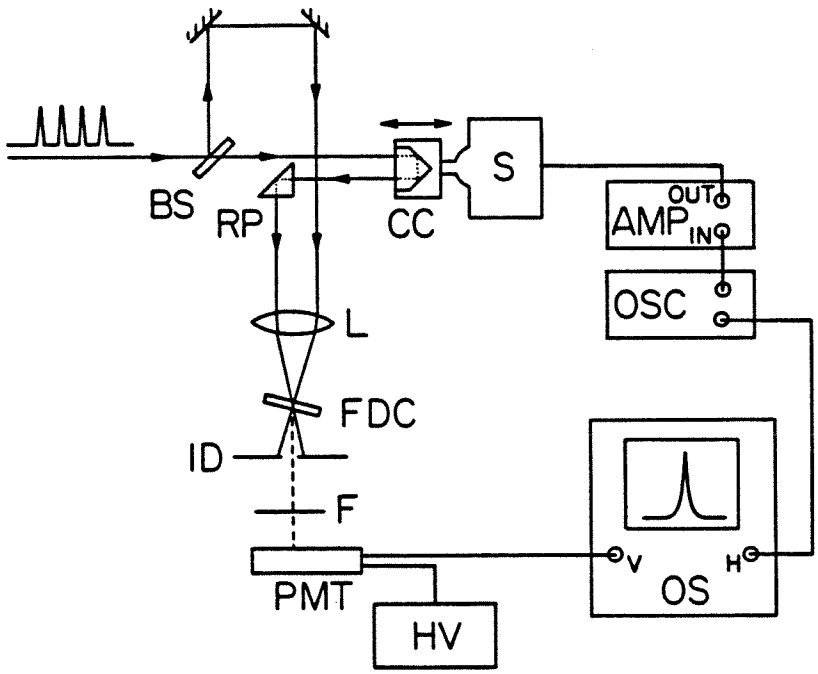
BS
RP
CC
S
AMP
OUT
IN
OSC
L
FDC
ID
F
PMT
HV
V
H
OS

B

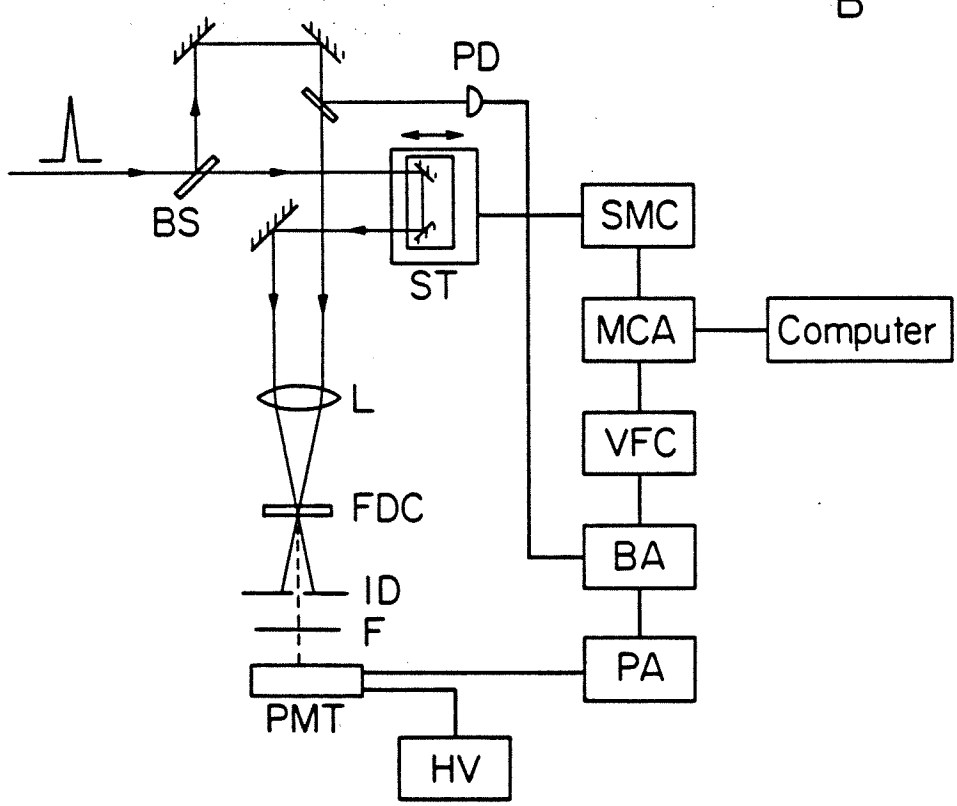
PD
BS
ST
SMC
MCA
Computer
VFC
BA
PA
L
FDC
ID
F
PMT
HV

Figure 7: Representative decays showing the "long" and "short" time behavior of the trans-stilbene MPI delay time decay. The temperature was 296K; pressure was about $5 * 10^{-5}$ torr. The wavelengths were λ_{pump} = 2976 Å and λ_{probe} = 5952 Å. The solid lines are the best fit convolutions of a biexponential decay with Gaussian pulses of about 4 ps FWHM. Also shown is the weighted deviation of the long time scan.

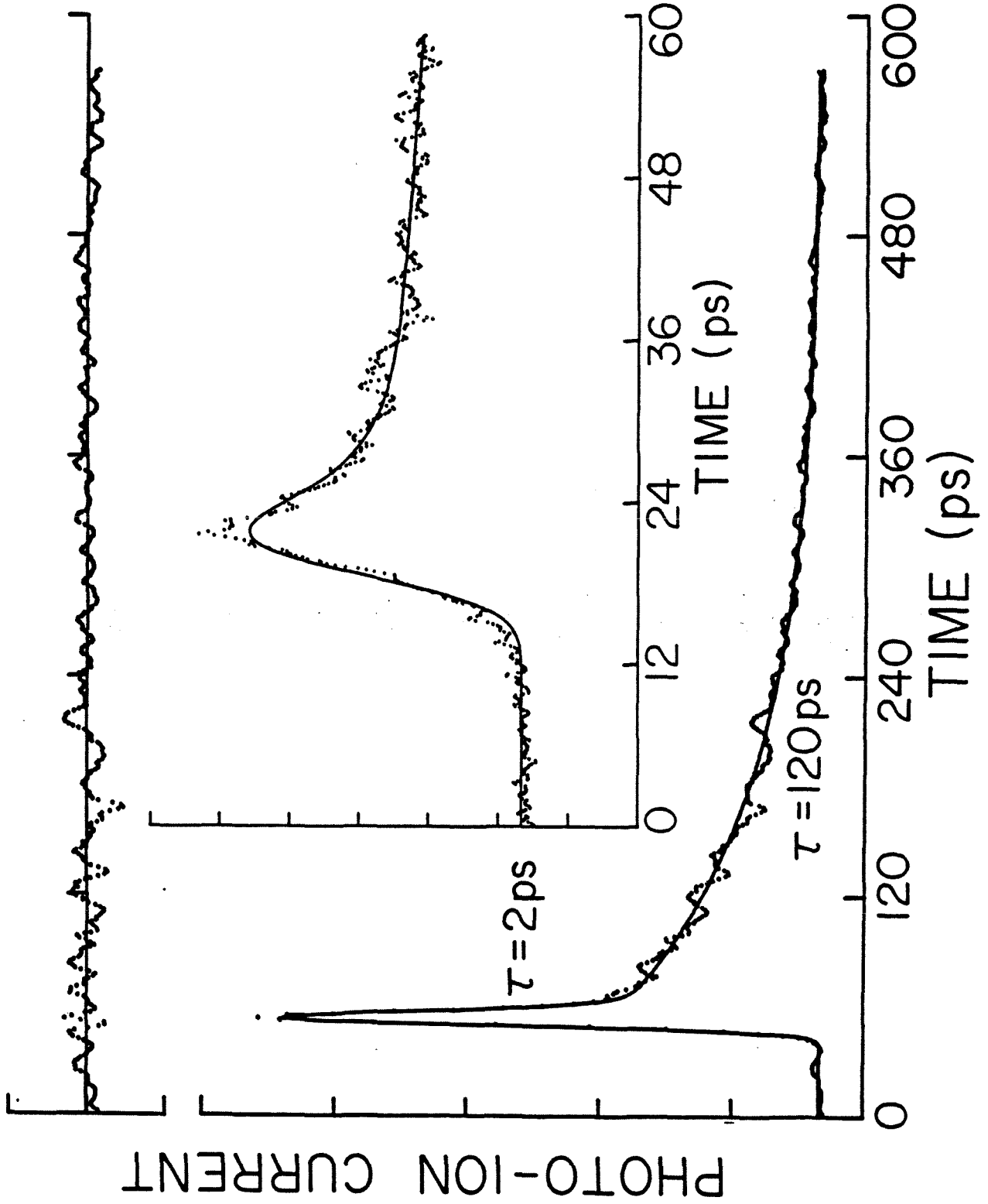
PHOTO-ION CURRENT
0
120
240
360
480
600
TIME (ps)
τ=120ps
0
12
24
36
48
60
TIME (ps)
τ=2ps

Figure 8A: Log-log plot of the integrated ion current vs the UV pulse energy (constant pulse width) for UV-VIS pump-probe experiment of trans-stilbene vapor (296K). λ_{UV} = 2975 Å, λ_{VIS} = 5950 Å. Note the essentially linear behavior with a slope $\sim$ 1.

B: Log-log plot of the integrated ion current vs the VIS the pulse energy for the UV-VIS pump-probe experiment. Same wavelengths used as above. Note the slope of the line indicated is $\sim$ 1.

C: Log-log plot of the fraction of the total amplitude which decays by the fast decay rate vs the VIS pulse energy. The slope of the line indicated is $\sim$ 1, however the actual behavior seems to be a form of saturation. Same wavelengths used as above.

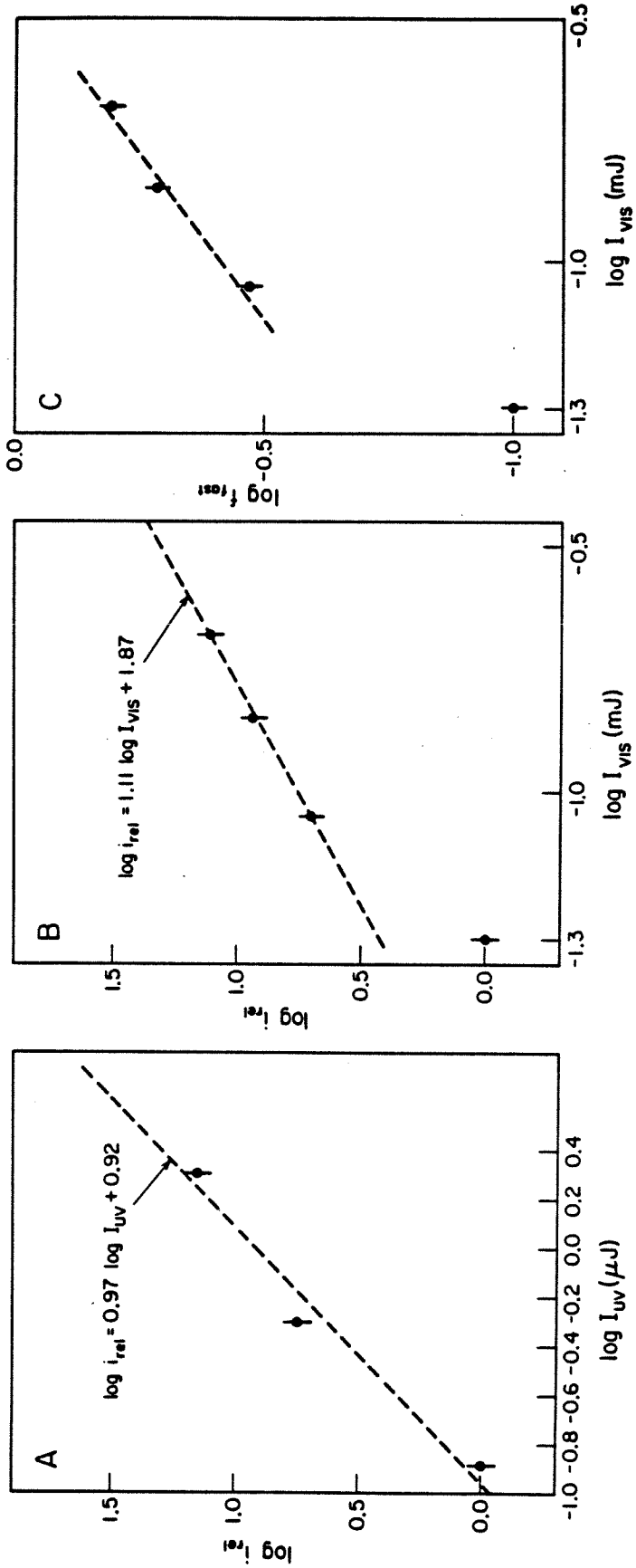
A
log i_{rel} = 0.97 log I_{UV} + 0.92
log i_{rel}
log I_{UV} (μJ)
B
log i_{rel} = 1.11 log I_{VIS} + 1.87
log i_{rel}
log I_{VIS} (mJ)
C
log f_{ass}
log I_{VIS} (mJ)

Figure 9: Representative picosecond pump-probe MPI decay of aniline vapor (side arm temperature 273K) for UV pumping and visible probing. The same result was obtained for excitation of the 0_0^0, $6a_0^1$ or 12_0^1 transitions. The transient shown is a single scan. The solid line is the best fit single exponential funciton with a lifetime of 2 ns. The known lifetime of the fluorescence is $\sim$ 6.7 ns,[11] however the limited range and signal to noise of this scan do not allow an accurate determination of the lifetime; also it would not be possible for us to extend the range of the scan enough to make such a measurement due to the limit of the interferometer scan ($\sim$ 2 ns). Note the absence of a very fast decay component as described in the text.

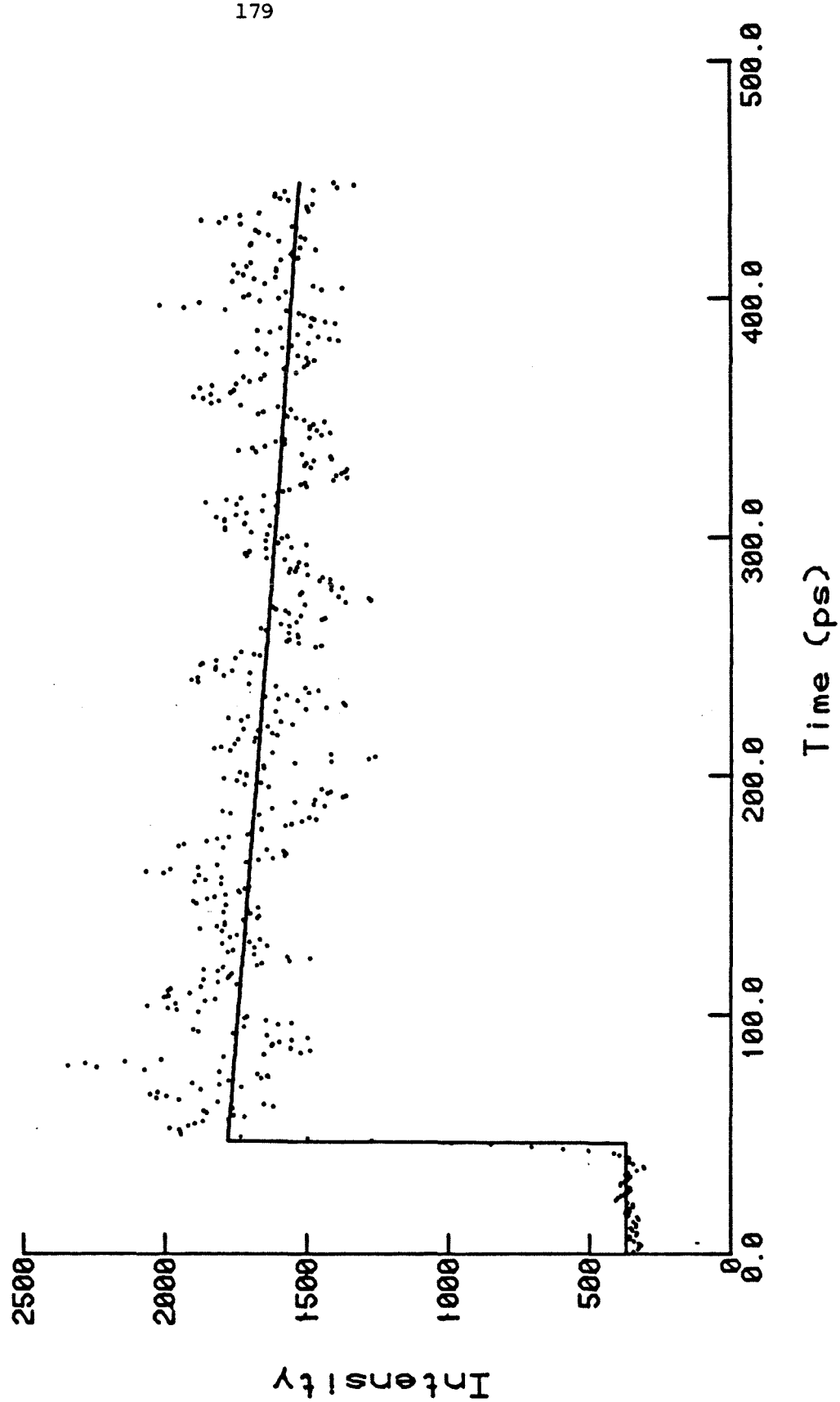
Intensity
2500
2000
1500
1000
500
0
0.0
100.0
200.0
300.0
400.0
500.0
Time (ps)

Figure 10A: Representative picosecond MPI delay-time decays of trans-stilbene vapor (T = 296K; P = 5 * 10^{-5} torr). The upper plot shows the decay for λ_{pump} = 3075.5 Å and λ_{probe} = 6195 Å; E_x = 200 cm^{-1}. The lower plot is for λ_{pump} = 2876 Å and λ_{probe} = 5752 Å; E_x = 2500 cm^{-1}. Note the different timescales for the two plots. The solid lines are the best fit single exponential for the upper plot and the best fit convolution of a Gaussian pulse and a biexponential decay for the lower plot. Also shown are the weighted deviations.

B: Excess energy dependence of trans-stilbene S_1 decay rates. Results from several experimental studies (points) and the calculated thermally averaged rates are plotted. The lower abscissa is the excess energy for room temperature (296K). The free-jet data should not be referred to this axis. The upper abscissa is the total energy and may be used as a common axis for all the experimental data, as discussed in the text.

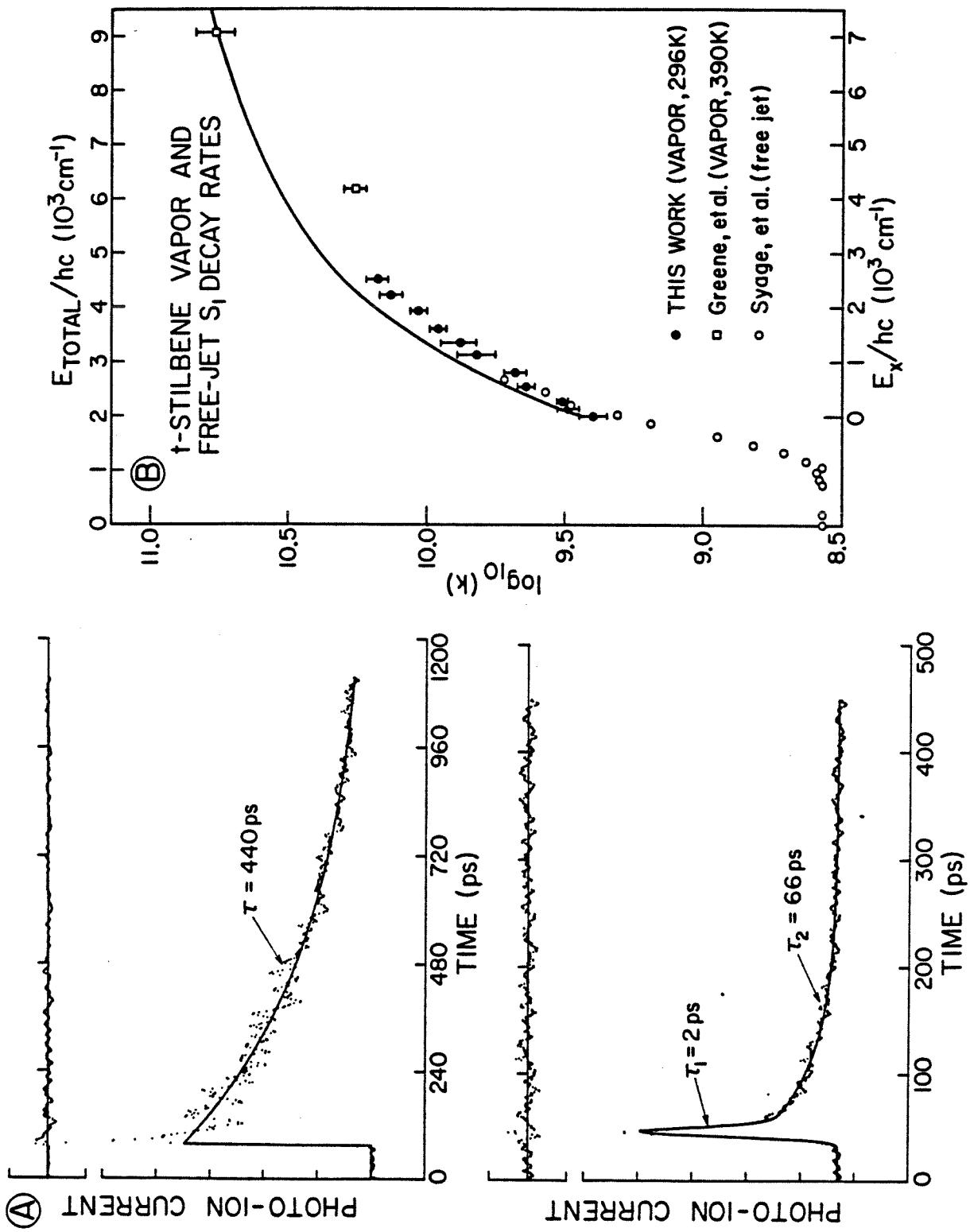
(A)
PHOTO-ION CURRENT
τ = 440 ps
TIME (ps)
τ1 = 2 ps
τ2 = 66 ps
(B)
t-STILBENE VAPOR AND
FREE-JET S1 DECAY RATES
ETOTAL/hc (10³cm⁻¹)
log10 (k)
Ex/hc (10³ cm⁻¹)
• THIS WORK (VAPOR, 296K)
□ Greene, et al. (VAPOR, 390K)
○ Syage, et al. (free jet)

Figure 11: Calculated thermal probability distributions for trans-stilbene at 296K (solid lines). The excitation of the ground state distribution to an electronically excited state +4000 cm^{-1} of excess vibrational energy is shown. The probability scale is 10x actual value. The energy scale is in cm^{-1} for energy above the ground state (E) or the excited state (E_x). The dashed curve is the distribution for complete thermalization of the total vibrational energy of the excited electronic state.

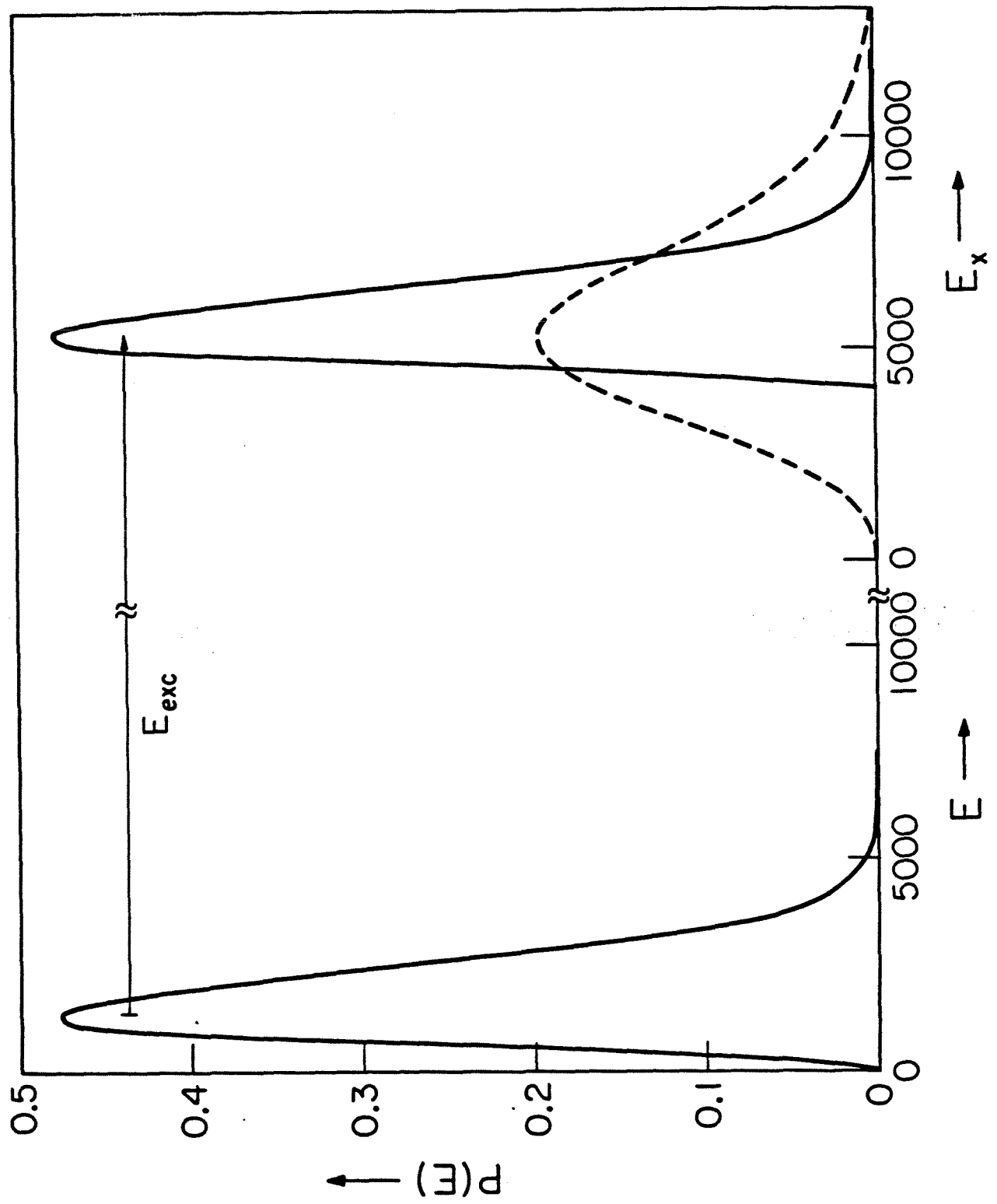
0.5
0.4
0.3
0.2
0.1
0
P(E)
0
5000
10000
≈
0
5000
10000
E
E_x
E_exc

Figure 12A: Schematic diagram of the levels and transitions relevant to the kinetic analysis of the UV-UV resonant two-photon time-resolved MPI (single manifold case). Solid lines are stimulated processes and the curvey lines are spontaneous decay processes.

B: Schematic diagram relevant to the kinetic analysis of a simplified model of the UV-VIS resonant three-photon time-resolved MPI (single manifold case).

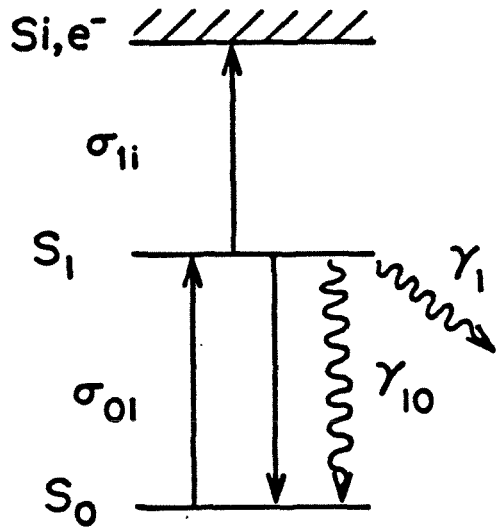

A

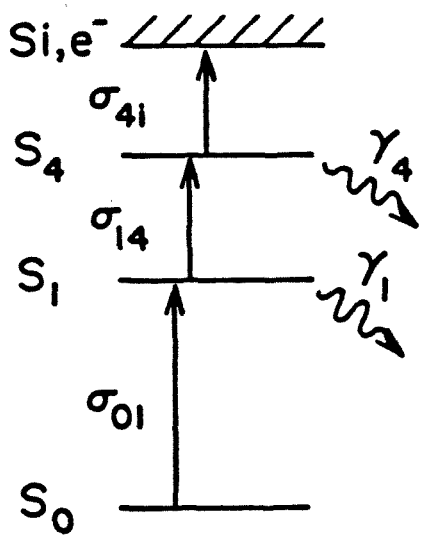

B

APPENDIX I

Reprinted from The Journal of Physical Chemistry, 1983, 87, 1480.

Laser Spectroelectrochemistry of a Ruthenium(II) Tris(bipyridyl) Derivative Adsorbed on Graphite Electrodes

Joseph W. Perry, A. James McQuillan,† Fred C. Anson,* and Ahmed H. Zewail*‡

Arthur Amos Noyes Laboratory of Chemical Physics, ⊥ California Institute of Technology, Pasadena, California 91125
(Received: February 4, 1983)

The luminescence spectra of laser-excited films of $[Ru(bpy)_2pbpy]Cl_2$ (bpy = 2,2′-bipyridine; pbpy = 4,4′-bis(2-(diphenylamino)ethyl)-2,2′-bipyridine) adsorbed on pyrolytic graphite electrode surfaces are reported. The graphite electrode surface is shown to be effective in quenching the excited state and the resulting decay of the luminescence is analyzed. The intensity of the luminescence from the molecules in the film can be modulated by controlling the potential of the underlying electrode. It is shown that the emitting molecules are in electronic contact with the electrode.

Introduction

There has been considerable recent interest in molecular luminescence as a probe of charge propagation mechanisms in films and coatings on electrode surfaces.[1-7] For example, fluorescence has been observed from amorphous zinc tetraphenylporphyrin films adsorbed on basal plane graphite electrodes and the intensity of the emission responded to changes in the electrode potential.[4] Electrochemical control of the luminescent lifetime of $Ru(bpy)_3^{2+*}$ confined within a polyelectrolyte film on a graphite electrode also has been demonstrated[6] and a possible mechanism for the quenching of such luminescence has been discussed.[6,7] Very recently, the dynamics of luminescence of $Ru(bpy)_3^{2+}$ adsorbed on various powdered semiconductor surfaces were reported.[8] This study showed that the luminescence decay for adsorbed molecules was enhanced on the semiconductor surfaces and that the decay could be decomposed into two components. The emission spectrum obtained early in the decay was blue shifted relative to that observed late in the decay. These results were interpreted in terms of two types of emitting sites corresponding to $Ru(bpy)_3^{2+}$ molecules which were "tightly" or "loosely" bound to the surface. The tightly bound molecules were argued to be involved in an electron-transfer interaction with the semiconductor to explain the short lifetime and blue-shifted luminescence. However, the dependence of the luminescence on the film thickness was not reported owing to difficulties in uniformly varying the coverage on the powdered samples.

In this report, time and spectrally resolved emission studies of homogeneous films of the complex $[Ru(bpy)_2(pbpy)]Cl_2$ (bpy = 2,2′-bipyridine; pbpy = 4,4′-bis(2-(diphenylamino)ethyl-2,2′-bipyridine) adsorbed on pyrolytic graphite electrodes are described. The emission lifetime of the adsorbed complex was shown to increase with the thickness of the film suggesting that the excited state is quenched by the underlying graphite surface, consistent with the results obtained on powdered semiconductor surfaces.[8] The emission intensity could be reversibly decreased and increased by cycling the electrode potential, showing that the luminescing molecules are in electronic contact with the electrode.

Experimental Section

Materials. Rutheniumbis(bipyridyl) 4,4′-bis(2-(diphenylamino)ethyl-2,2′-bipyridine dichloride was generously donated by D. A. Buttry who prepared it by a slight modification of a published method.[9] Pyrolytic graphite electrodes (Union Carbide Co., Chicago) having the edges of the graphite planes exposed to the solution were cut and mounted as described previously.[10] The circular disk electrode surface (0.34 cm^2) was polished initially with fine silicon carbide paper followed by an aqueous slurry of 0.3-μm alumina. The electrode was then immersed in 0.1 M aqueous HCl solution for 10 min, washed with distilled water, and allowed to dry in air for 1 h. Circular Optosil (fused-quartz) plates with the same surface area as the graphite electrodes were used to prepare films for absorption spectral measurements. Films of the complex were deposited by transferring a few microliters of a 1 mM solution of the complex in methanol to the graphite disk or silica plate which was held in a horizontal position in an evaporation chamber containing methanol-saturated air. The resulting films were of fairly uniform thickness in the center of the disks but the thickness increased by a factor of ca. 3–5 toward the outside edge of the disk. This type of film thickness variation is commonly observed for evaporatively deposited films[6,11] and probably arises from a more rapid evaporation from the edge of the solution droplet. The relative thickness of the center and edge of the film was measured by a Sloan Dektak profilometer and confirmed qualitatively by the relative intensities of the emission obtained when the edge or center of the coated disks was irradiated. The deposited films were reasonably stable so long as the ruthenium was present as Ru(II). Repetitive cycyling of the coated electrode over a potential range where the ruthenium is successively oxidized and re-reduced led to gradual loss of the coating from the surface as evidenced by the decreased intensity of the luminescence and smaller area under the cyclic voltammograms. The loss is believed to result from the greater solubility of the Ru(III) complex.

The areas under cyclic voltammograms typically corresponded to about 10% of the total quantity of complex initially deposited in the films. The missing 90% represents the sum of complex that is lost from the surface by dissolution and the portion of the complex on the surface without adequate ionic contact to the supporting electrolyte solution for complete electroactivity to be obtained on the experimental time scale.

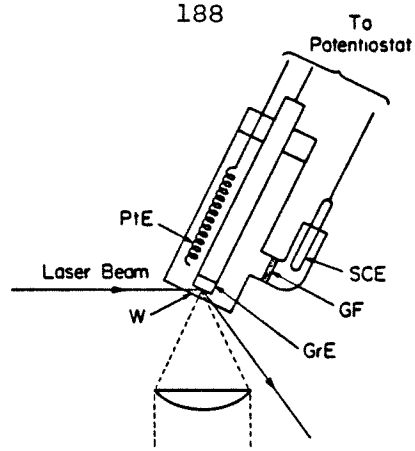

Figure 1. Schematic diagram of the electrochemical cell showing the geometry for laser excitation, and collection of emission from the film-coated electrode surface: PtE, platinum auxillary electrode; W, glass window; GrE, graphite electrode; GF, glass frit; SCE, saturated calomel electrode.

Electrochemical Apparatus. A sketch of the electrochemical cell employed is shown in Figure 1. A flat Pyrex glass window is provided for illumination of, and monitoring the emission from, the electrode surface. The surface of the graphite electrode was about 2 mm from the cell window. The auxiliary electrode was a platinum wire contained in the same cell compartment. The saturated calomel reference electrode (SCE) was separated from the test solution by a porous glass frit (quoted potentials are vs. this electrode). The potential of the graphite electrode was controlled by means of a PAR Model 174 polarographic analyzer (E G & G Instruments, Princeton, NJ). The luminescence intensity and cyclic voltammetric response were recorded simultaneously by means of a two-pen $X-Y_1Y_2$ recorder (Hewlett Packard 7046A). The cell and electrode placements in these preliminary experiments were not optimized to produce uniformity of current flow. As a result, the intensity of the luminescence was much more sensitive to the electrode potential when the exciting laser beam was directed near the edge of the graphite electrode closest to the platinum auxillary electrode. Although we did not explore the observations in greater detail it seems clear that the high intensities and spatial resolution available from laser sources could easily be exploited to probe variations in the uniformity of the current distribution at electrode surface where luminescent reactants are present.

A tunable dye laser system served as a source for film photoexcitation. The system consisted of a Molectron UV-24 nitrogen laser which pumped a DL-II dye laser. The dye laser, employing coumarin-481 (pulse width ~ 8 ns) delivered about 0.5 mJ at the sample after band-pass filtering and partial reflection to excite a photdiode. All experiments were performed with a laser pulse repetition rate of 10 Hz. The photodiode signal was used to trigger a boxcar integrator (Princeton Applied Research Model 164 with Model 162 integator and digital storage) which averaged the photomultiplier (EMI 9659QB) signal. The emission of the laser-excited films was collected, taking care to avoid the specular reflection of the laser beam. The emission was dispersed with a 0.75-m Spex spectrometer (Model 1402). The response time of the system was de-

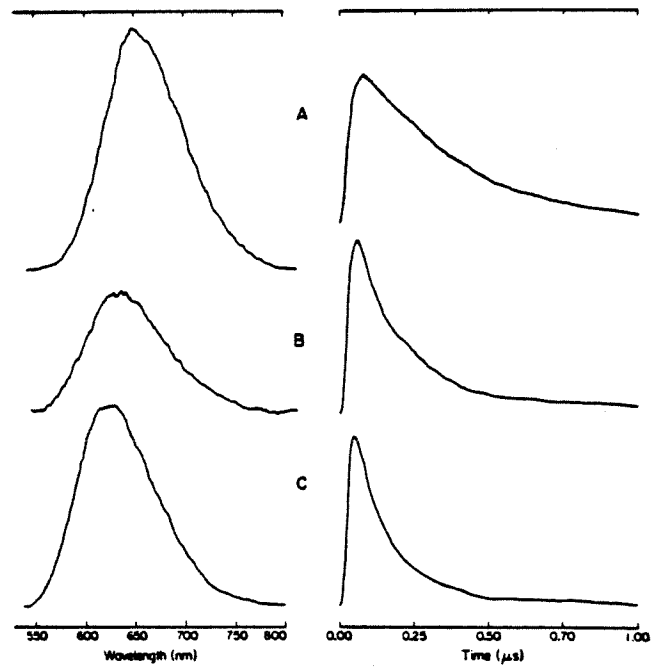

Figure 2. Spectrally (left) and temporally (right) resolved emission of $Ru(bpy)_2(pbpy)Cl_2$ in various media: (A) 10^{-5} M in 0.2 M aqueous $LiClO_4$; (B) film adsorbed on graphite electrode immersed in electrolyte; (C) dry film adsorbed on graphite electrode, measured in air. The spectra have not been corrected for the response of the system.

termined by the fall time of the photomultiplier tube: ca. 20 ns. Time decays were obtained by scanning the boxcar integrator gate (width = 5 ns) over the range of the transient PMT signal. For all optical measurements the excitation wavelength was 519 nm and for the transient decays the emission was detected at 650 nm. Emission spectra were obtained by holding the boxcar gate near the maximum of the transient and scanning the spectrometer wavelength. All experiments were performed at room temperature.

Results and Discussion

Spectroelectrochemistry of Films of $Ru(bpy)_2(pbpy)Cl_2$ Adsorbed on Graphite Electrodes. The emission spectra of films deposited on graphite were recorded in both the dry state and when immersed in aqueous supporting electrolyte solutions. These spectra were compared with that of the same complex dissolved in solution in Figure 2. The wavelength of the emission maximum appears at 625 nm in the dry film, 635 nm for the film in contact with the aqueous electrolyte (0.2 M $LiClO_4$), and 650 nm for the complex in bulk solution. We infer from this trend that the complex in the deposited film is partially solvated by the electrolyte solution. Further evidence for this comes from the decays of the emission that are also shown in Figure 2. In the homogeneous solution the decay is exponential with a lifetime of 315 ± 20 ns. The dry film exhibits nonexponential decay and the behavior of the partially solvated film is intermediate between that of the other two as expected from the relative shifts in the emission maxima.

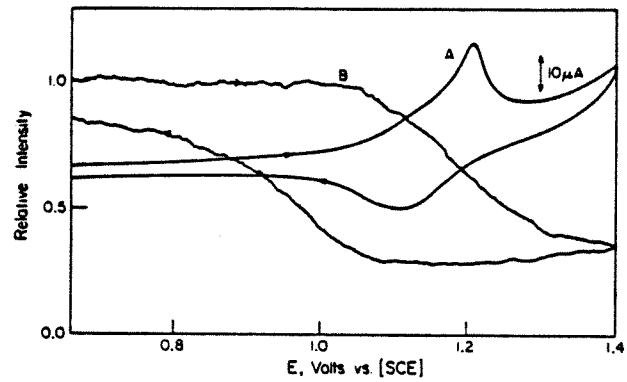

Figure 3. A simultaneous recording of (A) a cyclic voltammogram and (B) the emission intensity for a film of $Ru(bpy)_2(pbpy)Cl_2$ adsorbed on a graphite electrode: total quantity of material in film, 1.1×10^{-8} mol cm^{-2}; scan rate, 20 mV s^{-1}; electrolyte, 0.2 M aqueous $LiClO_4$. The current scale for the cyclic voltammogram is indicated by the arrow maker.

In Figure 3 are shown a cyclic voltammogram and the corresponding potential-dependent emission intensity recorded simultaneously for the laser-excited, film-coated electrode. The peak current for the oxidation of Ru^{II} to Ru^{III} appears at +1.2 V and the broad reduction wave has a peak at +1.1 V. The emission intensity begins to decrease just as the conversion of Ru^{II} to Ru^{III} commences. This decrease results from both the oxidative loss of ground-state Ru^{II} complex and the quenching of $*Ru(bpy)_2(pbpy)^{2+}$ by the electrogenerated ground-state Ru^{III} complex. The emission intensity decreases most rapidly at potentials in the vicinity of the oxidation wave. The emission intensity continues to decrease slowly following the reversal of the direction of potential scan until reductive current begins to flow. The intensity then begins to recover although more slowly than it decreased during the oxidative half of the cycle. At the end of the potential scan the intensity had not returned to its original value. However, almost all of the original intensity was regained as the electrode was held at the initial potential for several minutes. This trend of rapid loss of luminescence followed by slower recovery has been observed recently in a study of $Ru(bpy)_3^{2+}$ incorporated in polyelectrolyte coatings where the behavior was attributed to structural changes in the medium in which the luminescent molecule was incorporated.[6] In the present case the delay in the recovery of the luminescence upon re-reduction of the film may arise from the continuous diffusion of the electrogenerated $Ru(bpy)_3^{3+}$ into the irradiated portion of the film from surrounding nonirradiated portions.

Time-Resolved Emission from $*Ru(bpy)_2(pbpy)^{2+}$ in Dry Films on Quartz and Graphite. One of our objectives in this study was to examine the role of the underlying surface in quenching the luminescence from films of $Ru(bpy)_2(pbpy)^{2+}$. To determine if the luminescent lifetime of the complex was decreased on a graphite surface, we found it convenient to prepare a suitable reference film in which the intrinsic decay of the excited states could be measured. Films of the complex deposited on quartz plates served in control experiments in which the underlying surface was assumed to be inert. In Figure 4 the luminescence decay of such a film is shown. The decay does

not follow an exponential curve but it can be approximated crudely as the sum of two exponentials.[12] Doing so leads to short-time and long-time "lifetimes" of 130 ± 20 and 280 ± 70 ns, respectively. These lifetimes are independent of film thickness in the range of 0.6×10^{-8} to 2.9×10^{-8} mol/cm^2. The nonexponential decay of the luminescence could be the result of a triplet–triplet annihilation (TTA) process such as has been reported recently for $Ru(bpy)_3^{2+}$ in micelles,[13] cation-exchange resins,[14] and solutions of polyelectrolytes[15] at high concentrations of the complex and intense irradiation. By observing the variation in emission decay with the intensity of laser irradiation of films of $Ru(bpy)_2(pbpy)^{2+}$ on quartz as well as single crystals of $Ru(bpy)_3^{2+}$, we infer that TTA probably makes a significant contribution to the decay until the laser intensity is decreased to less than 1% of the its nominal value (0.5 mJ). However, such low irradiation intensities produced emissions too weak for reliable measurements with films of $Ru(bpy)_2(pbpy)^{2+}$ deposited on graphite substrates because of the low quantum yield exhibited by this complex.[16] For this reason we utilized laser intensities at levels where TTA was probably a significant quenching pathway that competed with the quenching by the graphite that we were attempting to monitor. Typical decay curves for dry coatings of $Ru(bpy)_2(pbpy)^{2+}$ deposited on graphite and quartz surfaces are compared in Figure 4. The yield of emitting complex on graphite is clearly smaller than that

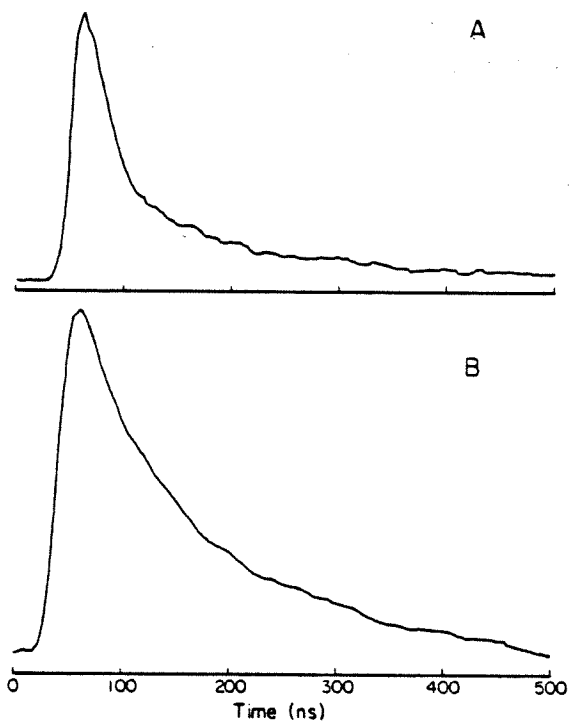

Figure 4. Typical decay curves for $Ru(bpy)_2(pbpy)Cl_2$ films adsorbed on (A) EPG electrode and (B) quartz plate, showing the enhanced decay on the graphite surface. Total quantity of material in film is 1.7×10^{-8} mol/cm^2.

on quartz. In addition, the plots of ln (intensity) vs. time show the rate of decay of the excited complex to be greater on graphite than quartz. Approximate values of the "short-" and "long-time" constants of the decays on graphite (approximated as two exponentials) are listed in Table I for three film thicknesses. The time constants for decay decrease with the film thicknesses as expected if participation of the underlying graphite surface in the quenching became more and more important with thinner and thinner films. Both triplet excitation transfer and electron transfer mechanism could contribute to such surface quenching. The presently available data are inadequate in both quantity and quality (low signal-to-noise ratio) to permit a distinction between these two pathways. We are hopeful that time-correlated photon-counting experiments currently in progress may provide the additional information necessary to allow a clear identification of the evident surface quenching process that we have observed.

TABLE I: Luminescence Decay Time Constants for Films of $[Ru(bpy)_2(pbpy)]Cl_2$ Adsorbed on Graphite

$10^8\Gamma$,[a] mol/cm²	τ,[b] ns
2.9	120 ± 20 short
	290 ± 50 long
1.7	70 ± 10 short
	150 ± 50 long
0.6	40 ± 20

[a] Total quantity of complex deposited on the graphite. The film thickness varied somewhat between the center and edge (see Experimental Section). [b] Approximate time constants obtained from the slopes of logarithmic plots of the initial (short) and later (long) portions of the decay. The film was irradiated at 519 nm and the emission observed at 650 nm. The lifetimes reported here have not been corrected for the finite response time of the system.

Acknowledgment. This work was supported by the U.S. Army Research Office and by the National Science Foundation. We thank Daniel Buttry for the sample of $[Ru(bpy)_2(pbpy)]Cl_2$ and helpful discussions. A.J.M. acknowledges a Fullbright-Hays Travel Grant.

†Present address: Department of Chemistry, University of Otago, Dunedin, New Zealand.
‡Camille and Henry Dreyfus Foundation Teacher–Scholar.
⊥ Contribution No. 6792.

(1) W. Arden and P. Fromherz, *Ber. Bunsenges. Phys. Chem.*, **82**, 868 (1978).
(2) W. Arden and P. Fromherz, *J. Electrochem. Soc.*, **127**, 370 (1980).
(3) T. Iwasaki, T. Sawada, H. Kamada, A. Fujishima, and K. Honda, *J. Phys. Chem.*, **83**, 2142 (1979).
(4) J. S. Pflug and L. R. Faulkner, *J. Am. Chem. Soc.*, **102**, 6144 (1980).
(5) I. Rubinstein and A. J. Bard, *J. Am. Chem. Soc.*, **103**, 5007 (1981).
(6) D. A. Buttry and F. C. Anson, *J. Am. Chem. Soc.*, **104**, 4824 (1982).
(7) M. Majda and L. R. Faulkner, *J. Electroanal. Chem.*, **137**, 149 (1982).
(8) T. Kajiwara, K. Hasimoto, T. Kawai, and T. Sakata, *J. Phys. Chem.*, **86**, 4516 (1982).
(9) S. Sprintschnik, H. W. Sprintschnik, P. P. Kirsch, and D. G. Whitten, *J. Am. Chem. Soc.*, **99**, 4967 (1977).
(10) N. Oyama and F. C. Anson, *J. Am. Chem. Soc.*, **101**, 3450 (1979).
(11) D. A. Buttry and F. C. Anson, unpublished results.
(12) We have considered the possible contribution to the emission decay due to stimulated emission. We conclude that this is not a significant effect in our experiment since typically only ~5% of the molecules in the interaction volume are excited by a laser pulse.
(13) V. Lachish, M. Ottolenghi, and J. Rabani, *J. Am. Chem. Soc.*, **99**, 8062 (1977).
(14) S. Kelder and J. Rabani, *J. Phys. Chem.*, **85**, 1637 (1981).
(15) A. Slama-Schwok, Y. Feitelson, and J. Rabani, *J. Phys. Chem.*, **85**, 2222 (1981).
(16) J. Van Houten and R. J. Watts, *J. Am. Chem. Soc.*, **98**, 4853 (1976).

APPENDIX II

Thermal Lensing Spectroscopy with Picosecond Pulse Trains and a New Dual Beam Configuration

J. W. PERRY, E. A. RYABOV[a] and A. H. ZEWAIL[b]

Arthur Amos Noyes Laboratory of Chemical Physics,[c] California Institute of Technology, Pasadena, California 91125 USA

(Received May 17, 1982)

It is now well-known that thermal lensing (TL)[1,2] induced by CW or pulsed lasers can be used for spectroscopic study of weak transitions,[3] for trace analysis,[4] for investigation of chemical kinetics[4] and for nonlinear spectroscopy.[5,6] TL spectrometers employing single and dual (pump, probe) beam methods have been reported.[3] The time dependence of the thermal lensing signal is determined by the rate of thermalization of the deposited energy, the velocity of sound in the material, and the rate of thermal conduction. The rate of thermalization (with time constant τ), may depend on the lifetime of the excited state (population depletion), while the time constant for dissipation of the thermal lens is given[1] by $t_c = w^2\rho C_p/4k$, where w is the laser beam diameter, ρ is the density of the material, and C_p and k are the specific heat and thermal conductivity, respectively. The thermalization time constant (τ) is typically short (microsecond timescale).[7,8] In contrast, t_c is usually long, on the order of milliseconds.[2]

---

[a]Visiting Research Associate. Permanent address: Institute of Spectroscopy, USSR Academy of Sciences, 142092 Moscow Region, Troitzk, USSR.

[b]Alfred P. Sloan Foundation Fellow and Camille & Henry Dreyfus Foundation Teacher-Scholar.

[c]Contribution No. 6648

COMMUNICATIONS

In this communication, we wish to report on the use of synchronously mode-locked picosecond lasers in a pump-probe configuration for TL spectroscopy. The peak power for these picosecond lasers is very high and, of course, the fundamental of the dye laser (red beam) can be efficiently (~10%) doubled in frequency (U.V. beam) by second harmonic generation in nonlinear crystals. We use this generated U.V. beam as a probe to monitor the very weak absorption of the red beam. An arrangement[4] of the beams involving different waist positions for the pump and probe is used. This arrangement results in an enhancement of sensitivity (at least a factor of three to seven). Also, a different dependence of the signal on the cell position compared to the single beam method is obtained. Finally, we have obtained the $\Delta v = 5$ CH-stretching overtone absorption spectrum of liquid toluene with this method (see Figure 1). Suggestions are made regarding new applications of this picosecond pulse thermal lensing technique.

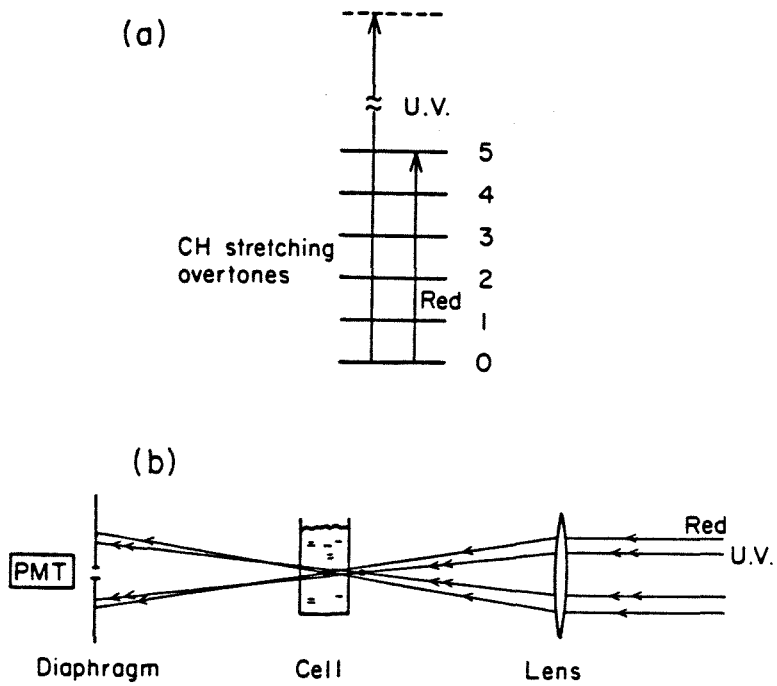

FIGURE 1 Schematic of energy levels (upper) and experimental geometry (lower).

A mode-locked argon ion laser (Spectra Physics 171) (frequency ~82 MHz), which produces a 0.9 W pulse train at 5145 Å with pulse widths of ~100 ps, was used to pump a dye laser. The dye laser gain medium[9] was 1:1 mixture of DCM and LD700 (1.2 *M*) dissolved in 25% benzyl alcohol, 25% glycerol and 50% dimethyl sulfoxide. This dye laser operates over the range of 705–770 nm and produces ~100 mW at the peak, with an 8% output coupler. The dye laser had a pulse width of <10 ps. A 1.5 mm thick $LiIO_3$ crystal, cut for phase matching at 720 nm, was used to frequency double the dye laser output. The beams were focused, in a colinear geometry, into the cell with toluene using a 75mm focal length lens. The fundamental power at the sample was ~50 mW and U.V. power was ~30-50 times lower. Heating of the sample due to absorption of the U.V. beam was negligible.

Using a telescope to adjust the U.V. beam, separated from the red by a dichroic mirror, allowed variation of the relative position of the beam waists. The quartz cell (1 or 10 mm) filled with toluene was translated along the beam axis. The intensity of the red or U.V. beam, transmitted through a 1 mm diameter (φ) diaphragm (placed ~120 mm from the red beam waist position) was measured in the experiments on the cell position dependence of the signal (Figure 1).

Figure 2a shows the observed dependence[10] of the red beam intensity on cell position for the *single beam* experiment with a 1 mm cell. The shape of this curve is in good agreement with that predicted by theory.[1] The maximum signal ($S = I_0 - I/I_0$) achieved in this experiment was 9.4%. In the double beam experiment, with mismatched focusing, the intensity of the UV beam had a different dependence on the cell position. In these experiments, the UV beam waist position occurs before the red beam waist position. Thus, the cell position dependence of the transmitted intensity shows no change in sign, Figure 2b. We find only a decrease in the UV intensity as the cell approaches the red beam waist position, as expected. The maximum signal for the dual beam experiment was 30% at the red beam waist position, showing a *much larger* value than for the single beam experiment. In fact, a "black-hole" appeared visible to the naked eye on the UV beam!

For the long cell (l = 10 mm) the position dependence of the red beam intensity is more complicated than for the thin (1 mm) cell, Figure 3a. In this case $l \gg z$ where $z = \pi w_0^2/\lambda$ (z ~ 1 mm), the confocal length parameter. Thus, the thermal lens cannot be considered as thin. This is probably why there exists a "plateau" between the maximum and minimum. For the dual

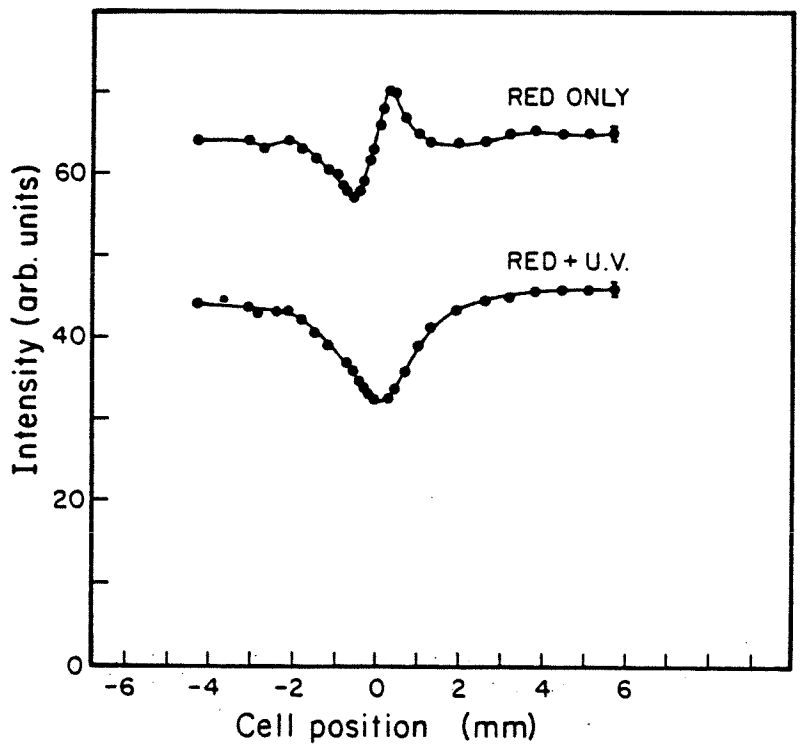

FIGURE 2 Observed cell position dependence of transmitted probe beam intensity for the 1 mm thick cell with toluene liquid, λexc. = 715 nm. a) upper curve is with red beam only and b) lower curve is for the dual beam method (red and UV beams) and the UV intensity is plotted.

beam experiment with the thick cell the intensity follows roughly the same dependence on cell position as for the thin cell, except for being broader, close to the cell length. Again, the maximum signal for the thick cell for the dual beam case is more than six times the signal in the single beam case. With these results, we have demonstrated experimentally that an increased signal (larger defocusing effect) results when a dual beam method with *mismatched focusing*[4] from a short focal length lens is used, relative to the single beam case, for the thermal lensing.[11]

Using the new dual beam configuration we have obtained the $\Delta\upsilon = 5$ CH-stretching overtone spectrum of liquid toluene, Figure 4. This spectrum agrees reasonably well with the spectrum measured with a conventional

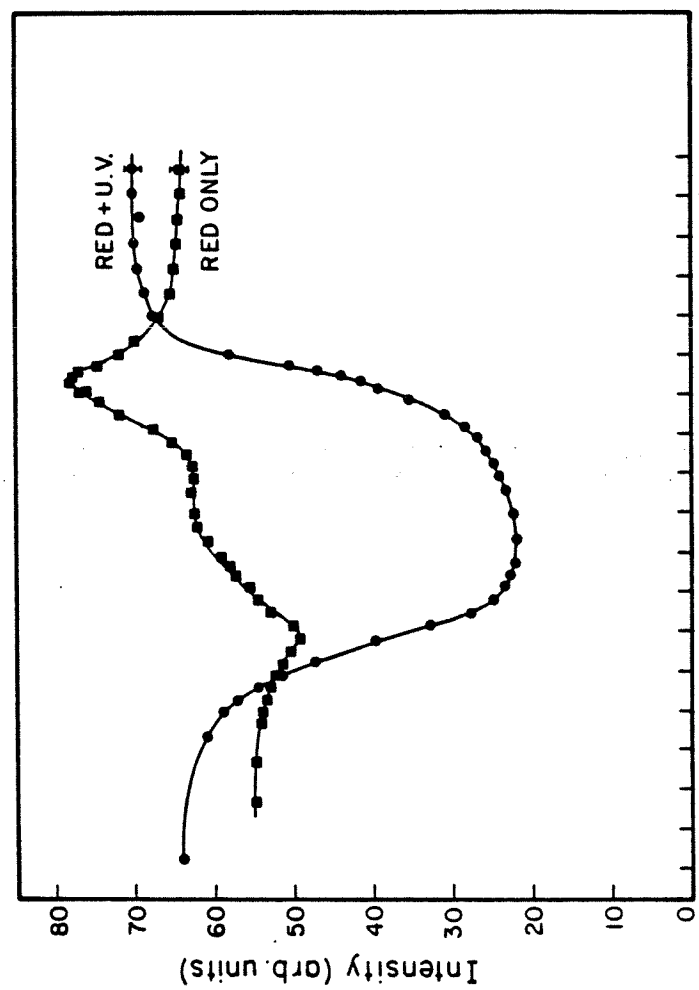

FIGURE 3 Observed cell position dependence of transmitted intensity for the 10 mm thick cell with liquid toluene, $\lambda_{exc.}$ = 715 nm. a)Red only, single beam method, b) red + UV dual beam method, UV intensity is plotted.

spectrophotometer and using a 10 cm path length. Thus, the picosecond pulse thermal lensing spectrometer gives reasonable linear absorption spectra, as is confirmed again by the absence of absorption by benzene-d_6 in this spectral region. In contrast with benzene-d_6, the "black hole" was seen in benzene-h_6 ($\Delta\upsilon = 5$), and toluene ($\Delta\upsilon = 6$).

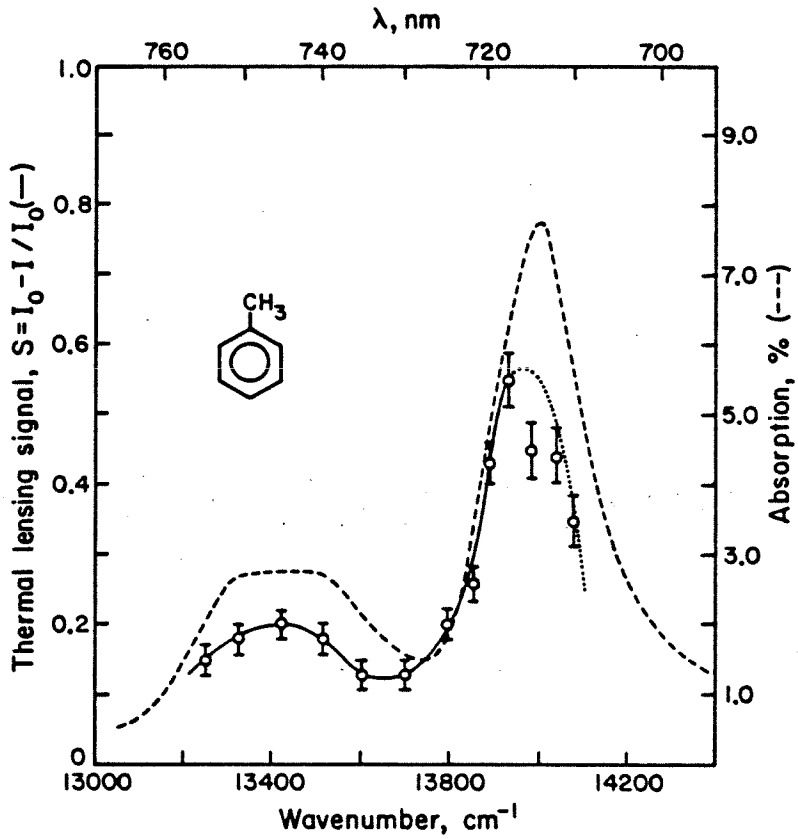

FIGURE 4 CH stretching overtone spectrum ($\Delta\upsilon_{CH} = 5$) of liquid toluene at room temperature (23°C). (----) spectrum obtained with 10 cm cell path length and Cary-17 Spectrophotometer. (——, with error bars) spectrum obtained with dual-beam picosecond thermal lensing spectrometer. The absorption scale is defined as 100% minus the transmission. It should be mentioned that the peak around 13400 cm^{-1} exhibits clear structure in the gas phase[12]; however, broadening of the bands in the liquid results in near coalescence, thus giving the unusual bandshape. Also, the conditions under which the TL spectrum was obtained were far from optimum. However, the spectrum suffices for the purpose of showing that we are dealing with linear overtone absorption. The spectra agree with that obtained previously.[13]

New applications of this method can be anticipated, such as the measurement of nonlinear absorption (e.g., two-photon absorption) in liquids and gases. These measurements should be successful because of the possibility of high peak power from picosecond pulses. Using these lasers with the appropriate repetition rate and delays between the pump and probe pulses, a means for monitoring the risetime of nonthermal transient lensing[6] (e.g., plasma formation) should be obtained.

Acknowledgment

This work was supported by grants from the National Science Foundation (CHE8112833 and DMR8105034). We would like to thank Professor D. Kliger for his useful comments.

References

1. J. P. Gordon, R. C. C. Leite, R. S. Moore, S. P. S. Porto, and J. R. Whinnery, *J. Appl. Phys.* **36**, 3 (1965).
2. C. Hu and J. R. Whinnery, *Appl. Optics* **12**, 72 (1973).
3. R. L. Swofford, M. E. Long, and A. C. Albrecht, *J. Chem. Phys.* **65**, 179 (1976).
4. J. P. Haushalter and M. D. Morris, *Appl. Spectrosc.* **34**, 445 (1980).
5. D. S. Kliger, *Acc. Chem. Res.* **13**, 129 (1980).
6. G. C. Nieman and S. D. Colson, *J. Chem. Phys.* **68**, 2994 (1978).
7. F. W. Dabby, R. W. Boyko, C. V. Shank, and J. R. Whinnery, *IEEE J. Quantum Electron.* QE-5, 516 (1969).
8. D. R. Siebert, F. R. Grabiner and G. W. Flynn, *J. Chem. Phys.* **60**, 1564 (1974).
9. E. Marason and R. Boggy (Spectra Physics)—private communication.
10. Note that the maximum signal for the single beam case occurs at ~0.5 mm (~ one confocal length) from the zero cell position (red beam waist) in agreement with prediction.[1]
11. This observation may be physically justified in that the temperature gradient generated from the pump beam is large (with a short focal length lens) and the resulting thermal lens is located near one confocal length, the maximum defocusing position,[2] from the probe beam waist.
12. K. V. Reddy, D. Heller, and M. Berry, *J. Chem. Phys.* **76**, 2814 (1982).
13. M. S. Burberry, J. A. Morrell, A. C. Albrecht, and R. L. Swofford, *J. Chem. Phys.* **70**, 5522 (1979).